Assessment of macro-instability using SHANSEP in RFEM

The application of SHANSEP in combination with RFEM for safety assessment of dikes.

Esat Ünal

TUDelft

Assessment of macro-instability using SHANSEP in RFEM

The application of SHANSEP in combination with RFEM for safety assessment of dikes.

by

Esat Ünal

to obtain the degree of Master of Science
at the Delft University of Technology,
to be defended publicly on Monday September 15, 2021 at 3:00 PM.

Student number:	4384008
Project duration:	November 16, 2020 – September 15, 2021
Thesis committee:	Prof. dr. ir. M. A. Hicks, TU Delft
	Dr. ir. A. P. Van den Eijnden, TU Delft, supervisor
	Dr. ir. R. C. Lanzafame, TU Delft

TUDelft

Preface

This Master's thesis sets the end of my time at TU Delft. For me, this university was a place where a lot of smart people come together to think and learn about how they could improve the world. Some do this by finding new clever solutions, others improve existing methods. I am grateful to have had the opportunity to meet those great people and to make new friendships. Like every good thing in life, also my great time at this wonderful university has come to an end.

First of all, I want to thank my supervisors and other professors for their knowledge and valuable feedback along this journey.

I want to thank my friends and colleagues for being a listening ear and supportive at all times.

Above all, I want to thank my lovely family for, although being at a distance, keeping to believe in me despite all hardships I have faced. It would probably have not been possible without their support.

Esat Ünal
Rotterdam, September 2021

Abstract

The Dutch Water board revised their guidelines for the safety assessment of dikes in 2017. A major change for the assessment of macro-stability is the use of the SHANSEP method to estimate the strength of impermeable cohesive layers. The failure probabilities are estimated with a deterministic analysis using limit equilibrium methods. The use of design values and safety factors to account for uncertainty is basic and proven to be conservative leading to over engineering.

In this thesis, it is investigated how the SHANSEP method can be incorporated to the more advanced Random Finite Element Method. It is found that three random fields for SHANSEP parameters S,m and POP are required. The random fields do not show particular trends in mean or standard deviation. A random field generator is coded in Python. a simple version of the in-house FEM is modified to read the generated random fields. This code is used to test various geotechnical assumptions.

A final version of the assumptions is coded into a more advanced version of the simulator to do the comparison. The output of the FEM code are the FOS and failure mechanism of a single evaluation with a combination of three random fields. A mean and standard deviation of the FOS results are calculated. The probability of failure is estimated by the area under the probability density function of a lognormal distribution for values below unity. The probability of failure of the deterministic case is estimated using the First Order Second Moment method.

The results show that the probability of failure is overestimated in a FOSM analysis by one order of magnitude compared to the most conservative RFEM simulation. It is expected that this difference is even higher for the more conservative deterministic approach the Dutch guidelines prescribe. The slip surfaces of RFEM were found to be similar to their deterministic counterpart. The RFEM slip surfaces went through local weak zones in random fields.

It is recommended to Dutch policy makers to investigate the use the random finite element method. Although conservatism is preferable in safety assessments, an conservatism of this significance compared to the RFEM approach is unnecessarily costly.

Contents

List of Figures

Shear stress

List of Symbols

α	Orientation of major principal stress with respect to the vertical axis
Δt_c	Critical time step
ϵ	Strain
ϵ_{vp}	Viscoplastic strain
η	Horizontal position in local coordinates
$\gamma(T)$	Variance reduction function
γ	Shear strain
γ_m	Model factor
γ_{dry} & γ_d	Dry volumetric weight
γ_{sat} & γ_w	Saturated volumetric weight
μ	Mean
μ_{ln}	Mean of logarithm
ν	Poisson's ratio
ϕ'	Effective friction angle
ρ	Correlation
σ	Stress or standard deviation
σ_1 & σ'_1	Major principal effective stress
σ_h & σ'_h	Horizontal effective stress
σ_p & σ'_p	Preconsolidation stress
σ_v & σ'_v	Vertical effective stress
σ_{ln}	Standard deviation of logarithm
σ_{v0}	Initial vertical effective stress
σ_{vc}	Vertical consolidation stress
τ	Shear stress or distance
θ	Correlation length
ξ	Vertical position in local coordinates
c'	Effective cohesion
C	Covariance
c_f	Reduced undrained shear strength
c_u	Undrained shear strength
$CADP$	Continuous ADP
E	Young's Modulus
e	Void ratio
F_b	Body forces
F_t	Yield function
f_x	Probability density function
FEM	Finite Element Method
FOS	Factor of Safety
$FOSM$	First Order Second Moment method
m	Strength increase exponent
$nreal$	Number of realisations
OCR	Overconsolidation ratio
$P10$	10 percentile value
$P90$	90 percentile value
p	Mean effective stress
p_f	Probability of failure
POP	Pre-overburden pressure
Q	Plastic potential function
q	Deviator stress
RF	CADP reduction factor

$RFEM$	Random Finite Element Method
S	Normalised undrained shear strength at normal consolidation
s_u	Undrained shear strength
$s_{u,A}$	Undrained shear strength in the active zone
$s_{u,min}$	Lower bound of undrained shear strength
$s_{u,p}$	Undrained shear strength in the passive zone
s_u^{DSS}	Undrained shear strength in Direct Simple Shear
s_u^{TXC}	Undrained shear strength in triaxial compression
s_u^{TXE}	Undrained shear strength in triaxial extension
SRF	Strength reduction factor
t	time
u	Horizontal discplacement in global coordinates
URL	Slope of the unloading-reloading line
v	Specific volume
v	Vertical displacement in global coordinates
VCL	Slope of the virgin compression line
W_i	Weight factor
X	Random variable
Z	Random field
Z_{ln}	Transformation function

1

Introduction

A large part of the Netherlands is located below sea level. These areas are protected against flooding by a network of flood defence systems that consists of dikes, dunes and engineering structures. The Netherlands has 53 dike rings with a total of 3500km of dikes. Large cities with high economic value and vital infrastructure like Amsterdam, Rotterdam and The Hague are protected by these dikes. A breach would lead to billions of euros of damage and thousands of casualties.

The Dutch defence system differentiate two types of dikes: (1) primary dikes, which acts as a direct shield against the North Sea and large rivers, and (2) regional dikes, which protect low lands from water in the branches of large rivers, canals and lakes. Both types of dikes consist of a substantial amount clay and peat. Although the amount of these low permeable soils is often higher in regional dikes. Presence of these soils affect the strength of both types of dikes significantly.

The Dutch government requires administrators to assess whether a dike complies to safety standards every 12 years. An important part of the assessment is macro-stability, the resistance of dikes against failure of a slope on both sides. This assessment is usually performed using a combination of geotechnical investigation and numerical methods. Multiple methods to evaluate the risk of macro-stability exist. An advanced method is the Random Finite Element Method (RFEM) in which multiple random strength fields representing heterogeneity due to inherent spatial variability in soil properties are generated and their stability is assessed with the Finite element Method (FEM). Heterogeneity is estimated using geotechnical laboratory and field tests and expressed as statistical parameters. The Dutch government has published new guidelines for its administrators, WBI2017, to assess Dikes and Dams in 2017. A major improvement is the recommendation to incorporate Critical State Soil mechanics (CSSM) (Schofield and Wroth, 1968), using the Stress History And Normalized Soil Engineering Properties (Ladd and Foott, 1974) method for soft layers (van Duinen, 2014). The model assumes the undrained shear strength to be a function of the vertical effective stress and overconsolidation ratio (OCR). In contrast to the traditional way of modelling (Mohr-Coulomb) in which the shear strength in every layer is usually taken constant, SHANSEP allows to have depth dependent variation in shear strength within a layer in a natural way. This approach is more realistic as typical dike geometry results in higher (vertical) effective stresses, and thus a higher shear resistance, in the middle compared with the effective stresses at the toe.
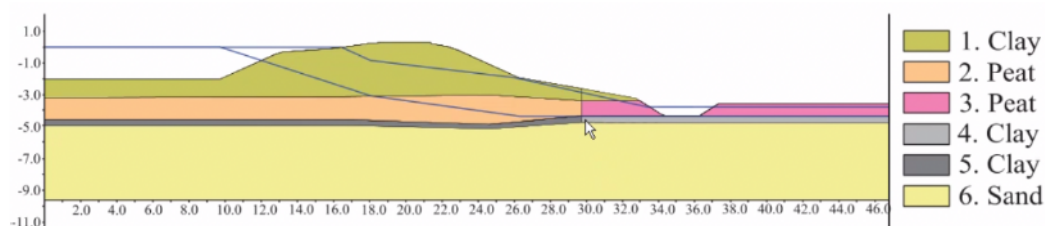
Figure 1.1: A 2D model of a regional dike in a FE program in which SHANSEP is not used. The impermeable layers (peat and clay) need to be divided horizontally to account for the difference in strength in the same geological layer.

1.1. Research Problem

Although the use of SHANSEP in the FEM with a low-level risk analysis (i.e. a deterministic analysis using partial factors) is common in practice for the evaluation of the stability of dikes, it's use in combination with a more advanced RFEM has not been done. A possible reason could be complexity as two sources of strength variation needs to be combined and modelled: (1) depth dependent variations caused by SHANSEP and (2) statistical variation in a random field. However, it is worth investigating whether the combination yields significant different results with respect to existing methods in the evaluation of failure caused by macro-instability.

1.2. Main objective and research questions

The main objective of this Master thesis is to investigate the effect of using statistical spatial variability in combination with SHANSEP in a FEM. In order to fulfil this aim, the following research questions are formulated:

- In what ways can the variation in a random field be combined with variation of shear strength created by SHANSEP? Which method is practical?

- How can random fields be generated to avoid physically impossible circumstances?

- What difference in failure mechanism, factor of safety and probability of failure does the SHANSEP RFEM combination yield with respect to its deterministic counterpart?

1.3. Outline

In order to answer the research questions a thorough literature review will be performed, with a summary of the most relevant findings presented in chapter 2. The literature review will give us insight on possible ways to combine RFEM and SHANSEP. Based on the literature review a random field generator will be coded to generate random fields, which will later be fed to FEM programs developed at the TU Delft. The inner workings of the random field generator, the modifications to a simple FEM program and the interaction of the two will be discussed in chapter 3. Geotechnical assumptions are tested with this code. Findings of this conceptual development phase will be used to modify an advanced FEM code. This code will be used to perform deterministic and RFEM analyses of a hypothetical slope. The modifications and the comparison of results are reported in chapter 4. An RFEM analysis will be run with data of a real case. Its findings will be reported in chapter 5. The thesis will be concluded with chapter 6 in which the research questions are answered with the results of this thesis. A section will be dedicated to reflect on the methodology used in this thesis and recommendations will be given for future research.

2

Literature review

2.1. Failure mechanism: Macro-instability

Dikes are water retaining structures made of (organic) soils. They fulfil their function by two means, (1) they are impermeable enough to prevent water from leaking inwards and (2) they are high and stable enough to keep water away from the hinterland.

A dike loses its water retaining capabilities when either of those characteristics is altered. The water level could rise above a dike's crest, the geometry of the dike could change due to instability in such a way its crest becomes lower than the water level, or the dike could become more permeable. Typical failure mechanisms related to the aforementioned reasons are illustrated in figure 2.1. The failure mechanism that will be of concern in this thesis is macro-instability (E and C in figure 2.1). Macro-instability is the sliding of large chunks of soil along a deep, straight or curved, slip surface. It is caused by the loss of equilibrium between the driving moment and resisting moment (see figure 2.2). The driving moment is induced by the soils body's self-weight on the active side. The resisting moment is induced by the soil body's self-weight on the passive side and the soil's shear resistance along the slip surface(Ministerie van Infrastructuur en Milieu, 2016a).

Macro-instability can happen towards both sides of the dike. Although the mechanisms are identical, external factors driving them are different. Inner slope failure happens when the phreatic surface within the dike rises due to increased water levels or heavy rainfall. The pore pressures increases, the effective stress decreases and, subsequently, the shear resistance decreases. Another phenomenon contributing to the inner slope failure is Uplift reducing the shear strength along a part of the slip surface. It happens when there is a soft low permeable layer on top of permeable sand layer in the hinterland. The hydraulic head of the more permeable layer rises and at the boundary of the two layers, the pore pressure becomes higher than the buoyant self-weight of the weak layer lifting up the weak layer and decreasing most of the shear resistance. Outer slope failure is caused, similar to the inner slope failure, by an elevated phreatic surface or water head
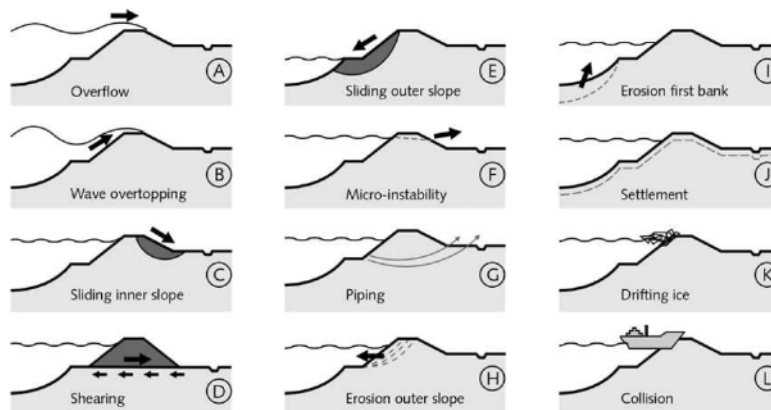
Figure 2.1: Mechanisms that could induce failure in a dike.(Vrijling et al., 2011)
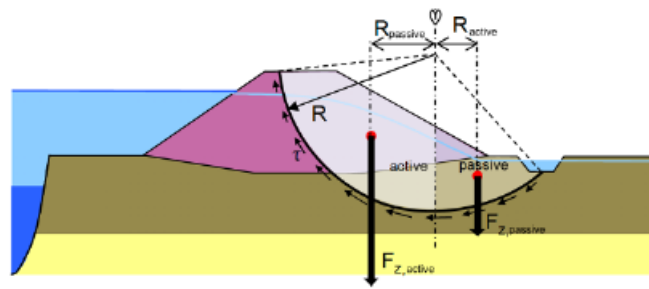
Figure 2.2: The moment equilibrium of a dike with circular slip surface schematised. (Ministerie van Infrastructuur en Milieu, 2016a)

in the soil. However, as the weight of the water body in the river contributes to the resisting moment, outer slope surface is usually less of a concern. The only scenario which could cause an outer slope failure is a rise in water level followed by extreme drought. This causes a reduction in shear resistance which is not counterbalanced by the water body's self-weight.

2.1.1. Significance of SHANSEP in Dutch guidelines.

The Dutch law requires dikes to be assessed every 12 years. Ideally, dikes are as safe as possible. However, as dike maintenance is expensive, a trade-off between protection and cost has to made. The minimum required probability of flooding of a trajectory of dike is prescribed by law (Water act) for primary dikes and by norms for regional dikes. Dikes which do not protect highly populated and economically important areas are allowed to have higher probabilities of flooding. This probability includes every mechanism that could lead to a breach of a trajectory of dike and is translated to a probability of failure for every mechanism. In the assessment, a trajectory of dike is divided into sections based on geometrical and geological similarities. A representative cross section is selected, and site investigation techniques and laboratory tests are performed. A ground model based on those data is made in Ringtoets or a finite element program and the probability of failure is calculated.(Ministerie van Infrastructuur en Milieu, 2017)

The Dutch waterboards has released Ringtoets, software to assist the assessment of dikes. Ringtoets allows to analyse the stability of slip surfaces with three methods; Bishop (Bishop, 1955), UpliftVan (Van, 2001) and Spencer-VanderMeij(Van de Meij, 2012). All of these methods are a variation of the method of slices in which the sliding mass is divided into slices. The forces acting on the slices are calculated, and the stability is assessed using moment and force equilibrium equations. The most advanced is the Spencer-VanderMeij method as it uses a genetic algorithm to find the most critical slip surface. This is a more realistic approach as the geometry and size of the slip surface is not predefined.

There are two types of analysis that can be distinguished. Drained analysis assumes that the pore fluid is able to drain out of the soil matrix during shearing. An increase in load will not affect pore pressures. On the other hand there is undrained analysis which assumes a restricted movement of pore fluid. Some of the loads are transferred to the incompressible pore fluid, increasing pore pressures. The pore pressure acts as a counter force to the interlocking forces of the particles and subsequently, its frictional resistance decreases. The actual behaviour of natural soils is in between those extremes. The Dutch guidelines recommend using drained analysis for sands and undrained analysis for clays and peat. The motivation behind this choice is based on the observed speed at which dike failure happens with respect to the soils' permeability. It is assumed that a sand's permeability is sufficient to allow free movement of pore water. Clays and peat do not.(Ministerie van Infrastructuur en Waterstaat, 2017)

Another recommendation is to use the SHANSEP method (Ladd and Foott, 1974) to calculate the undrained shear strength of soft and organic soils. The SHANSEP method is based on the Critical State Soil Mechanics (CSSM) (Schofield and Wroth, 1968) theory (Ministerie van Infrastructuur en Waterstaat, 2017). CSSM describes certain soil behaviour (i.e. shearing, volume changes) in terms its state. A soil's state is defined as a combination of the soils specific volume (v) and the effective volumetric (p) and deviator stresses (q) acting on the soil. The theory suggests that there exists combinations of volume and stresses at which the soil fails. Failure occurs at a soil's critical state, a state where the soil shears continuously under constant volume and deviator stress. A soil tends towards this critical state irrespective of its initial state (2.4). All possible critical
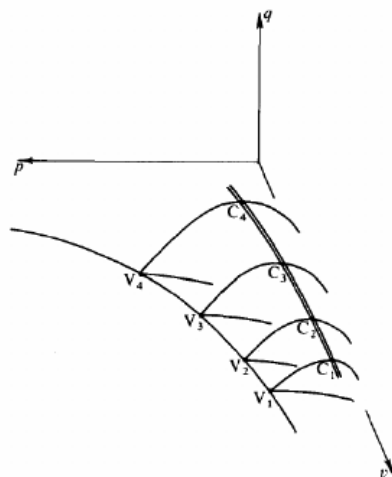
Figure 2.3: A 3D representation of state in the CSSM based Cam Clay model. The q,p and v axes refer to the deviator and volumetric stress and specific volume, respectively. C1 til C4 is the critical state for a particular pre-consolidation pressure (V1 till V4). The line going through these points is the Critical State Line (CSL). From Schofield and Wroth(1968).
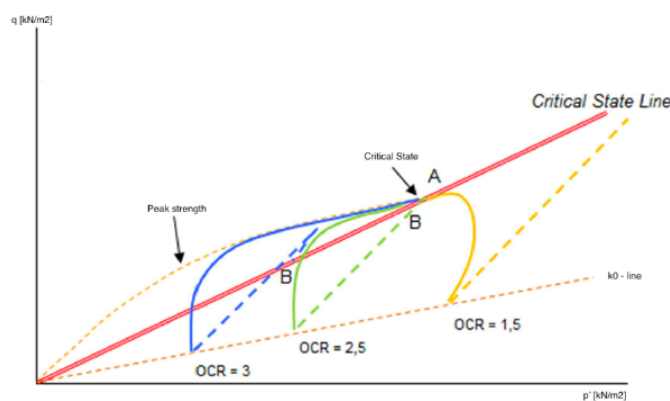
Figure 2.4: Stress paths of the same soil at different initial OCR and same pre-consolidation pressure. Note that the slope of the dached lines is 3:1 in reality. Adapted from Ministerie van Infrastructuur en Milieu(2016b)

states are represented by a line in the three-dimensional q,p,v-space (2.3). The exact point depends on the stress history which is expressed by the pre-consolidation pressure. The behaviour of soil depends on the state it is in with respect to the critical state line. The soil shows contractive behaviour when its state is below the critical state and dilative behaviour when its state is above the critical state line. This is of particular interest, because in undrained conditions, dilation of the soil, leads to the development of negative pore pressures due to surface tension, and consequently, to an increase in shear strength. Dilative behaviour is observed in soils with a high over consolidation ratios (OCR). OCR is defined as the ratio between current effective stress and pre-consolidation pressure. It is an indication of the stress history.

The SHANSEP model is a simplified representation of CSSM in the sense that the undrained shear strength depends on the actual stress and stress history. While CSSM aims to describe full stress-strain behaviour of soils, SHANSEP concerns with just the behaviour (strength) at a single point of the full behaviour, usually being the peak or ultimate state strength.

2.2. SHANSEP

SHANSEP revolutionised the industry by introducing a new method of determining and expressing the undrained shear strength of (organic) soft soils. The method was proposed by keeping recent research on the behaviour of clays into consideration. The four key insights on the behaviour of clays of that time were sample disturbance, strength and stress-strain anisotropy, strain rate effects and normalized behaviour. These four findings will be briefly elaborated.
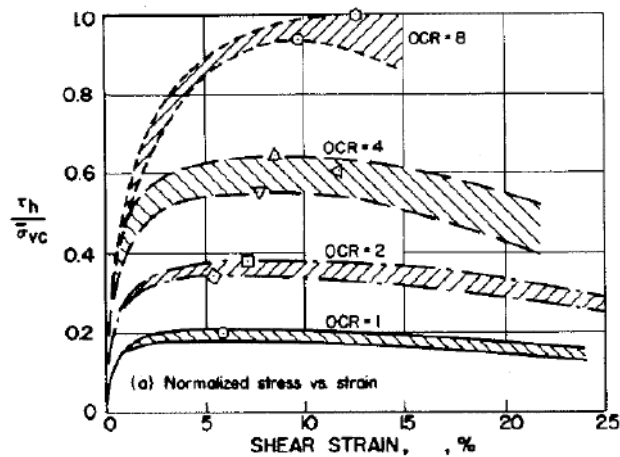
Figure 2.5: Data of CK0U triaxial tests performed on reconsituted Boston Blue Clay. After Ladd and Foott(1974).

2.2.1. Normalized behaviour

It has been shown through laboratory tests that clays with the same OCR that are consolidated at different pressures show very similar stress-strain behaviour. Theoretically, when the deviator stress is normalized by their pre-consolidation pressure, their stress-strain curves should be identical. Figure 2.5 shows the normalised stress-strain data for K0 consolidated triaxial compression tests on reconstituted Boston Blue Clay obtained by four different people. It can be seen that there is very small variation between the measured normalised shear strengths. The small scatter in results can be dedicated to differences in testing procedures and spatial variability. Further extensive research on normalised behaviour of cohesive soils showed that the maximum divergence of scatter in similar stress-strain curves is generally found to be 10% of the mean.(Ladd and Foott, 1974)

2.2.2. Sample disturbance

A part of the strength of natural soils cannot be dedicated to stress effects. Post-depositional processes such as cold welding at inter particle contacts under high pressure, deposition of carbonates, hydroxides and organic matter from solution, recrystallisation of minerals during weathering, the modification of the adsorbed water layer and interparticle attractive forces causes bonding between particles (Leroueil and Vaughan, 1990) contributes to the strength by increasing the pre-consolidation pressure (Tanaka et al., 2003; Leroueil and Vaughan, 1990). These processes are simply referred to as cementation and ageing. The binding effect of cementation and ageing is called the fabric structure of a soil.

Sample disturbance is the inevitable disturbance of the soil fabric structure during sampling. A major source of disturbance is stress relief (Ladd and Foott, 1974). If the structure is destroyed in the process of sampling or during preparation of a specimen for laboratory testing, it is impossible for the specimen to represent the in-situ conditions perfectly even if the stress conditions are reproduced in a laboratory test. (Tanaka et al., 2003). However, the effect of sample disturbance can be minimised by using good quality samples(Ladd and Foott, 1974). The SHANSEP method tries to overcome effects of sample disturbance by erasing the effect of soil fabric.

This is achieved by consolidating the specimen under stresses several times its in-situ pre-consolidation stress and swelling it back to its original OCR. The question arises whether this procedure is representative for the true in-situ behaviour of clay. An experiment performed by Tanaka et al. (2003) compares the undrained shear strength obtained from the SHANSEP method to the undrained shear strength obtained from the recompression technique using low and high quality samples on six different natural clays. The results from the SHANSEP method were just slightly off, a factor between 0.9 and 1.1. It may be concluded that although SHANSEP is not capable of capturing the effect of fabric structure, it still is a useful technique for obtaining the peak undrained shear strength. It should be kept in mind that this conclusion relies heavily on the assumption that the recompression technique is capable of representing the in-situ conditions perfectly.
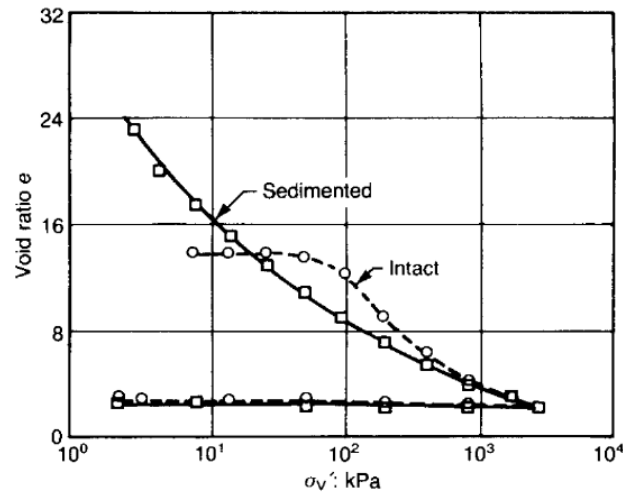
Figure 2.6: One dimensional compression curves for intact samples of soft (Mexico city) clay (Mesri, 1975) and for samples sedimented in the laboratory. It can be observed that the intact (natural) clay sample does not follow the normal compression line of the sedimented clay after reloading. The pre-consolidation pressure is slightly higher for the samne vertical effective stress. The increase is dedicated to cementation and ageing. After Leroueil and Vaughan(1990).
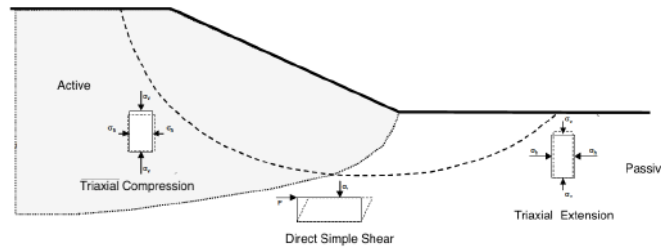
Figure 2.7: A schematic cross-section of a dike indicating three zones of stress conditions and laboratory test with strong correlations. After(Ministerie van Infrastructuur en Waterstaat, 2017).

2.2.3. Anisotropy

Multiple researchers have proven that natural clays show anisotropy in strength and stress-strain behaviour (Lewin, 1973; Duncan and Seed, 1966; Nishimura et al., 2007). Anisotropy in soft soils, the dependency of stress-strain behaviour on stress direction, has two major sources. The first is inherent anisotropy which is the result of differences in soil structure which occurred during formation of the soil. Varved clays, soil composed of alternating layers of silt and clay, show high inherent anisotropy(Ladd and Foott, 1974). The other source of anisotropy is induced and is the result of the rotation of principle stress directions. A load applied to a soil is carried by a small fraction of particles forming force chains, the remaining particles carry little or no load. These load-carrying particles undergo reorientation during a loading process. They tend to reorient themselves perpendicular to the major principle stress. The stress strain behaviour is affected by the orientation of these particles(Anandarajah et al., 1996).

As the undrained shear strength of clays is dependent on the load direction, the shear strength of the soil in the semi-circular slip surface of an embankment depends on its specific location as the load direction varies. This requires the use of different types of tests in order to obtain shear strength parameters for a certain zone under a dike. As illustrated in figure 2.7, the stress conditions in the active zone is strongly correlated by a triaxial compression test, the triaxial extension test is representative for the passive zone and the intermediate zone close to the toe of the dike is best imitated by the direct simple shear test.(Ladd and Foott, 1974) Although the Dutch guidelines recognizes this principle, it recommends the use of a single set of undrained shear strength parameters obtained at large strain rather than the peak strength. This is decided considering the effect of strain compatibility.(Ministerie van Infrastructuur en Waterstaat, 2017) Strain compatibility is the assumption that strains along a slip surface are equal. This assumption complicates the prediction of the undrained shear strength along the slip surface.Consider the results of laboratory tests on marine clay in figure 2.8. By keeping the principle of strain-compatibility in mind, the mobilised shear strengths at a cer-
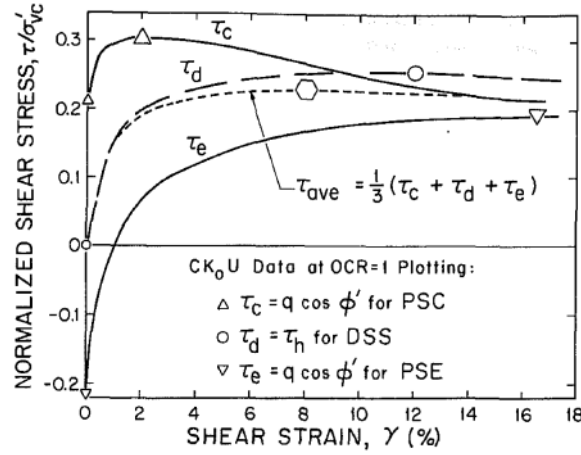
Figure 2.8: A comparison of the stress-strain behaviour of AGS Marine clay in Triaxial extension (τ_e), triaxial compression (τ_c) and direct simple shear test (τ_d). After Ladd(1991).

tain shear strain are compared. For example, at around 8% shear strain, the peak shear stress (indicated by a hexagon) is mobilised in a DSS test. At the same shear strain, the same soil in a triaxial compression test would have been loaded beyond its peak strength. This means that in the calculation of the shear resistance along a slip surface, is somewhat complicated However, figure 2.8 shows that the mobilised shear strength in the three different tests converge at large strain. This phenomenon and the fact that macro-instability causes large strains justifies the assumption of the Dutch guidelines.

2.2.4. Strain rate effect
It is now well-known that the undrained shear strength of soil depends on the strain rate. This affects the undrained shear strength measured from a laboratory test. The strain rate effect of clays is amplified in highly plastic and creep susceptible clays. The effect is the result of creep during undrained loading leading to increased pore pressures, thus lower effective stresses, leading to a decreased shear strength. The slower the loading of the soil, the more creep can develop and the lower the undrained shear strength will be(Ladd and Foott, 1974).

2.2.5. SHANSEP equations and parameters
In contrast to the traditional way of modelling, in which the undrained shear strength is estimated using the c-phi method which results in constant strength within a single layer, the SHANSEP method allows to have variation in shear strength within a layer depending on the magnitude of vertical effective stress. The base for this is the previously mentioned normalised behaviour observed in cohesive soils. In figure 2.9, the normalised peak undrained shear strength of 5 different clays are plotted against OCR. The lines are a trend line through data points. The maximum scatter is 10% from the regression line. The curves are similar, they all resemble exponential functions. The curves can be expressed mathematically as:

$$\frac{S_u}{\sigma'_{v0}} = S * OCR^m \tag{2.1}$$

$$OCR = \frac{\sigma'_{vc}}{\sigma'_{v0}} = \frac{\sigma'_{v0} + POP}{\sigma'_{v0}} \tag{2.2}$$

in which S is the normalised shear strength at normal consolidation and m is the shear strength increase exponent. In order to calculate the undrained shear strength, model parameters S and m and the pre-consolidation pressure and in-situ vertical effective stresses needs to be determined. The in situ stress conditions can be estimated using field tests (i.e. CPT) or laboratory tests. The procedure recommended by the Dutch guidelines can be summarised as follows.

S is the normalised undrained shear strength at OCR=1. The parameter can be calculated by first consoli-dating the soil specimen at pressures equal to or larger than its in-situ pre-consolidation pressure. An esti-
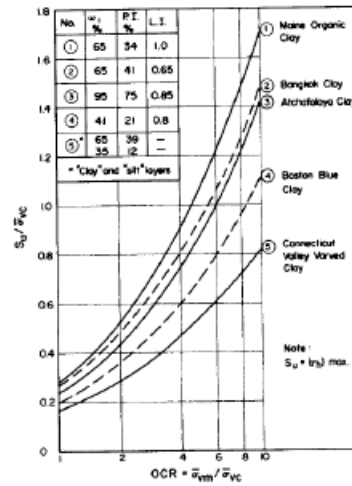
Figure 2.9: Normalised (peak) shear strengths of 5 different clays plotted against OCR. After Ladd and Foott(1974).

mation of the in-situ pre-consolidation pressure is made by performing an oedometer test. Then it is recommended to perform a k0 consolidated undrained triaxial compression test or direct simple shear test. The shear strength at 25% and 40% axial strain for a CK0U or DSS is taken as the undrained shear strength, respectively. The calculated shear strength is divided by the applied pre-consolidation pressure.

Parameter m can be determined in two ways. The first method is by performing multiple laboratory tests at the same pre-consolidation pressures but different OCR. An exponential regression line is drawn through the results. The exponent is parameter m.

The second method of determining parameter m is by performing an oedometer test. Parameter m is related to the slopes of the virgin compression line (VCL) and unloading-reloading line (URL) by the following formula.

$$m = \frac{VCL - URL}{VCL} \tag{2.3}$$

2.2.6. SHANSEP NGI-ADP in PLAXIS

The Norwegian Geotechnical Institute launched a constitutive model for bearing capacity problems in 2011. The main feature of this model is the application of the ADP concept wherein the slip surface in the foundation, similar to a slope stability problem, goes through three stress zones. Plaxis added the use of SHANSEP formulation to compute s_u^A, the plain strain active shear strength. The plane strain DSS and passive shear strengths (s_u^{DSS} & s_u^P) are derived from s_u^A and the corresponding input ratios.

The SHANSEP formulation implemented in PLAXIS has a subtle difference compared to the original SHANSEP formulation; the major principal stress is considered rather than the vertical effective stress. The major principal stress is thought to be a more objective parameter as it is the most compressive stress in every stress condition. It is expected that the PLAXIS approach will give lower values of OCR, but higher values of S_u, as the major principal stress is always higher (or equal) to the vertical effective stress. (Panagoulias and Brinkgreve, 2017)

$$\frac{S_u}{\sigma_1'} = S * OCR^m \tag{2.4}$$

$$OCR = \frac{\sigma_{1,max}'}{\sigma_1'} = \frac{\sigma_1' + POP}{\sigma_1'} \tag{2.5}$$

2.2.7. 1-D example ground model

In order to illustrate a typical evolution of S_u with depth using the SHANSEP method, the S_u of a hypothetical clay layer is plotted against depth. The layer is 5 meters thick and has the properties listed on the caption of figure 2.10. As can be seen from the figure, two cases can be distinguished. The OCR in the clay layer could be constant. In this case, the S_u increases linearly with depth. The OCR could also be variable. This is achieved by assuming a constant pre-overburden pressure (POP)in equation 2.2. Due to the relatively high value of

Typical 1-D s_u ground models of a clay layer made with SHANSEP
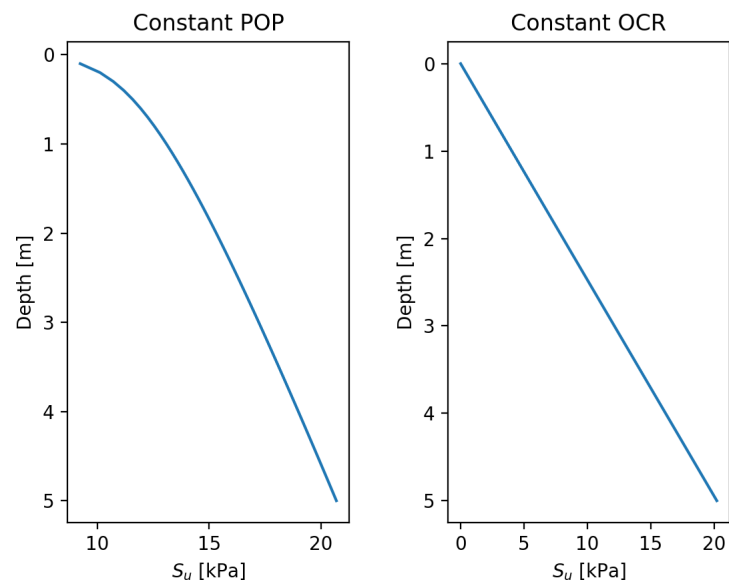
Figure 2.10: Typical 1-D ground model made with the SHANSEP formulation. The SHANSEP parameters of the hypothetical clay are as follows: $\gamma_{sat} = 14.8 kN/m3, \alpha = 0.32, m = 0.88$. For the first graph a POP of 50 kPa is used. For the second graph an OCR of 3.0 is used.

POP with respect to σ'_{vo}, the OCR at the upper part of the layer will be high. The OCR will quickly decrease as, with increasing depth, the in-situ vertical effective stress increases and the relative contribution of POP decreases. This effect can be seen in the figure on the left hand side. the graph is curved initially and as the depth increases, the curve becomes linear as OCR approaches 1.

2.3. Finite element method

The Finite Element Method (FEM) is a widely used method to solve engineering problems. Its application varies from structural analysis to heat transfer, fluid flow and mass transfer. FEM subdivides the geometry of the engineering problem into smaller elements. An analysis is performed at the smaller scale by solving partial differential equations numerically. All solutions combined make up the output of the full analysis.The method's popularity increased significantly with the rise in computational power of personal computers in the early 2000s.

The most common use of FEM for geotechnical applications is structural analysis. It is very much suitable for slope stability analysis. Although Ringtoets makes use of the more traditional methods of slices, due to some advantages of FEM, it is becoming more common to use the FEM in the assessment of Dutch dikes. A range of of possible failure mechanisms (consisting of a single slip surface) is defined a priori in Ringtoets, with the exception of the computationally expensive Spencer-VandeMeij method. In FEM, the failure mechanism (consisting of possible multiple slip surfaces) is computed during the analysis yielding more accurate results.

The inner workings of a simple FE code is demonstrated in the following subchapters. The code is used at early stages of the project to perform quick slope stability simulations for generated random fields in order to test geotechnical assumptions. The more advanced FE program that will be adapted uses an identical program flow; a viscoplastic SRF iteration algorithm. The first subchapter will give an overview of the several parts within the program. The subsequent chapters explain relevant parts of the program in more detail. The book by Smith et al.(2014) can be consulted for further details about the program.

2.3.1. Structure chart of FE program

Figure 2.11 illustrates schematically the structure of the FE program. The program is developed for 8-node quadrilateral reduced integration viscoplastic 2-D slope stability analysis. It starts with an initialization, where geometry and soil property data are loaded, the mesh is discretised and memory is allocated to vectors and matrices. This is followed by the assembly of the global elastic stiffness matrix. The global stifness matrix is the third variable, alongside deformation and force, in the governing equation. The values within the matrix depend on the soil stiffness. Thirdly, the critical time step is worked out to be used in the viscoplastic analysis. After that, the viscoplastic analysis starts.The strength reduction factor (SRF) is calculated iteratively using the bisection method. The choices for the SRF selection is assisted by an elasto-viscoplastic iteration. In case the maximum displacement remains small, the overall deformation within the slope is assumed to be elastic. In the other case, the slope failed.

2.3.2. Discretization

FEM is a technique for solving partial differential equations by first discretising these equations in their space dimensions. The discretization is carried out locally over smaller elements of simple but arbitrary shapes. This results in matrix equations relating the input at specified points in the elements (the nodes) to the output at these same points. In order to solve equations over large regions, the matrix equations for the smaller subregions can be summed node by node, resulting in global. Alternatively, 'element-by-element' techniques can be employed to avoid creating large global matrices.Smith et al., 2014

The simple program uses quadrilateral elements with 8 nodes (see figure 2.12). Every node has two degrees of freedom; translation in both the horizontal x- direction (u) and vertical y-direction (v). 4 nodes are located at the corners and the remainder are in the middle of each leg. The geometry of an element is defined by nodal positions. The continuous displacement vector [u] is approximated by nodal deformations, through simple weight functions of the space variable called 'shape functions'. Nodes in the proximity carry more weight(Smith et al., 2014). The 8 node approximation of a quadrilateral element results in a quadratic (2nd order) shape functions. As the true variation of deformation is of higher order, greater accuracy could be achieved by introducing more nodes in element, leading to higher order shape functions(Smith et al., 2014). Shape functions of an 8-node quadrilateral element can be found in the appendix.

If shape functions were to be defined for a general (deformed) quadrilateral in 'global' (x,y) coordinates, very complex shape functions would be needed to be defined which had to be updated every load step. This would lead to the use of computationally expensive algebra packages to find shape functions. In order to solve this problem, shape functions are defined in their own 'local' coordinate systems in ξ,η-space. In this system, full length of every side is at a distance of unity from both axes (see figure 2.12, sides 12, 23, 24 and 14 are at $\eta =$

Initialization

Load geometry and soil property data
Discretize mesh
Allocate memory

Assemble of global stiffness matrix

For all elements:
Calculate elastic stiffness [D]
Assemble element stiffness matrix [km]

> For all integration points:
> Calculate shape functions
> Calculate [B]
> Calculate contribution of integration point to element stiffness matrix
> Sum all contributions

Calculate gravitational load

Assemble and factorize global stiffness matrix

Work out critical time step

Viscoplastic SRF analysis

Assume initial strength reduction factor (SRF)

Work out iteratively strength reduction factor (SRF) with bisectional method:
Add body loads to gravitational loads

> For all elements:
>
> > For all integration points:
> > Reduce field strength by SRF
> > Calculate elastic strain increments
> > Calculate stress increments and add to loads leftover from previous load increment
> >
> > Failure criterion exceeded?
> >
> > Yes   No
> > Accumulate visco plastic strains.   Go to next
> > Form integrals for element body   Gaus point
> > loads
>
> Assemble global body loads

Check convergence

Yes   No
Quit iteration   Iterate again

Compute deformation vectors
Update mesh
Print results
Clear memory

Figure 2.11: Structure chart of the simple FE slope stability analysis program. Adapted from figure 6.8 in (Smith et al., 2014)
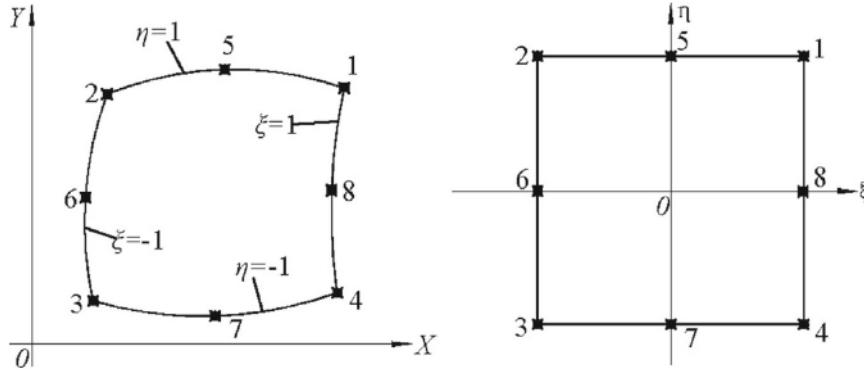
Figure 2.12: An example of a rectangular 8-node quadrilateral element. The corners of the element are always at a distance of 1 from the axes in the axis system of the element. After Zhang and Wang (2019).

1, $\xi = -1, \eta = -1$ and $xi = 1$,respectively. The advantage of defining local coordinates this way is that a single set of equations is sufficient to describe the shape of every element. The elements are isoparametric, meaning that the same shape functions could be used in both global and local coordinate systems to approximate the value of a continuous variable. The approximation of deformation in horizontal [u] and vertical [v] directions are as follows:

$$u = N_1 u_1 + N_2 u_2 + N_3 u_3 + N_4 u_4 + N_5 u_5 + N_6 u_6 + N_7 u_7 + N_8 u_8 \tag{2.6}$$

$$v = N_1 v_1 + N_2 v_2 + N_3 v_3 + N_4 v_4 + N_5 v_5 + N_6 v_6 + N_7 v_7 + N_8 v_8 \tag{2.7}$$

2.3.3. Governing equations

The governing equation will be derived ftom the 2-D force equilibrium.

$$\frac{\partial \sigma_x}{\partial x} + \frac{\partial \tau_x y}{\partial y} + F_x = 0 \quad , \quad \frac{\partial \sigma_y}{\partial y} + \frac{\partial \tau_{xy}}{\partial x} + F_y = 0 \tag{2.8}$$

Note that the shear stresses are equal. The matrix notation of the equations is:

$$[\mathbf{A}]^T \boldsymbol{\sigma} = -\mathbf{F}, \quad [\mathbf{A}] = \begin{bmatrix} \frac{\partial}{\partial x} & 0 \\ 0 & \frac{\partial}{\partial y} \\ \frac{\partial}{\partial y} & \frac{\partial}{\partial x} \end{bmatrix}, \quad \boldsymbol{\sigma} = \begin{Bmatrix} \sigma_x \\ \sigma_y \\ \tau_{xy} \end{Bmatrix} \quad and \quad \mathbf{F} = \begin{Bmatrix} F_x \\ F_y \end{Bmatrix} \tag{2.9}$$

Stress $\boldsymbol{\sigma}$ in equation 2.9 can be replaced by the elastic constitutive equation for plane strain conditions.

$$[\mathbf{A}][\mathbf{D}]\{\boldsymbol{\varepsilon}\} = -[\mathbf{F}], \quad \{\boldsymbol{\varepsilon}\} = \begin{pmatrix} \varepsilon_x \\ \varepsilon_y \\ \gamma_{xy} \end{pmatrix} and [\mathbf{D}] = \frac{E(1-v)}{(1+v)(1-2v)} \begin{bmatrix} 1 & \frac{v}{1-v} & 0 \\ \frac{v}{1-v} & 1 & 0 \\ 0 & 0 & \frac{1-2v}{2(1-v)} \end{bmatrix} \tag{2.10}$$

Eliminiating $\{\boldsymbol{\varepsilon}\}$:

$$[\mathbf{A}][\mathbf{D}][\mathbf{A}][\mathbf{S}]\{\mathbf{u}\} = -\{F\}, \quad [\mathbf{S}]\{\mathbf{u}\} = \begin{Bmatrix} [\mathbf{N}]\{\mathbf{u}\} \\ [\mathbf{N}]\{\mathbf{v}\} \end{Bmatrix} \tag{2.11}$$

where {u} and {v} are nodal displacement vectors in the x and y directions, respectively. Applying Galerkin's method and substituting [A][S] with [B] :

$$\iint_A [\mathbf{B}]^T [\mathbf{D}][\mathbf{B}]\{\mathbf{u}\} dx dy = \iint_A = [\mathbf{S}]^T [\mathbf{F}] dx dy \tag{2.12}$$

As nodal displacements and body forces are not a function of x and y, the two quantities could be taken out of the integral and the governing equation can be written in its more general form.

$$[\mathbf{k_m}]\{\mathbf{u}\} = [\mathbf{F}] \tag{2.13}$$

in which $[\mathbf{k_m}]$ is called the element stiffness matrix. In order to calculate displacements from forces directly, this matrix needs to be assembled. The integral can be approximated numerically using Gauss-Legendre quadrature. Integrals are evaluated by calculating the function at multiple (integration) points within the element, assigning a weight factor depending on the position and taking the sum.

$$\int_{-1}^{1} f(\xi, \eta) d\xi d\eta \approx \sum_{i=1}^{nip} W_i f(\xi, \eta)_i \tag{2.14}$$

The integral of the stiffness matrix must be transformed to the ξ, η-space in order to be able to evaluate it such as in equation 2.14. This can easily be done by applying the chain rule for the derivatives in the $[\mathbf{B}]$ matrix. It is convenient to use a matrix for the application of the chain rule. The matrix is of form:

$$\left\{ \begin{matrix} \frac{\partial}{\partial \xi} \\ \frac{\partial}{\partial \eta} \end{matrix} \right\} = \begin{bmatrix} \frac{\partial x}{\partial \xi} & \frac{\partial y}{\partial \xi} \\ \frac{\partial x}{\partial \eta} & \frac{\partial y}{\partial \eta} \end{bmatrix} \left\{ \begin{matrix} \frac{\partial}{\partial x} \\ \frac{\partial}{\partial y} \end{matrix} \right\} = [\mathbf{J}] \left\{ \begin{matrix} \frac{\partial}{\partial x} \\ \frac{\partial}{\partial y} \end{matrix} \right\} \tag{2.15}$$

The transformation requires the determinant of the Jacobian matrix ($[\mathbf{J}]$). Reflex angles in elements should be avoided as the Jacobian matrix could become indeterminate. The transformation is formulated mathemtically as:

$$\iint dxdy = \int_{-1}^{1} \int_{-1}^{1} det|\mathbf{J}| d\xi d\eta \tag{2.16}$$

Applying Legendre quadrature (eq. 2.14) and the jacobian (eq. 2.15) to the integral in eq. 2.12 gives the following numerical element stifness approximation euqation.

$$\sum_{i=1}^{nip} [\mathbf{k_m}] = W_i det|\mathbf{J}|_i ([\mathbf{B}]^T [\mathbf{D}][\mathbf{B}])_i \tag{2.17}$$

2.3.4. Viscoplastic algorithm

The stability of the slope is assesed with a viscoplastic iteration loop that uses a constant stiffness approach. Every iteration represents an elastic analysis with a constant material stiffness [Km]. The excess stress is projected on the stress-strain curve of the material (see figure 2.13). At every integration point, displacement computed with the governing equation (2.13) is converted to strains by multiplying it with the $[\mathbf{B}]$ matrix. Strains are converted to stresses with the elastic constitutive equation $[\boldsymbol{\sigma}] = [\mathbf{D}][\boldsymbol{\varepsilon}]$. Obtained stresses are used to check if yielding occurs. The Von Mises yield criterion is used for this. The yield criterion reads:

$$F_t = \frac{\sigma_q}{\sqrt{3}} - c_f \qquad c_f = \frac{c_u}{SRF^n} \tag{2.18}$$

in which σ_q is the deviatoric stress and c_f is the strength of the soil reduced by the assumed SRF. Values of c_u will be generated with a random field generator (will be discussed in a future section) by taking into account the SHANSEP method described in the previous section 2.2.

In case the value $F_t \geq 0$, the integration point has yielded and (visco)plastic strains need to be computed. In contrast to other plastic algortihms, the viscoplastic allows stresses in the integration point to overshoot the yield criterion temporarily(Smith et al., 2014). The rate of viscoplastic strains is related to the amount by which yield is violated through the following expression:

$$\left(\frac{\partial \varepsilon_{vp}}{\partial t} \right) = F \left(\frac{\partial Q}{\partial \sigma} \right) \tag{2.19}$$

In which Q is the plastic potential function, a mathematical formulation of the relative magnitude (and direction) of plastic strains. This expression assumes a pseudo-viscosity property equal to unity(Smith et al.,
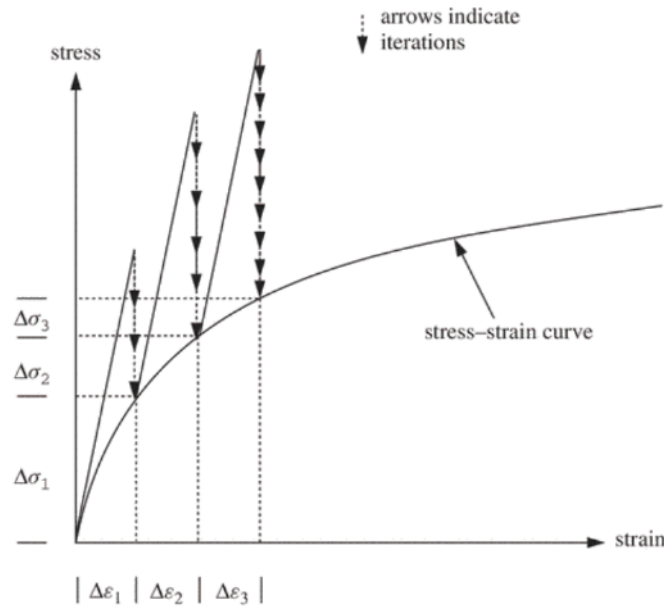
Figure 2.13: Illustration of the calculation of stresses within a viscoplastic algorithm,

2014). The multiplication of the strain rate by the time step gives the viscoplastic strain increment which is accumulated for the next plastic iteration step.

$$\{\delta\varepsilon_{vp}\}^i = \left\{\frac{\partial\varepsilon_{vp}}{\partial t}\right\}^i \Delta t \tag{2.20}$$

and

$$\{\Delta\varepsilon_{vp}\}^i = \{\Delta\varepsilon_{vp}\}^{i-1} + \{\delta\varepsilon_{vp}\}^i \tag{2.21}$$

Δt is the (critical) time step for which unconditional numerical stability is ensured. A formulation derived by Cormeau(1975) is used. According to this formulation, the critical time step is a function of soil properties and depends on the failure criteria used. The critical time step for the Von Mises yield criterion is calculated using the following expression:

$$\Delta t_c = \frac{4(1+v)(1-2v)}{E(1-2v)} \tag{2.22}$$

in which E, v, ϕ are elastic moduli. The soil properties need to be computed at every integration point in case a random field is used and the elastic properties are assumed to be a function of the strength. The combination of soil properties at a specific point which results in the lowest critical time step should be taken in the analysis. Body forces of an element is approximated using the following formulation.

$$\{\mathbf{F_b}\}^i = \{\mathbf{F_b}\}^{i-1} + \sum_{i=1}^{nip} W_i det|\mathbf{J}|[\mathbf{B}]^T[\mathbf{D}]\Delta\boldsymbol{\varepsilon_{vp}} \tag{2.23}$$

The plastic iteration loop is repeated by continuously updating the body forces. The iteration is stopped if the solution converges. The solution converges if the maximum displacement remains within a certain tolerance after redistribution of body forces meaning that the slope did not fail. In case there is no convergence (the maximum displacement in the soil exceeds tolerance), after a specified amount of iterations, it is assumed that the slope fails.

2.3.5. Factor of safety
The factor of safety is computed iteratively by reducing the undrained shear strength (eq.2.18) by some strength reduction factor within the viscoplastic iteration loop. The factor of safety is the lowest possible value for SRF for which the plastic iteration loop does not converge. The bisection iteration scheme with the following equation for the u is used for this purpose.

The initial value of SRF_0 5 plus a random value between 0 and 1. This tested SRF is updated at the end of the viscoplastic iteration loop according to following equation.

$$SRF^n = SRF^{n-1} \pm \frac{\Delta SRF^{n-1}}{2} \qquad (2.24)$$

where n denotes the iteration number. Initially ΔSRF is equal to SRF_0. The exact sign of equation 2.24 depends on the convergence of the plastic iteration loop. If the plastic iteration loop converges, or in other words, if the displacements are elastic, the SRF is increased by half the change in SRF. The iteration is continued until the value of ΔSRF falls below a specified tolerance.

2.4. Random Fields

Soils and their properties are variable over space (and time). This variability is the result of many complex random physical processes during deposition and/or consolidation. Data on soils are collected at discrete points in a geotechnical investigation. The random nature of spatial variability of soil properties adds a layer of difficulty to the estimation of soil property values in between those points. This imposes a big uncertainty on the estimation of slope strength.

The focus of the previous section was to introduce to you the FEM, a method to perform a stability analysis. It was mentioned briefly that, in a finite element analysis (FEA), soil behaviour is characterised by some properties. In this section, we will touch on the theory of random fields, which is used as an extension to the FEM to account for uncertainty of properties created by spatial variability. The use of random fields in combination with the FEM is referred to as the Random Finite Element Method (RFEM).

Random fields are a collection of values for a certain (soil) property. Every value is linked to a certain location (at a specific time). When a FE mesh is considered in which the yield of soil is evaluated at every integration point, a random field could be created for the strength of the soil at every integration point. Possible values for every location are drawn from a distribution obtained from geotechnical data. Such distributions are characterised by a mean value and the standard deviation. Theoretically, there are infinite possible random fields that could be generated from a single (continuous) distribution.

The idea behind RFEM is that by generating a lot of fields, corresponding to the many different forms the unknown strength variation of the soil could take, and evaluating their stability, one can estimate a slope's probability of failure. The following subchapters will explain briefly the assumptions behind random field theory in geotechnical engineering, introduce a method to generate random fields and summarize the steps involved in the generation process.

2.4.1. Variability and Spatial dependency

There are some considerations involved in characterizing spatial variability in geotechnical engineering; variability at a point and spatial dependence.

Suppose that at a specific position (t'), possible property values $X(t')$ have a probability density function $f_{x'}(t)$. Another position ($t*$) would possibly have another distribution $f_{x*}(t)$ of possible values. In other words, variability at a point refers to the evolution of pdf's with position. In practice, it is quite difficult to estimate the evolution of pdf's beyond a simple trend in mean or variance.(Fenton and Griffiths, 2008)

Consider again two positions separated by distance $\tau = t' - t*$. Presumably, the two random values will exhibit some dependence on each other. It is expected that the two random values to be quite similar when τ is small and probably very dissimilar when τ is large. Thus, random values generally have some sort of dependence that often decreases with separation distance (and time). The interdependence can be characterized by a joint bivariate distribution $f_{x',x*}(t)$ which specifies the probability that $X(t')$ and $X(t*)$ hold at the same time. If we would generalize this idea to all points in a field (f.e. FEM mesh), the complete probabilistic description would be a high dimensional pdf. Such a pdf is difficult to use as it would be impossible to estimate all of its parameters.(Fenton and Griffiths, 2008) In order to simplify the difficulties of both considerations, a number of assumptions are made.

1. Gaussian Process: The joint pdf is a multivariate normally distributed random process. Such a process is referred to as a Gaussian process. The great advantage is that the complete distribution can be characterized by the mean vector and covariance matrix(Fenton and Griffiths, 2008). This assumption is in line with the central limit theorem. which states that the probability distribution of the sum of M independent, identically distributed random variables tend to Gaussian as M increases. In our case the distributions are not identical. However, the principle also holds if the fractional contribution of any
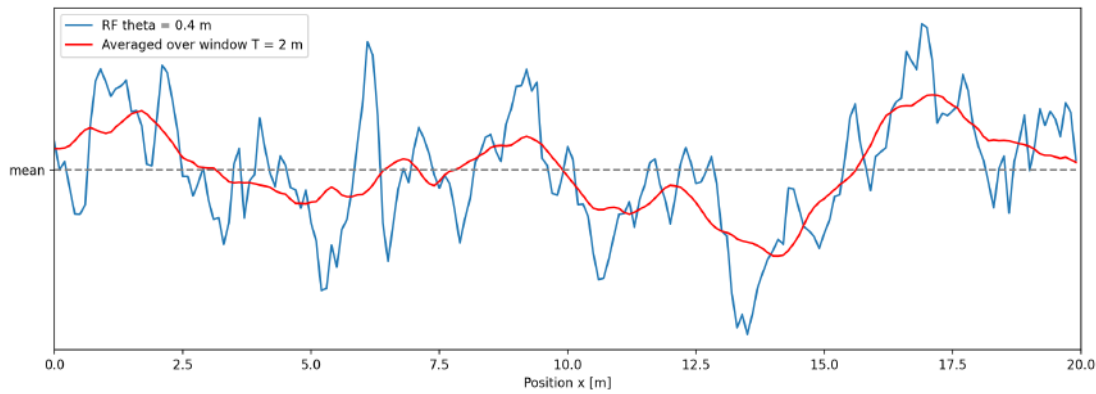
Figure 2.14: The effect of local averaging on a random field. Averaging act as a low pass filter. Local effects are dampened decreasing the variance of the field while the mean is preserved.

one of the random variables to the total variance vanishes when M tends to infinity(Vanmarcke, 2010). In other words, the sum of distributions tend to gaussian if there are no outliers in variance.

2. Stationarity, statistical homogeneity: The joint pdf is independent of spatial position, it only depends on the separation between points. This assumption implies that the mean and covariance (and higher moments) are constant over space(Fenton and Griffiths, 2008).

3. Isotropy: The joint pdf is invariant under rotation. The correlation between points depends only on the distance, not on their orientation relative to one another(Fenton and Griffiths, 2008).

2.4.2. Local averaging

Whenever an engineering property is quantified, the value of a local average is taken. For example, the measured cone resistance in a CPT is the average resistance exerted by a small volume of soil particles around the cone tip, and similarly, the measured shear strength of a soil in a triaxial test, is the average shear strength over the soil sample's volume. If it was possible to evaluate the shear strength at microscopic level, let's say particle level, the measured shear resistance of particle contacts would be different in the sense that it is expected that the variance of measured values would be very large. Measured values of engineering properties depend on the scale it is evaluated. This phenomenon can be illustrated by the application of the moving average function on a random field.

$$X_t(t) = \frac{1}{T} \int_{t-T/2}^{t+T/2} X(\xi) d\xi \tag{2.25}$$

In which $X_T(t)$ is the local average of $X(t)$ over a window of width T centered at t. The effect of this function is illustrated in figure 2.14. The line in blue is a random field with zero mean, standard deviation σ, correlation length μ. The line in red represents the same random field averaged over a moving window T using equation 2.25. By comparing the two plots we can come to the conclusion that local averaging decreases the standard deviation and acts as a low pass filter, in the sense that it dampens the effect of high frequency content in the random field. This is achieved while preserving the mean (Fenton and Griffiths, 2008). Likewise, averaging a soil property over a certain volume acts as a low pass filter in which the high frequency effects (small scale effects) are dampened and the variance of observable values is reduced. The reduction in variance is quantified by the variance reduction function $\gamma(T)$:

$$\gamma(T) = \frac{1}{T^2} \int_0^T \int_0^T \rho(t_1 - t_2) dt_1 dt_2 = \frac{2}{T} \int_0^T \left(1 - \frac{\tau}{t}\right) \rho(\tau) d\tau \tag{2.26}$$

in which γ is the reduction factor for an averaging window (T).

2.4.3. Correlation function and Covariance matrix

The covariance quantifies the magnitude of interdepence between points. Another more objective quantification of interdepence is correlation, the degree of linear interdepence between points. Let us again assume
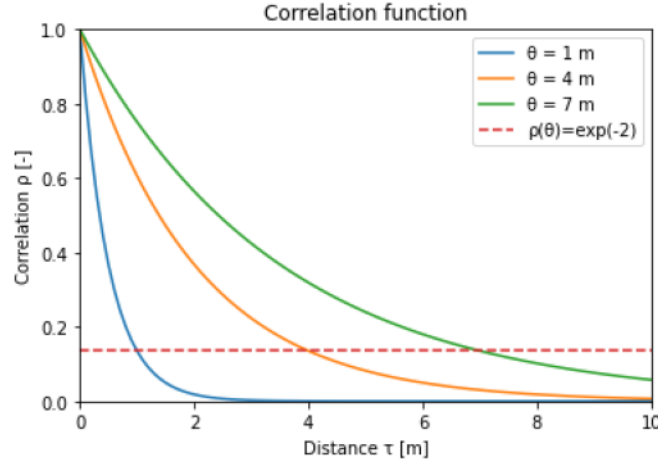
Figure 2.15: The correlation function plotted against distance for correlation lengths one, four and 7 meter for comparison. Note that, in case theMarkov correlation function is used, the correlation length corresponds to a correlation of e^-2.

two points in the subsurface with random values $X(t')$ and $X(t*)$. The relationship between their covariance C and correlation ρ would be (Fenton and Griffiths, 2008):

$$\rho(\tau) = \frac{C(t', t*)}{\sigma_x(t')\sigma(t*)} \tag{2.27}$$

where $\sigma_x(t')$ and $\sigma_x(t*)$ are the standard deviations of points t' and $t*$, respectively. Correlation can take values between -1 and 1, where -1 and 1 indicate perfect (inverse) linear dependence and 0 indicates a lack of correlation. For stationary fields, the mean and covariance are independent of (spatial) position. This assumption allows equation 2.27 to be written as a function of distance $\tau = t' - t*$.(Fenton and Griffiths, 2008)

$$\rho(\tau) = \frac{C(\tau)}{\sigma_x^2} \tag{2.28}$$

Because $C(t', t*) = C(t*, t')$ and the field is stationary, we must have $C(\tau) = C(-\tau)$ and $\rho(\tau) = \rho(-\tau)$.

There are multiple correlation functions defined in literature. However, the Markov correlation function is commonly used in engineering practices because of its simplicity. Aside from being a relatively simple exponential function to calculate with, it has an inherent simplifying assumption that the process is Markovian. The Markov property states that the conditional probability of the future state depends only on the most recently known state. This assumption is generally valid for engineering models, as they rarely depend on the entire past history (exceptions are creep models)(Fenton and Griffiths, 2008). The 1-D Markov correlation function reads:

$$\rho(\tau) = \exp\frac{-2|\tau|}{\theta} \tag{2.29}$$

in which θ is the correlation length, also known as scale of fluctuation. Physically is it a measure of distance within which points are significantly correlated ($\geq e^{-2} \approx 0.135$) (Fenton and Griffiths, 2008). Mathematically, θ is the area under the correlation function (Vanmarcke, 2010).

$$\theta = \int_{-\infty}^{\infty} \rho(\tau)d\tau = 2\int_0^{\infty} \rho(\tau)d\tau \tag{2.30}$$

Figure 2.15 illustrates the development of Markov correlation with distance for several values of θ. The Markov correlation function satisfies the requirements that were stressed throughout this subchapter; the correlation decays (exponentially) with increasing distance, has a value between 0 and 1(which is a subset of -1 and 1), there is full linear dependence for $\tau = 0$ and $\rho(\tau) = \rho(-\tau)$ (follows from the absolute sign in the function). Geotechnical problems are rarely evaluated in one dimension. The correlation function needs to be extended for higher dimensions. Furthermore, due to depositional effects a higher correlation of soil
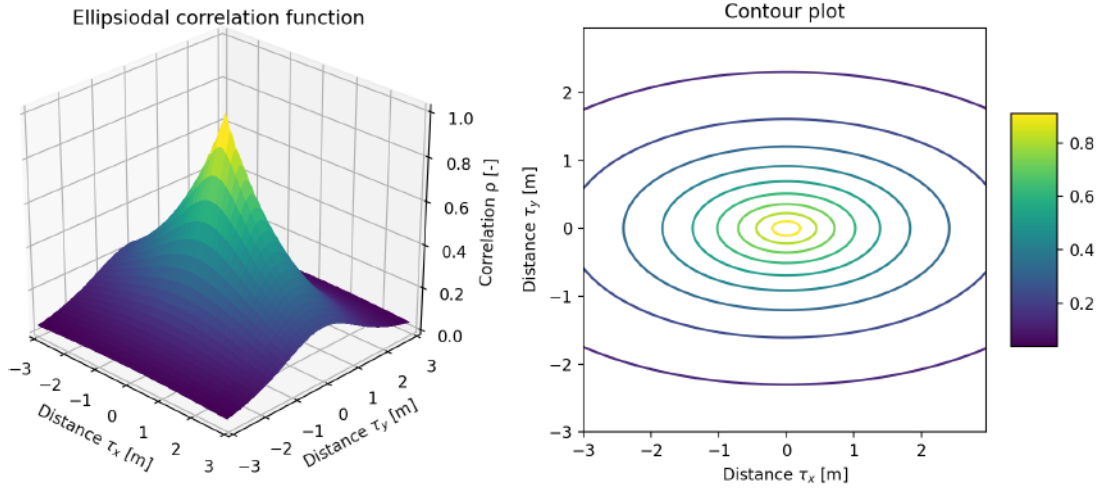
Figure 2.16: A plot and contour plot of a ellipsoidal (2-D) Markov correlation function with $\theta_x = 4m$ and $\theta_y = 2m$. As expected, the contour lines form an ellipse stretched in the horizontal direction with an aspect ratio of 2.

properties is expected in horizontal direction with respect to the vertical direction. The following multidimensional (ellipsoidal) correlation function with variable correlation length is formulated.

$$\rho(\tau) = \exp -|\tau| \quad |\tau| = \sqrt{\left(\frac{2\tau_1}{\theta_1}\right)^2 + ... + \left(\frac{2\tau_n}{\theta_n}\right)^2} \tag{2.31}$$

in which index n represents the dimension number.

2.4.4. Random field generation

A correlated random field can be viewed as the moving average of an ideal white noise, an uncorrelated random field with infinite variance (Vanmarcke, 2010). The application of equation 2.14 on an ideal white noise is mimicked in the Covariance Matrix Decomposition method (CMD) by using the "square root" of the covariance matrix as a transformation function of a set of random variables drawn from a standard normal distribution. The transformation results in a random field of correlated random vales with mean $\mu = 0.0$ and standard deviation $\sigma = 1.0$. The method works as follows.

Given that Z is a random field, the autocovariance matrix C, is defined as the expected covariance between any two points of Z.

$$\mathbf{C} = E[\mathbf{Z}\mathbf{Z}^{\mathbf{T}}] \tag{2.32}$$

Suppose the random field is characterized as a set of orthogonal vectors and a set of uncorrelated numbers. With L being the set of vectors and U being the set of random numbers sampled from a standard normal distribution, the random field is defined as:

$$\mathbf{Z} = \mathbf{L}\mathbf{U} \tag{2.33}$$

Combining equations 2.32 and 2.33 yields:

$$E[\mathbf{Z}\mathbf{Z}^{\mathbf{T}}] = E[\mathbf{L}\mathbf{U}(\mathbf{L}\mathbf{U})^{\mathbf{T}}] = E[\mathbf{L}\mathbf{U}\mathbf{U}^{\mathbf{T}}\mathbf{L}^{\mathbf{T}}] = \mathbf{L}\mathbf{I}\mathbf{L}^{\mathbf{T}} = \mathbf{L}\mathbf{L}^{\mathbf{T}} = \mathbf{C} \tag{2.34}$$

From this relation, it follows that L is a decomposition of the covariance matrix(van den Eijnden and Hicks, 2017).

The decomposition is achieved using Cholesky decomposition, provided that the covariance matrix is positive definite (Fenton and Griffiths, 2008; Green et al., 2015). The covariance matrix could lose its positive definiteness in case non-diagonal values become to 1.0. This could happen when the distance between points is very small with respect to the correlation length and at rounding of the value becomes 1.0. The standard normal values computed with 2.33 need to be transformed to a distribution fitting the data of the geotechnical

property. The Dutch guidelines recommend the use of lognormal distributions for all parameters of SHANSEP (Ministerie van Infrastructuur en Waterstaat, 2017).The transformation function (Z_{ln}) reads:

$$Z_{ln} = \exp\left\{\sigma_{ln}Z + \mu_{ln}\right\} \tag{2.35}$$

in which μ_{ln} and σ_{ln} are mean and standard deviation of logarithm, respectively. Those statistical parameters are computed using the following equations:

$$\sigma_{ln} = \sqrt{\log\left(1 + \frac{\sigma^2}{\mu^2}\right)} \quad \mu_{ln} = \log(\mu) - 0.5\sigma_{ln}^2 \tag{2.36}$$

where μ and σ are the mean and standard deviation of the geotechnical property.

Vanmarcke(2010) warns that the transformation to a lognormally distributed set of random values could change the correlation structure of the random field. The possible change in correlation structure will be investigated and verified. In case a correction is required, the following equation is formulated as an correction, which is the inverse of the equation by Vanmarcke(2010). .

$$\rho_y(\tau) = \frac{\exp(\sigma^2\rho(\tau)) - 1}{\exp(\sigma^2) - 1} \tag{2.37}$$

2.5. Spatial variability

Additional to statistical variables mean and standard deviation, a random field requires a measure of the spatial variability expressed as the correlation length. The literature has been consulted to look for specific requirements regarding the spatial variability of SHANSEP paramters.

2.5.1. Spatial variability of properties S and m

A paper by Koning et al.(2019) on the variability of SHANSEP parameters for probabilistic analyses of macro-instability suggests that a geotechnical survey consisting of CPTs and laboratory tests performed for the dike strengthening project KIJK, showed that there were no particular differences in S and m values under a dike and at the foundation layer away from the dike. This indicates that there is no trend in horizontal variation.

Data from the same study also suggest that there seems to be a relationship between the wet volumetric weight and m (figure 2.17). It is interesting to see that the same trend in mean is observed for various geomaterials (clay, peat and). One could argue that this data could indicate a potential depth-dependency of m as deeper soils are usually more dense due to consolidation under higher stresses. The effect of the volumetric weight as a stochastic parameters will not be taken into account. These findings that apply to both parameters are observed for values obtained at large strain. Their applicability to peak strength values is unknown.

No other reports of trends in the variability of both parameters are encountered in literature. This is to be expected as SHANSEP is based on a objective representation of soil behaviour through parameters for which any stress effects are canceled.

2.5.2. Spatial variability of pre-overburden pressure

The pre-overburden pressure is defined as the difference between the pre-consolidation pressure and the actual pressure acting on the soil. The majority of this extra pressure can be dedicated to the consolidation of the soil at higher loads in the past. This is referred to as mechanical overconsolidation. The primary source is a constant geological load applied vertically which is (partially) removed at a later stage. An example is the erosion of a geological layer. These type of loads affect the whole layer equally.

Secondary effects of chemical and biological origin are described in a previous section and have smaller impact on the total pre-consolidation. In addition to this, some other smaller mechanical effects like ageing and repeated rapid loading (due to fluctuations in phreatic levels affecting the pore pore pressures and effective stresses in the short term) could be considered as secondary as their contribution to the total POP is relatively small.

The literature does give us some insight on the vertical variability of POP. Let us consider vertical profiles of the pre-consolidation pressures (figure 2.18). This data suggests that there seems to be vertical variation around a constant mean value. It is thought that the constant mean value can be attributed to the primary source of overconsolidation, the natural deposition and erosion of soil layers. The variation is thought to be the result of the smaller effects of secondary origin.

(a) S against vertical consolidation stress   (b) m against volumetric weight
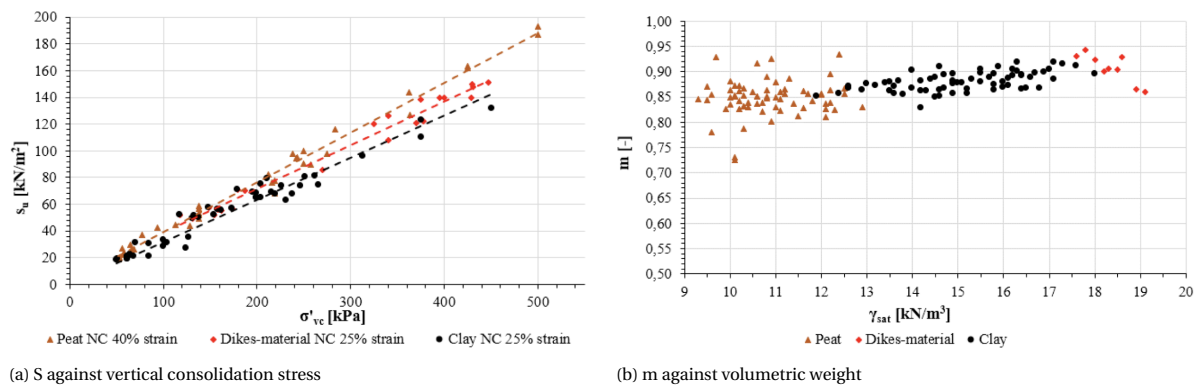
Figure 2.17: Parameters S (a) and m (b) plotted against vertical consolidation pressure and wet volumetric weight, respectively from geotechnical data of dike strengthening project KIJK. (a) shows the relationship between the undrained shear strenghts at large strain of normally consolidated samples and their vertical consolidation pressure. The linear lines indicate a constant mean of S value independent of the consolidation stress for any material. (b) shows the relationship between the strength increase exponent and wet volumetric weight. There seems to be a linear (slightly) increasing relationship independent of the material. After Koning et al.(2019)

The horizontal variability of primary source of POP strongly depends on the geometry and location of historical loads. Natural loads (e.g. erosion of a horizontal soil layer) generally tend to result in small to none horizontal variability. Artificial loads (like human made roads) generally results in regional loads. Therefore it is better to induce the effect of artificial loads manually to specific regions in the dike.

The suggested method of creating random fields for the POP is to draw values from log normal distribution with a mean value which represent primary effects and a standard deviation based on secondary effects. The vertical scale of fluctuation can be estimated from CPT data.

2.6. Conclusion

Macro-stability refers to the failure of a dike through the massive displacement of the soil body (generally) initiated by its self weight and resisted by the soil's shear resistance. The Dutch guidelines propose the use of the SHANSEP method to calculate the shear strength of impermeable (cohesive) soils. This method approximates the strength with three parameters S, m and POP which are the normalised shear strength ratio at normal consolidation, strength increase exponent and the pre-overburden pressure, respectively, in combination with stresses acting at a point.

The FEM programs start with the assembly of an elastic stiffness matrix and the computation of the stresses acting at a point based on gravitational stresses. The critical time step is computed and an algorithm is started to compute the strengths and displacements of elements using the Mohr-Coulomb constitutive model. Failure of the whole system of elements is checked. The stability of a single evaluation is checked multiple times to iteratively find a factor of safety by applying a strength reduction factor to the strength.

The Covariance Decomposition Method is a way to generate standard normal random fields. A vector of uncorrelated standard normal random values are correlated by the matrix multiplying it with the Cholesky decomposition of the covariance matrix. The covariance matrix is assembled using Markov correlation and distance matrices. The standard normal values are transformed to lognormal values. There are no trends found in the spatial variability of SHANSEP parameters. There is cross correlation observed between parameter m and the volumetric weight of the soil.

(a) Burswood Clay/CRS-test   (b) Ballina Clay/CRS-test   (c) Bothkennar Clay/CPT
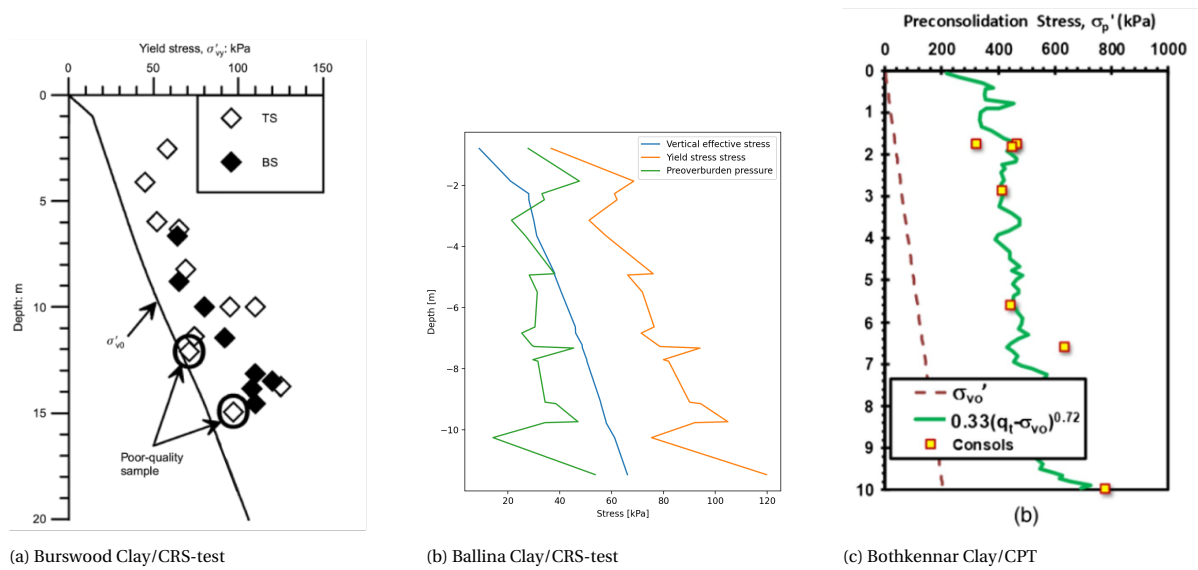
Figure 2.18: Vertical profiles of pre-consolidation pressure drawn with CRS tests(A & B) and CPT (C) of Burswood clay (Low et al., 2011), Ballina clay(Pineda et al., 2016) and Bothkennar clay(Agaiby and Mayne, 2019), respectively. The pre-consolidation pressure in all three test show some variation from a depth dependent mean. The POP, the difference between pre-consolidation pressure and vertical effective stress, is calculated for Ballina clay (C) and seems to vary around a constant mean. There was no access to the rough data of the other two clays, but from visual comparison, they are expected to comply to the reasoning of a variation around a constant mean.

3

Conceptual and numerical development

This chapter focuses on the development of geotechnical concepts and its numerical implementation. The geotechnical considerations will be founded on the findings of the literature review. The numerical implementation will consist of two stages. Firstly, a random field generator will be coded to generate random fields which will interact with a simple version of the in-house FEM program. Secondly, an overview of the interaction between the random field generator and FEM code will be presented. This is followed by the modifications made to the FEM code. Finally, some results will be presented to back up some assumptions.

3.1. Geotechnical Considerations

Two versions of the SHANSEP formulation are presented in chapter 2, the only difference being the use of the major principal stress in the Plaxis version instead of the vertical effective stress in the original function.

The relationship in the original SHANSEP formulation was discovered by the evalutaion of k0 consolidated undrained triaxial compression test results. In a perfect k0 triaxial compession setup, the major principal effective stress is equal to the vertical effective stress. The question could arise what would happen if the soil specimens where consolidated under a rotated stress field, rather than a k0 field, for which the two stresses are not equal. The Dutch guidelines refer to this as preshearing. This type of stress field rotation is common in the proximity of the slopes and the foundation layer of a dike (figure 3.2).

The effect of preshearing is compared to a conventional k0 consolidated triaxial and DSS tests for Calais clay in figure 3.1. It is observed that the undrained shear strength with respect to the vertical effective stress has increased both in triaxial compression and DSS in case pre-shearing is applied. This would indicate that most likely the undrained shear strength is related to the major principal stress and that a normalisation with respect to this most compressive stress is more objective provided that the soil is not subjected to perfect triaxial compression. Therefore the major principal stress convention will be used in our implementation.

3.1.1. Stress anisotropy and mobilised strength

Both in-house finite elements programs that are used will make use of the linear-elastic perfectly plastic Tresca yield criterion for which the friction angle is assumed to be 0 and the cohesion is equal to the undrained shear strength calculated with the SHANSEP formulation. In terms of plasticity, this yield criterion allows to only evaluate if yield (in this case failure) occurs at a certain integration point. Other (anisotropy) effects like strain hardening/softening or rotational hardening are disregarded.

This approach only allows to model the full stress-strain behaviour as a single value of strength, it lacks the directional dependency of strength. Schematisation 2.8 showed that the the full stress-strain behaviour strongly depends on the direction of the stress field.

A way to deal with these (anisotropic) effects is to take SHANSEP parameter values at large strain, which is suggested by WBI2017 and explained in a previous section. However, it is observed in our simulations that this approach leads to shallow slip surfaces. Although these types of failure definitely require the repair of a dike, it is questionable if their occurrence would lead to complete failure, the impairment of water retaining capabilities of a dike. The findings will be demonstrated in the next chapter.
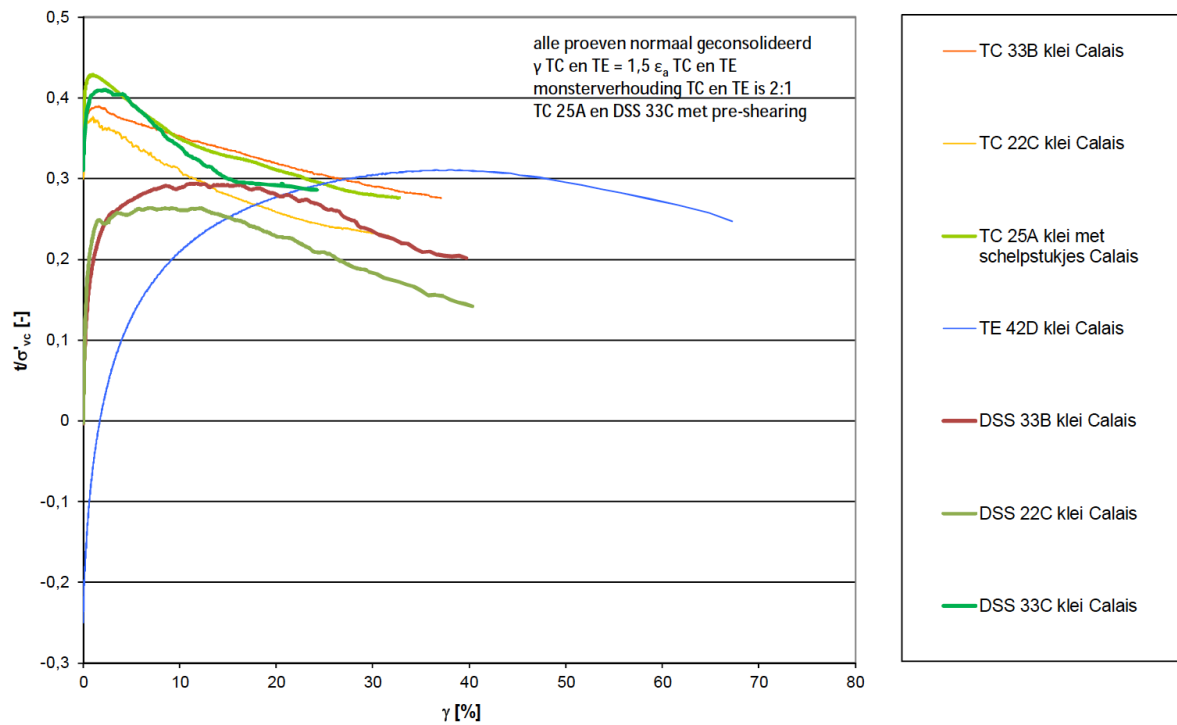
Figure 3.1: Normalised behaviour of Calais clay in triaxial compression, triaxial extension and DSS tests with and without preshearing. Pre-shearing is defined as a consolidation under a rotated major principle stress.It is observed that the normalised peak strength is higher when pre-shearing is applied (light and dark green) compared to conventional k_0 consolidation (orange, yellow, brown and green). The normalised strength becomes similar for DSS and TXC in case pre-shearing is applied.(Ministerie van Infrastructuur en Waterstaat, 2017)
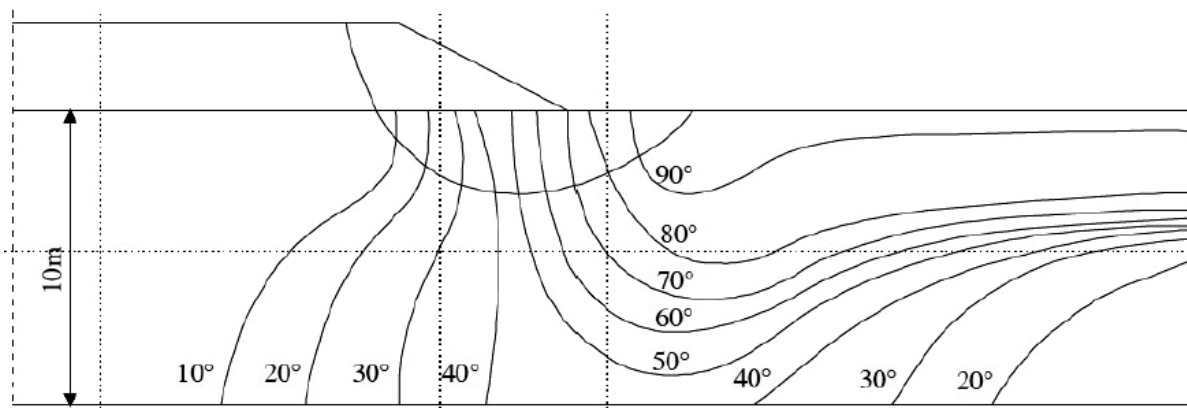
Figure 3.2: Schematisation of the expected orientation of the major principal stress with respect to the horizontal after construction of an embankment. The orientation is, from left to right, mostly vertical before the slope begins,the orientation starts increases in the slope and reaches a peak a little away from the the dike's foot. The orientations and locations are in line with the ADP approach as the orientation is 0 in triaxial compression, around 30 degrees in DSS depending on the friction angle and 90 degrees in a triaxial extension. After Jardine and Menkiti(1999)
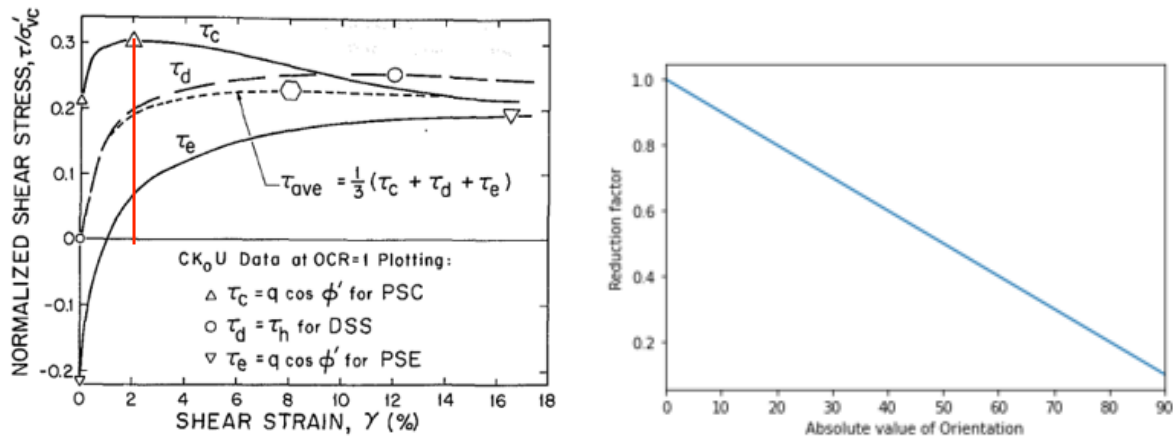
(a) Laboratory test results

(b) The relationship between reduction factor and orientation σ_1

Figure 3.3: In the first illustration is an adaptation from figure 2.8 in which a vertical line is drawn through the desired shear strain. the second illustrates a linear trend line with $s_u^{TXE}/s_u^{TXC} = 0.1$

Another approach in the light of the strain compatibility assumption is to take the mobilised shear strengths at a certain shear strain in all three laboratory tests and to formulate a strength reduction factor as a ratio with respect to the highest mobilised shear strength (usually peak strength in triaxial compression). The three ratios are plotted against the orientation of the major principal stress and are interpolated in between. This reduction factor is applied to the SHANSEP shear strength calculated in FEM with parameters values obtained from the highest mobilised shear strength. An example step by step procedure is:

1. The shear stress-shear strain curve of k0 consolidated laboratory test results of the clay in question is normalised by the major principal stress applied at consolidation and plotted together (similar to figure 2.8).

2. A vertical line through the peak triaxial compression strength (or any other desired shear strain) is drawn. The intersections of this vertical line and the stress-strain behaviour line is the mobilised shear strength for the other two tests.

3. The ratio between the mobilised shear strengths with respect to the peak strength in triaxial compression are taken and plotted against the corresponding orientation of the major principal in the test. The orientation is 0 in triaxial compression, around 30 degrees in direct simple shear and 90 degrees in triaxial extension.

4. A trend line is drawn through the points and used as a reduction factor. This relationship is either linear or quadratic. The reduction factor is applied to the calculated SHANSEP shear strength with the triaxial compression strength parameters based on the orientation of the major principal stress of the integration point.

This process is illustrated in figure 3.3. Note that the shear stress is normalised by the vertical effective stress at the end of consolidation. However, as the major principal stress is equal to the vertical effective stress in a triaxial setup, the graph also implies a normalisation with respect to the major principal stress at the end of consolidation for τ_c and τ_e.

In the simplest case, the points of the TXC, DSS and TXE in the reduction factor graph line up to give a linear trend line. The line can now be expressed mathematically with just one input value being the ratio between the the undrained shear strength at trixial compression and extension at a certain shear strain (s_u^{TXE}/s_u^{TXC}). The formulation reads:

$$RF = 1 - \left(\frac{1 - s_u^{TXE}/s_u^{TXC}}{90} \right) \alpha \tag{3.1}$$

The value of shear strain (vertical line) is soil specific and requires an engineer's judgement. An upper bound could be the minimum slip required for failure divided by an estimated length of slip surface. A lower

bound could be the shear strain at peak triaxial compression strength.

In addition to these approaches it was investigated if the implementation of the SHANSEP/NGI-ADP constitutive model in PLAXIS would be possible to use. However, also this constitutive model like any other advanced model only works in an elasto-plastic iteration scheme. The single time step viscoplastic iteration scheme does not allow a multi step integration to accurately model the full stress-strain behaviour.

3.2. Random field generator

The random field generator will be written in Python. The reason is that small adjustment are easily made and tested (plots are generated easily) in Python compared to FORTRAN, which will be beneficial during the development phase. After it is decided on a final version, the python script will be translated to FORTRAN and implemented to the advanced in-house FEM code.

The correlation between points is a function of their distance in space. This requires the random field generator to access to geometric information on the mesh in the FEM program. Due to the simple geometry of the problem that is used in the analysis, the mesh is generated with a handful of parameters in the FEM program with no external sources. The mesh generator of the FEM code is translated to python. The geometry parameters are defined in python and transferred in a separate text file. The mesh is regenerated in FORTRAN.

Algorithm 1 Random field generator

Class with geometry parameters (geom)
Class with soil parameters (SP)

Function (emb2Dgeom) to determine coordinates of element's nodes from element number.
Function (ShapeFun) to calculate coordinates of integration points from nodal coordinates.

for 1,2,...,$nels$ **do**
    Compute global coordinates of nodes. (emb2Dbody)
    for 1,2,...,nip **do**
        Compute coordinates of integration points. (ShapeFun)
        save coordinates
    end for
end for

Assemble distance matrices, one for every direction. (Spatial package)
Calculate covariance (matrix) Eq. 2.31 & 2.28
Decompose covariance matrix using Cholesky decomposition. (Numpy package)

for every SHANSEP parameter **do**
    Create matrix of standard normal values(Python function) and matrix multiply it to the covariance matrix (Eq. 2.33).
    Transform standard normal values to lognormal values using Eq. 2.35 & 2.36.
end for

Save random fields and geometry parameters (geom) in individual text files (Numpy package).
Run FEM program (os package).

The mesh generator starts with the computation of integration points' coordinates. This is followed by the assembly of distance matrices for every dimension. After this, the correlation matrix is computed using equation 2.31. The correlation matrix equals the covariance matrix for a standard normal random field according to equation 2.28. The correlation matrix is decomposed using Cholesky decomposition. It was pointed out in(Vanmarcke, 2010) that transforming standard normal values to lognormal values would alter the correlation structure of the field. It is verified (figure 3.4) that a correction is not necessary.

Correlated random fields with standard normal values are generated using the 'square root' of the covari-

ance matrix following equation 2.33. The values of those random fields are transformed to lognormal values of desired mean and standard deviation using equations 2.35 and 2.36.

Finally, the random fields and the geometry variables are saved into text files and the FEM program is launched automatically.

3.2.1. Verification of random field generator
The random field generator needs to be checked on the correctness of its implementation. As the generation process of random fields for every parameter (without modifications) is identical and only differs in values of generated standard normal values, the verification for one parameter would mean the verification for all parameters.

The verification is performed in two ways; a visual inspection of values and a check of covariances. The first inspection is a simple 1-D plot of parameter values along a straight line of integration points within a single random field.The same plot will include the arithmetic mean of 10000 random fields. It is expected that the mean over such a large amount of random fields equals the input value and it should be very unlikely to encounter values at a distance 3 times the standard deviation from the mean. The visual inspection can be found in figure 3.4.

Indeed in both 1D plots, taking the arithmetic mean of every point from 10000 random fields gives back the mean input value of 0.2. Furthermore, there are no values out of the 0.14-0.26 range.

In the second verification, the mean correlation between every point will be back calculated on a straight line of integration points for 10000 random fields. This correlation should equal the theoretical 1-D Markov covariance. The results of this verification show that indeed the covariance structure follow the theoretical 1D Markov correlation in both dimensions. There are some deviations observed at the tails. Those small deviations decrease with the amount of random fields generated. As the evaluation of every extra random field increases the computational time, a sweet spot needs to be found between the number of random fields generated and the accuracy of the correlation structure's tail.

3.3. Interaction with FEM code
The interaction between the random field generator and the FEM code is schematised in figure 3.5. The output of the random field generator is saved in text files. The mesh is regenerated in the FEM code from parameter values defined in one of the text files. The FEM follows the same steps of calculating the global stiffnes matrix and the critical time step is calculated as discussed in the previous chapter. Just before the start of the viscoplastic algorithm, there is an extra step added in which undrained shear strength is calculated. the calculation starts with the computation of gravitational stresses. The gravitational stresses are in Cartesian axes. In case the original SHANSEP formulation (eq. 2.1) is used (for the verification of the FEM code), the vertical effective stress value of the gravitational stresses can be extracted and together with the random fields of parameters S & m and the pre-overburden pressure (POP), the undrained shear strength is calculated.

$$s_u = max(S\sigma_{v0}OCR^m, 5kPa) \tag{3.2}$$

In all other cases, the Cartesian stresses need to be transformed to principal stresses. In order to achieve this, a subroutine is added that computes the eigenvalues of a 3D stress tensor with plane strain assumptions applied. The equations that follow from this approach are (note that the subscripts do not indicate an order in magnitude):

$$\sigma_1 = \sigma_z \tag{3.3}$$

$$\sigma_2 = \frac{\sigma_x + \sigma_y + \sqrt{(\sigma_x + \sigma_y)^2 - 4(\sigma_x + \sigma_y - \tau_{xy}^2)}}{2} \tag{3.4}$$

$$\sigma_3 = \frac{\sigma_x + \sigma_y - \sqrt{(\sigma_x + \sigma_y)^2 - 4(\sigma_x + \sigma_y - \tau_{xy}^2)}}{2} \tag{3.5}$$

in which subscripts x,y and z indicate the horizontal, vertical and the 3rd dimension, respectively. In plane strain, the stress in the third dimension is always equal to the intermediate stress. The major principal stress is either the second or third equation depending on the sign convention used for compression and extension. The convention used by the FEM code is the mechanical convention in which extension is positive. A square
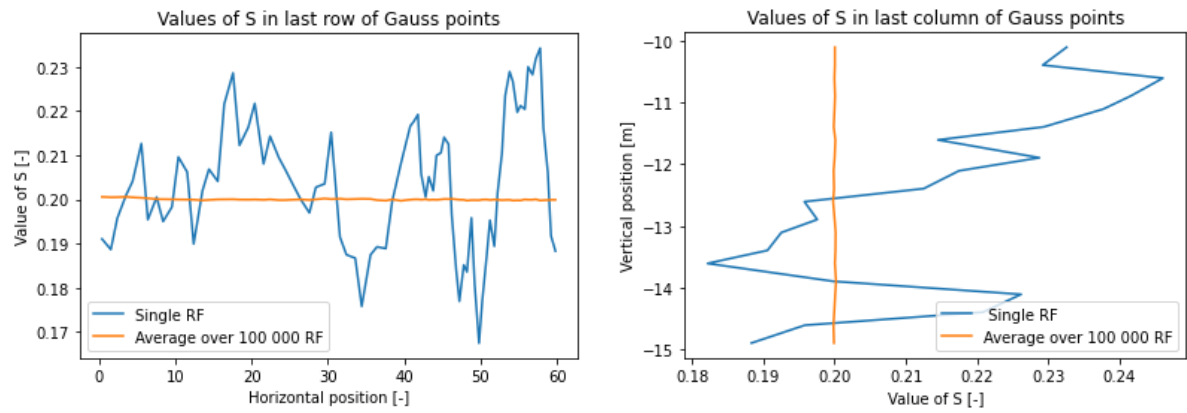
(a) Horizontal direction, $\theta_x = 10m$

(b) Vertical direction, $\theta_y = 2m$
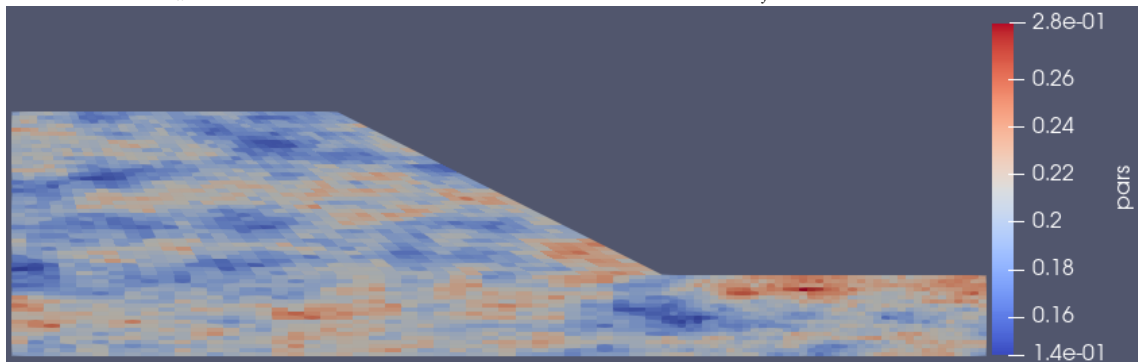
(c) The whole random field for a arbitrary dike geometry with a 1:2 slope
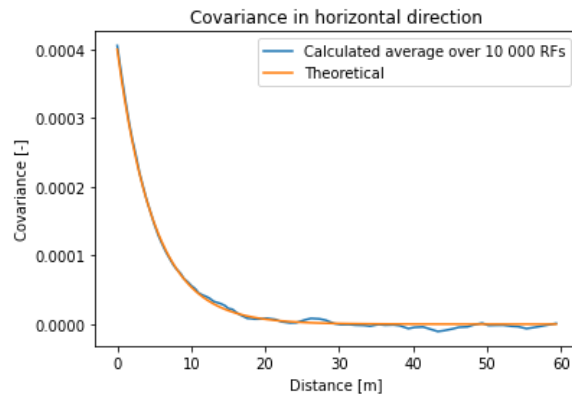
(d) Horizontal direction, $\theta_x = 10m$
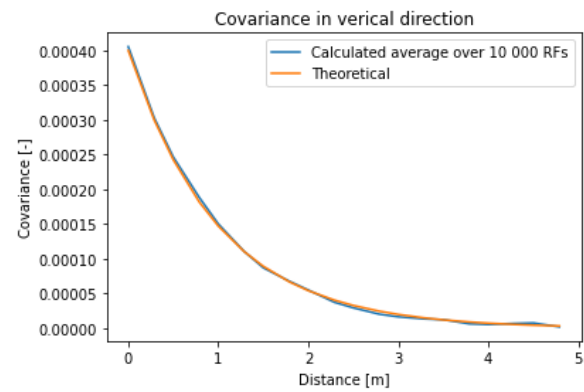
(e) Vertical direction, $\theta_y = 2m$

Figure 3.4: Verification 1; A random field generated for a soil geometry (c) and two linear sections in horizontal (a) and vertical (b) directions. Standard normal values are transformed to follow a lognormal distribution with $\mu = 0.2$ and $\sigma = 0.2$. Verification 2; The comparison of the mean covariance of 10000 fields between points along a linear horizontal (d) and vertical (e) line through the last (botton right corner) integration point in the mesh. There are some acceptable slight oscillations around the theoretical covariance structure. The correction was not applied. A change in the correlation structure proposed by Vanmarcke(2010) has not been observed.
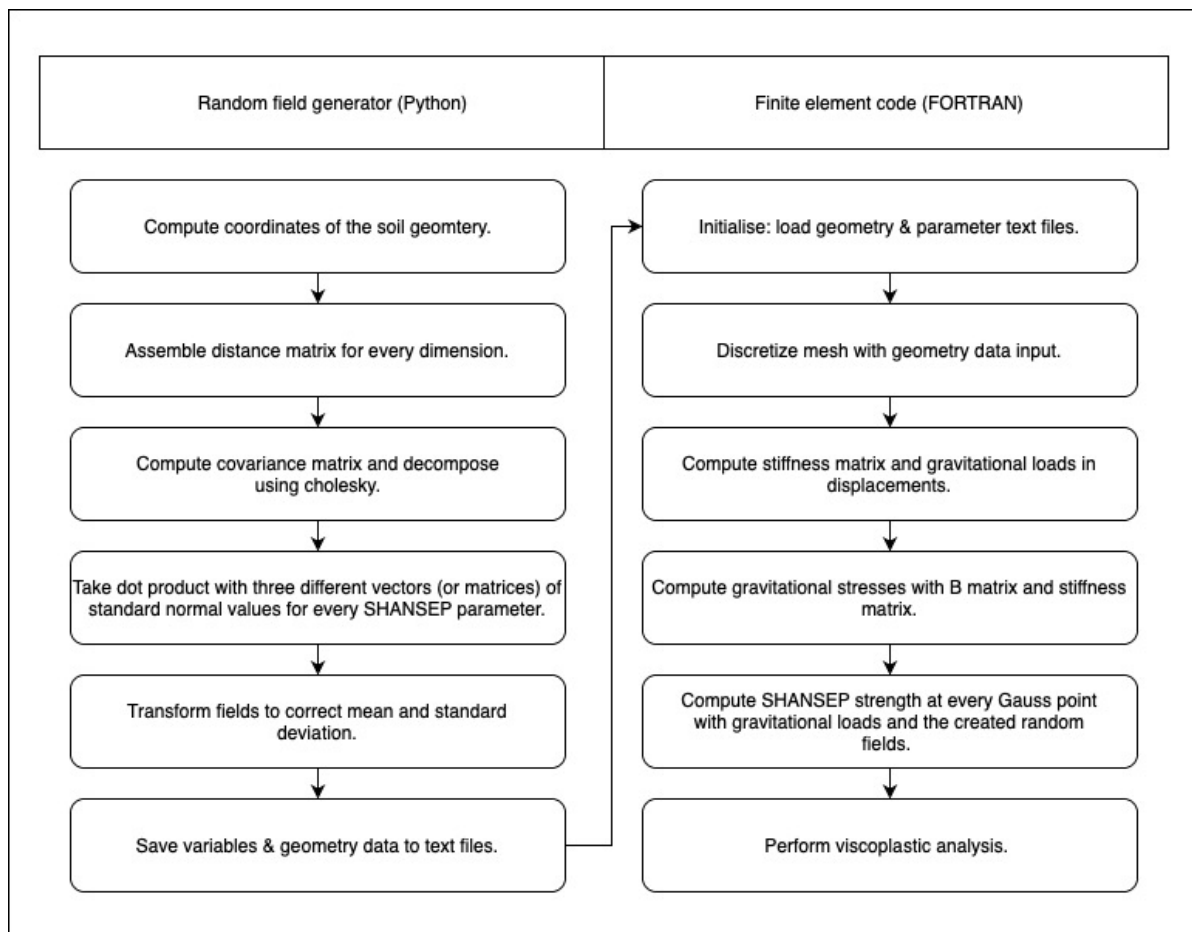
Figure 3.5: Schematisation of the interaction between the python and FEM codes.
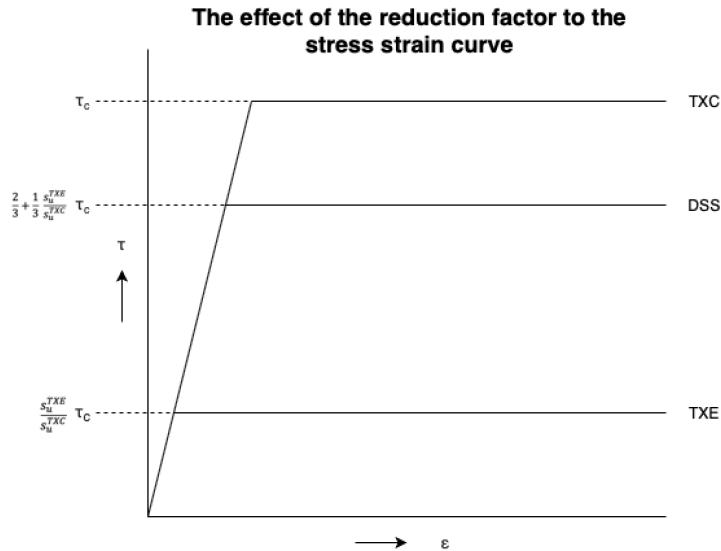
Figure 3.6: The effect of the reduction factor on the resulting stress strain curve of the constitutive model. The flat plastic part of the curve intersects with the elastic part at a different shear stress.

root can never give a negative value. Therefore we can conclude that if the major principal stress is defined as the most compressive stress, the third equation will always give the highest negative value and is the equation of the major principal stress.

The orientation of the major principal stress with respect to the horizontal is obtained by using the formulation for plane stress conditions. Although the plane stress and plain strain assumptions are different, because the shear stresses with respect to the third dimension are canceled, there is only one rotation direction possible, which is in the xy-plane. As the third dimension is perpendicular to this plane, its magnitude does not affect the rotation in this plane. As only shear stresses and normal stresses in the xy-plane matter, this is a semi-plane stress condition. The formulation reads:

$$\tan(2\alpha) = \frac{2\tau_{xy}}{\sigma_x - \sigma_y} \tag{3.6}$$

The derivation of the equation and the required correction are explained in the appendix. The orientation is used in order to calculate the reduction factor in equation 3.1.

The SHANSEP strength can now be calculated using the random fields and the major principal stress. The reduction factor is calculated with the orientation and multiplied by the SHANSEP strength. Due to to the cohesive nature of clays a lower bound is applied for the strength. The strength of the integration is calculated by:

$$s_u = max\left(RF\sigma_1 S\left(\frac{\sigma_1 + POP}{\sigma_1}\right)^m, s_{u,min}\right) \tag{3.7}$$

Figure 3.6 shows the effect of using the reduction factor on the stress-strain relation output of the constitutive model. Comparing the curves with the idealised behaviour of figure 3.3a, it is obvious that this representation is far from perfect. Strain hardening/softening is completely left out. This linear elastic perfectly plastic assumption is acceptable considering our goal of evaluating if failure occurs.

The reduction factor decreases the shear stress at which the perfectly plastic part of the curve intersects with the linear elastic part depending on the orientation of the stresses.

Preferably, in the light of strain compatibility, the plastic behaviour should start at a single shear strain. However, the stability analysis is performed with a single time step vicoplastic algorithm for which no deformation is accumulated and the yield is merely a function of stress conditions (deformation is computed afterwards), this difference in shear strain is not of importance.
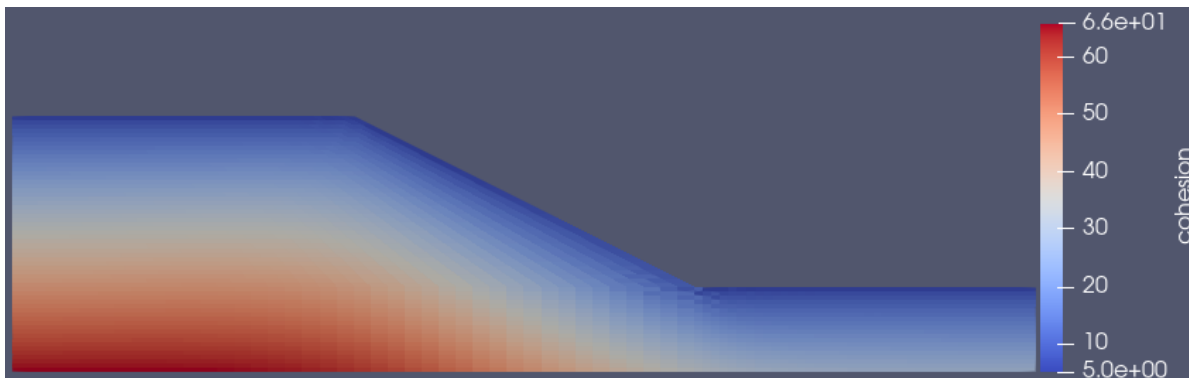
Figure 3.7: A strength field constructed from homogeneous SHANSEP parameter fields $S = 0.2, m = 0.8$ and $POP = 0$. As expected, the undrained shear strength increases with depth and there is a contour following the shape of the dike. There are no inconsistencies observed within elements. There has been strain oscillations noticed in the area in the proximity of the dike's foot caused by the irregular shapes of elements and the angle made at the foot. Their effect on performed analyses are not significant at this stage.

3.3.1. Verification of FEM code

Before proceeding with tests on assumptions, it is useful to verify that the random field generator and FEM code interact correctly to rule out any coding inconsistencies like integration point numbering mismatches.

The verification is an inspection of the output of a certain input of which the result is known. In this case, homogeneous fields for SHANSEP parameters are generated and the resulting strength field is inspected. It can be concluded from the original SHANSEP formulation that the strength field depends linearly (if $POP = 0$) on the vertical effective stress field and should therefore visually be similar. It is expected to encounter a depth dependent increase in strength, with contour lines following the dike geometry. The inspection is illustrated in figure 3.7.

Furthermore, it is useful to assess the accuracy of the FEM against another method. A Spencer-VanderMeij limit equilibrium analysis in D-stability is used. The same simple geometry is modelled with a single layer using the SHANSEP constitutive model. The stability of a slip surface similar to the output of the in-house FEM program (vertical effective stress convention) is assessed using the single slip plane tool. The result is presented in figure 3.8. The factors of safeties are very similar with a slight discrepancy around 5%. The discrepancy is expected to be even lower as a lower bound of 5 kPa is used in FEM giving some additional strength with respect to D-Stability. Such a small difference is acceptable.

3.4. Simulations

3.4.1. The effect of reduction factor

Let us investigate the effect of the reduction factor by comparing it to a simulation in line with WBI2017 assumption for which the strength is characterised by a single set of SHANSEP parameters. In order to highlight the differences, two deterministic analyses are performed and presented side by side in figure 3.9. The orientation of the major principal stress is (almost) vertical at the crest of the slope. The orientation starts to increase gradually (counter clockwise) towards the foundation layer at which it reaches a peak some distance away from the dike. The second figure shows that the reduction has a major impact around the foot of the dike and away from the dike. Although both slip surfaces go through the toe, the CADP model gives deeper failure mechanisms at the expense of the factor of safety. The simulation with anisotropy correction gives a 33% lower safety factor with respect to the corrected version as large parts (2/3) of the slip surface is within a highly reduced zone with more than 50% and up to 90% reduction.

3.4.2. Pre-calculation of strength

From a physical perspective, it is desirable to use actual stresses (including body forces) acting on the integration point to calculate the strength of the soil. However, it has been observed that this approach leads to numerical flaws, artificial rapid fluctuations of undrained shear strength, at such a degree that it affects results. The redistribution of forces is observed to affect both the magnitude and orientation (3.10e) of the major principal stress. This has a major impact on the strength field (3.10a) as a lot of numerical artefacts occur locally. Despite these artefacts, the slip surface in both cases match. However, when analysed closely,
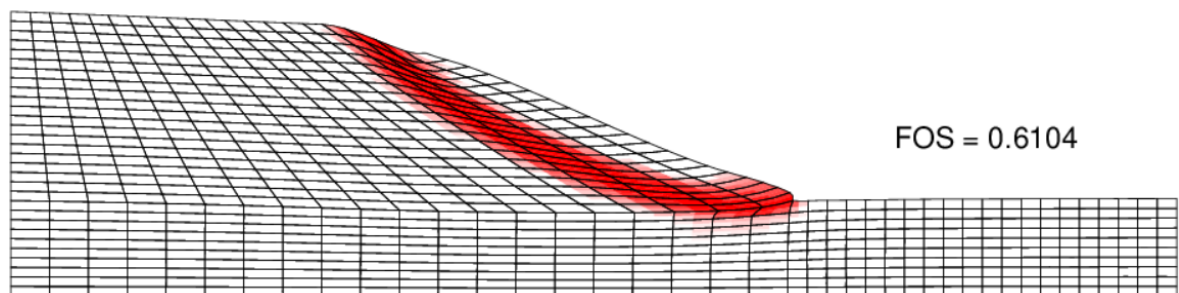
(a) In-house FEM code
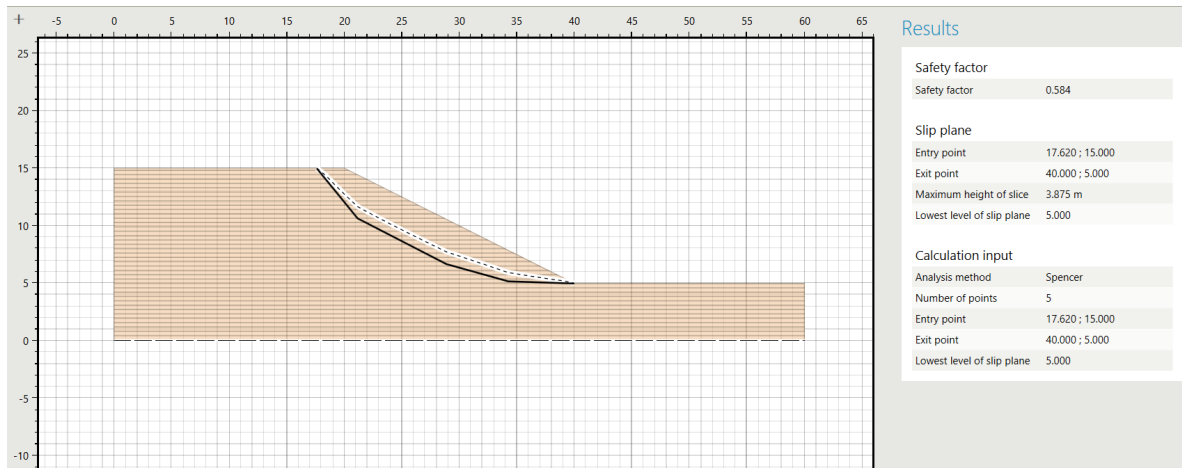
(b) D-Stability

Figure 3.8: Comparison of the in-house FEM code to a similar analysis in D-Stability. The slip surface in D-stability is a rough drawing by hand. The factor of safeties,0.584 and 0.6104.

(a) Orientation of major principal stress, α

(b) Reduction factor in decimals.

(c) Strength field ultimate state strength

(d) Strength field CADP

(e) Slip surface ultimate state strength

FOS = 0.9424

(f) Slip surface CADP

Deformed mesh (displ
color :: Von Mises equ
FOS = 0.6104

μ_S	σ_S	μ_m	σ_m	μ_{POP}	σ_{POP}	$s_{u,min}$	$\dfrac{s_{u,mob}^{TXE}}{s_u^{TXC}}$
0.2	0.0	0.8	0.0	25 kPa	0.0	1.0 kPa	0.1

(g) Input
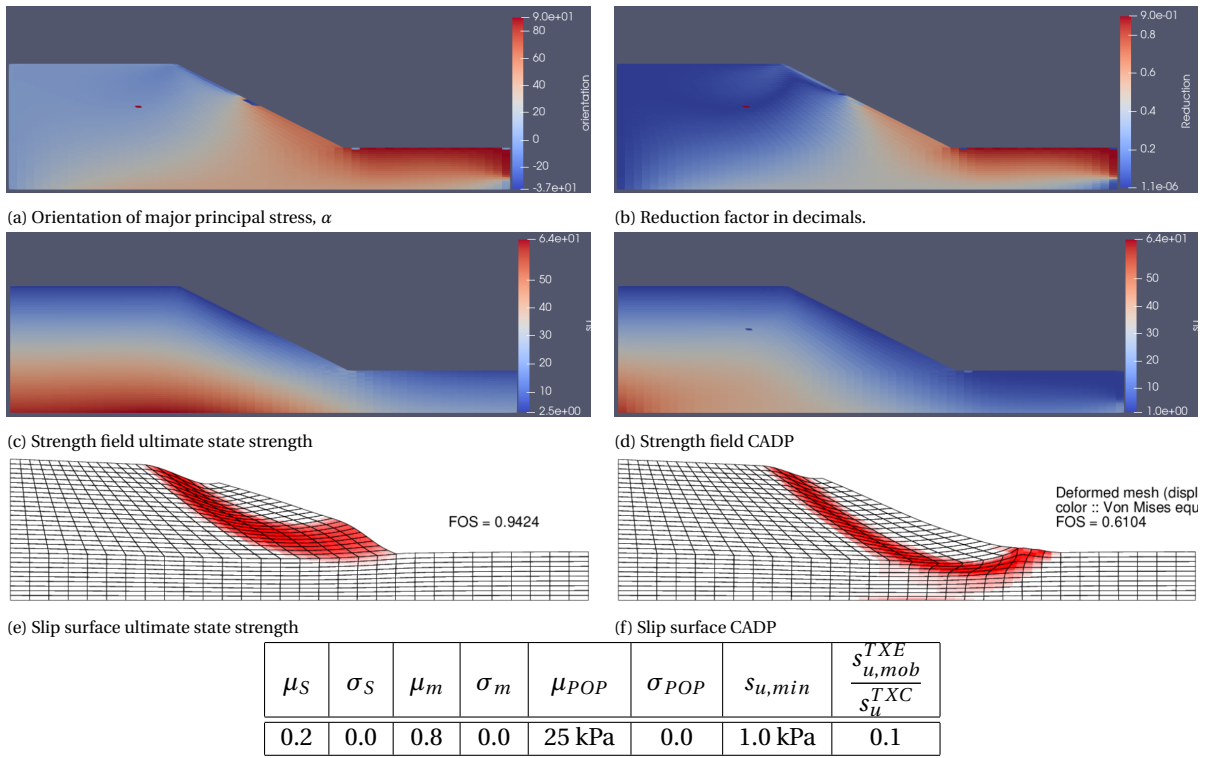
Figure 3.9: Comparison of the undrained shear strength and slip surface of two versions of the FEM code; ultimate state strength (c) & (e) and CADP (d) & (f). (a) and (b) show the orientation of the major principal stress and the reduction factor of the shear strength in case a linear reduction is employed. The input values in the model are tabled in (g). The value of the ratio is chosen randomly.

(a) Strength field actual stress

(b) Strength field pre-calculation

(c) Slip surface actual stress

FOS = 0.6397

(d) Slip surface pre-calculation

FOS = 0.5908

(e) Reduction actual stress

(f) Reduction pre-calculation

μ_S	σ_S	μ_m	σ_m	μ_{POP}	σ_{POP}	θ_v	θ_h	$s_{u,min}$	$\dfrac{s_{u,mob}^{TXE}}{s_u^{TXC}}$
0.2	0.02	0.8	0.08	25 kPa	2.5 kPa	1.0 m	15.0 m	1.0 kPa	0.1

(g) Input
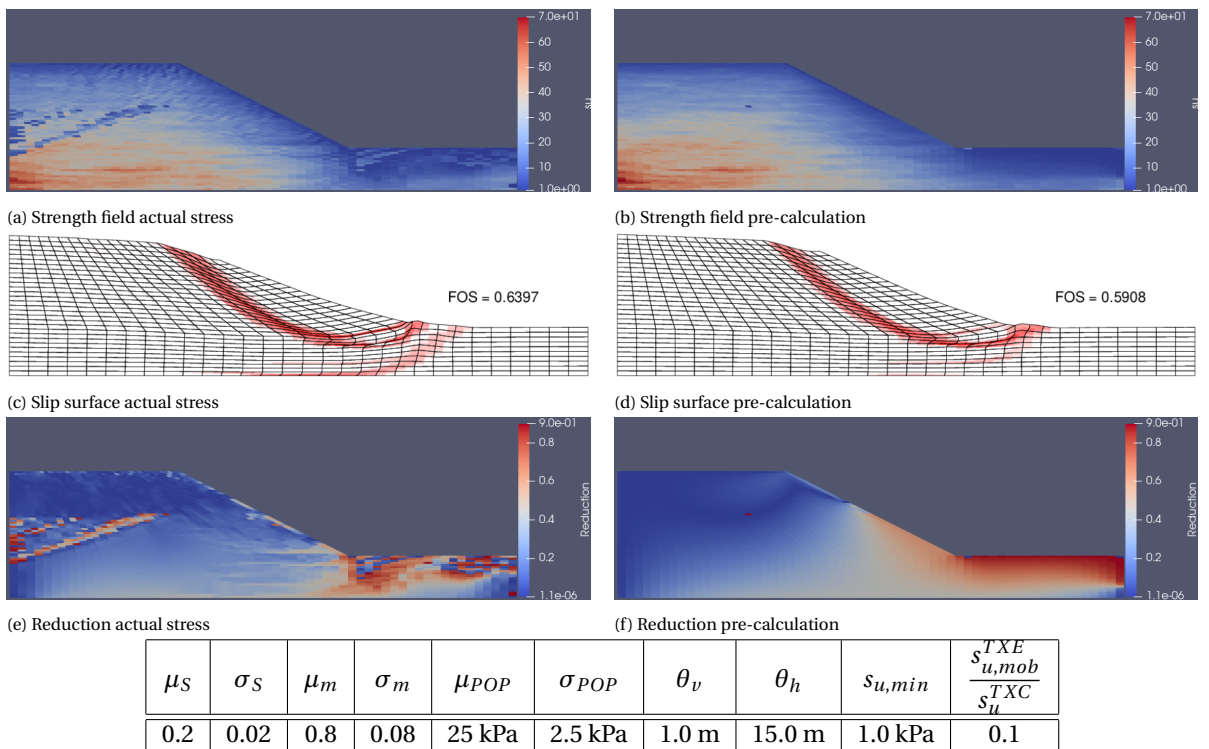
Figure 3.10: The evaluation of a single random field with pre-calculation of strength (3.10b,3.10d and 3.10f) and strength calculation within the viscoplastic algorithm (3.10a,3.10c,3.10e). The random fields to calculate the strength are exactly the same and are generated from input values tabled in 3.10g
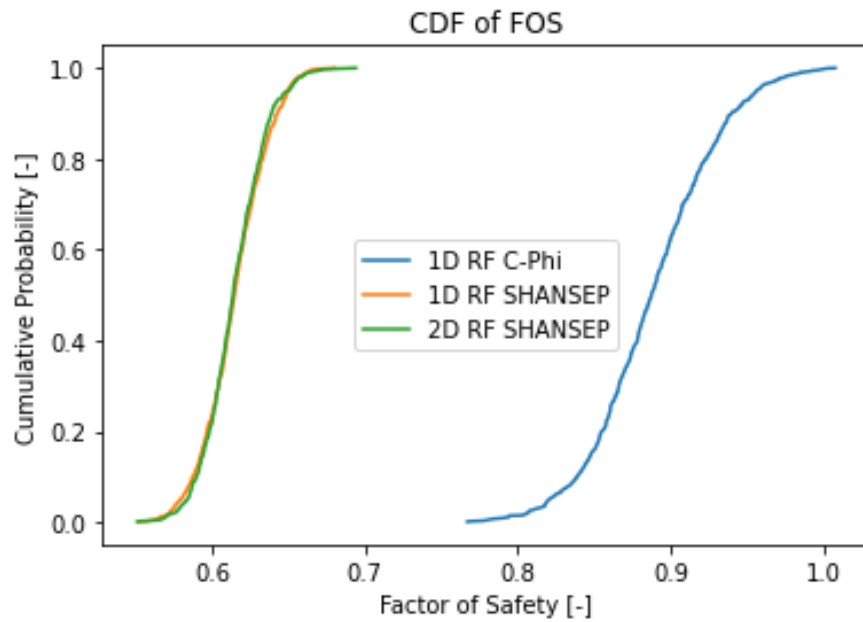
(a) Cumulative probability distributions

μ_S	σ_S	μ_m	σ_m	μ_{POP}	σ_{POP}	θ_v
0.2	0.02	0.8	0.08	25 kPa	2.5 kPa	1.5 m

θ_h	$s_{u,min}$	$\dfrac{s_{u,mob}^{TXE}}{s_u^{TXC}}$	C-Phi a	C-Phi b	C-phi CoV	nreal
15.0m	1.0 kPa	0.1	0 kPa	3 kPa/m	0.1	1000

(b) Input

Figure 3.11: CDFs of various simulatons' results (a) obtained from input values (b). Note that a very high value of θ_h is used for 1D SHANSEP simulation.

it is obvious that the slip surface of the case where strength calculation is performed within the viscoplastic algorithm suffers from oscillations locally. These oscillation affect the factor of safety.

3.4.3. Comparison 1-D c-phi Random Fields
To conclude this chapter, a comparison will be made between the initial code and the additions made in this thesis. The initial code applies the general assumption for cohesive soils in undrained conditions for the c-phi method; the contribution of the frictional component is cancelled ($\phi = 0°$) and the shear strength becomes merely a function of the cohesion. The initial code generates a depth dependent 1D random field for the cohesion and assesses it's stability.

In order to make the analyses comparable, a linear mean trend line will be matched to a vertical strength profile at the end of the crest of the strength field calculated from homogeneous fields of figure 3.9d. The same variation coefficient will be used in all random fields.

The linear representation in the original code of the SHANSEP strength profile is not prefect. The SHANSEP strength profile grows exponentially at low depth and smooths out to a linear line (figure 2.10).Furthermore, the undrained shear strength calculated with the SHANSEP method is stress dependent. The stress decreases towards the slope and therefore there is some horizontal decrease in shear strength which is not captured in the 1-D random field for the c-phi method. In figure 3.11 cumulative probability distributions of the obtained factor of safeties are compared.

What stands out is that both SHANSEP simulations give lower values of FOS compared to the c-phi method. There are two possible reasons for this. On the one hand, there is the reduction that anisotropy gives and on the other hand there is a general reduction in undrained shear strength horizontally towards the right hand side due to the stress dependency of the SHANSEP formulation. Both effects are non existent in the c-phi simulation. Furthermore, there is less scatter in the 2D SHANSEP results compared to the 1D results as the
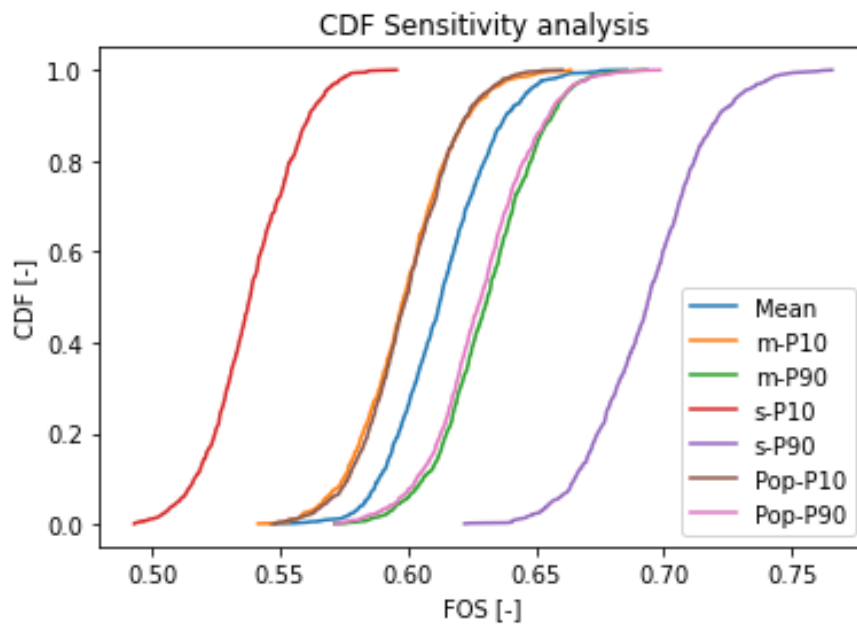
(a) CDFs

μ_S	CoV_S	μ_m	CoV_m	μ_{POP}	CoV_{POP}	θ_v	θ_h	$s_{u,min}$	$\dfrac{s_{u,mob}^{TXE}}{s_u^{TXC}}$	nreal
0.2	0.1	0.8	0.1	25 kPa	0.1	1.0 m	15.0 m	1.0 kPa	0.1	1000

(b) Input

Parameter	P10	P90	Diff. P10	Diff. P90	Average Variance	Sensitivity Factor
S	0.175	0.226	-0.0754	0.0804	6.1E-03	0.93
m	0.700	0.905	-0.0146	0.0176	2.6E-04	0.04
POP	21.886	28.263	-0.0134	0.0154	2.1E-04	0.03

(c) Sensitivity calculation

Figure 3.12: Sensitivity analysis; The CDF in (a) are obtained using the input parameters of (b). Every simulation differs only in one mean parameter value. The P10 and P90 values of (c) are used. The average variance is the the average of the two differences for a particular parameter squared. The sensitivty factor is obtained by dividing the average variance by the sum of the average variances.

distribution is slimmer. A possible reason is the occurrence of averaging towards the mean in the 2D simulation as the horizontal scale of fluctuation is smaller compared to the domain ($\theta_h = \infty$ and $\theta_h = 15m$). Finally, both SHANSEP distributions are slimmer compared to the c-phi method. A possible reason could be the use of three independent random fields which could lead to averaging towards the mean. This would require the three SHANSEP parameters to have equal contribution to the factor of safety. In order to tests this, a sensitivity analysis is performed.

The methodology adopted is as follows. A P10 and P90 value (the 10th and 90th percentile values, respectively) from distributions with statistical values in table 3.12b are obtained. Simulations are run for which only a single mean value input is changed to either a P10 or P90 value. The variance with respect to the mean simulation is calculated. The sensitivity factor is it's variances fractional contribution to the total variance. The results of this analysis is shown in figure 3.12.

The sensitivity analysis shows us that the three parameters do not have equal contribution to the FOS. The FOS depends mostly on parameter S, the normalised undrained shear strength at normal consolidation. There must be another unknown reason for the lower spread the FOS distribution of the SHANSEP method.

3.5. Conclusion
The major principal stress is found to be more objective than the vertical effective stress to represent stress conditions in the SHANSEP formulation. The FEM program uses a linear elastic perfectly plastic constitutive model, which do not allow for modelling of anisotropic effects. There are two solutions found to make up

for anisotropy in strength and stress conditions; (1) the SHANSEP parameters are obtained at ultimate state where the mobilised strengths converge or (2) the SHANSEP parameters are obtained at peak strength in triaxial compression after which the shear strength is reduced based on the orientation of the major principal stress to estimate the failure mode.

Both the random field generator and the modifications to the FEM program are coded and verified. The magnitude of the major principal stress is computed by taking the eigenvalues of the plane strain stress tensor and a formulation of its orientation is obtained by solving a force equilibrium. The reduction factor is a linear interpolation between unity at zero orientation and a ratio between the mobilised shear strength in traixial extension and triaxial compression at $\alpha = 90$. The reduction factor has a more profound effect close to the slope and at the foundation layer resulting in deeper failure mechanisms and lower factors of safety with equal input.

In a comparison of the ultimate state strength SHANSEP approach and the c-phi method with a linear increasing trend in the cohesion, it was found that the spread in factor of safety outcomes is higher. A sensitivity analysis pointed out that parameter S is the most influential SHANSEP parameter.

4

Complete FE calculations

The concepts developed in the previous chapter will be implemented into a more advanced FEM code. This code will be used to compare failure probabilities, factors of safeties and slip surfaces of RFEM against a deterministic analysis. The chapter begins with a brief introduction to the advanced code followed by a discussion on the results of the continuous ADP approach and a comparison to a deterministic analysis. The chapter will be concluded with a discussion on the results of the continuous ADP approach and differences with the ultimate state approach.

4.1. Introduction to advanced code
The advanced code is built on the simple code. Broadly speaking they share the same program flow; elastic stiffness is calculated based on gravitational stresses and an iterative viscoplastic algorithm is used to compute displacements and a safety factor. The advanced code is enhanced to include multistage loading, multiple soil layers, excess pore pressures, random field generation. Two constitutive models are available to use; mohr-coulomb and SHANSEP/Tresca model. The random field generator uses the Cholesky decomposition method.

   The advanced program is not able to create it's own mesh. The mesh has to be generated externally and loaded into the program. Modifications to the advanced code are presented in the appendix.

4.1.1. Mesh & Geometry
The goal of the comparison is to investigate the effect of using spatially varying SHANSEP parameters rather than fixed values in the evaluation of dike stability. The geometry and layering should be designed in such a way that effects of interactions of multiple layers and complex geometries are avoided. However, the geometry should include all areas, or failure modes, existing in a slope stability problem. The geometry of the experimental FEM code satisfies those requirements and is therefore reused. The mesh is regenerated and a phreatic surface is added to account for water loads. The embankment represents the inward part of a dike and is 20m wide with a slope of 1:2. An additional width of 20m are added to the crest and foundation layer. The foundation layer is 5m meters high.The phreatic surface consists of two line segments between (0;12), (40;4.5) and (60;4.5) The mesh is made up of unstructured quadrilaterals. While the bottom is fixed, the boundaries on the sides are only restricted horizontally. The whole soil body is composed of a single cohesive layer. The geometry, mesh and stress conditions are illustrated in figure 4.1.

4.1.2. First Order Second Moment method
Before starting the comparison, a way has to be found to express the factor of safety of the deterministic analysis to a failure probability. The Dutch guidelines recommend the following formulation to calculate the failure probability of primary dikes (Ministerie van Infrastructuur en Milieu, 2017).

$$p_f = \Phi^{-1}\left(-\frac{\dfrac{FOS_d}{\gamma_m} - 0.41}{0.15}\right) \tag{4.1}$$

(a) Mesh

(b) Geometry

(c) Orientation of σ_1

(d) σ_1
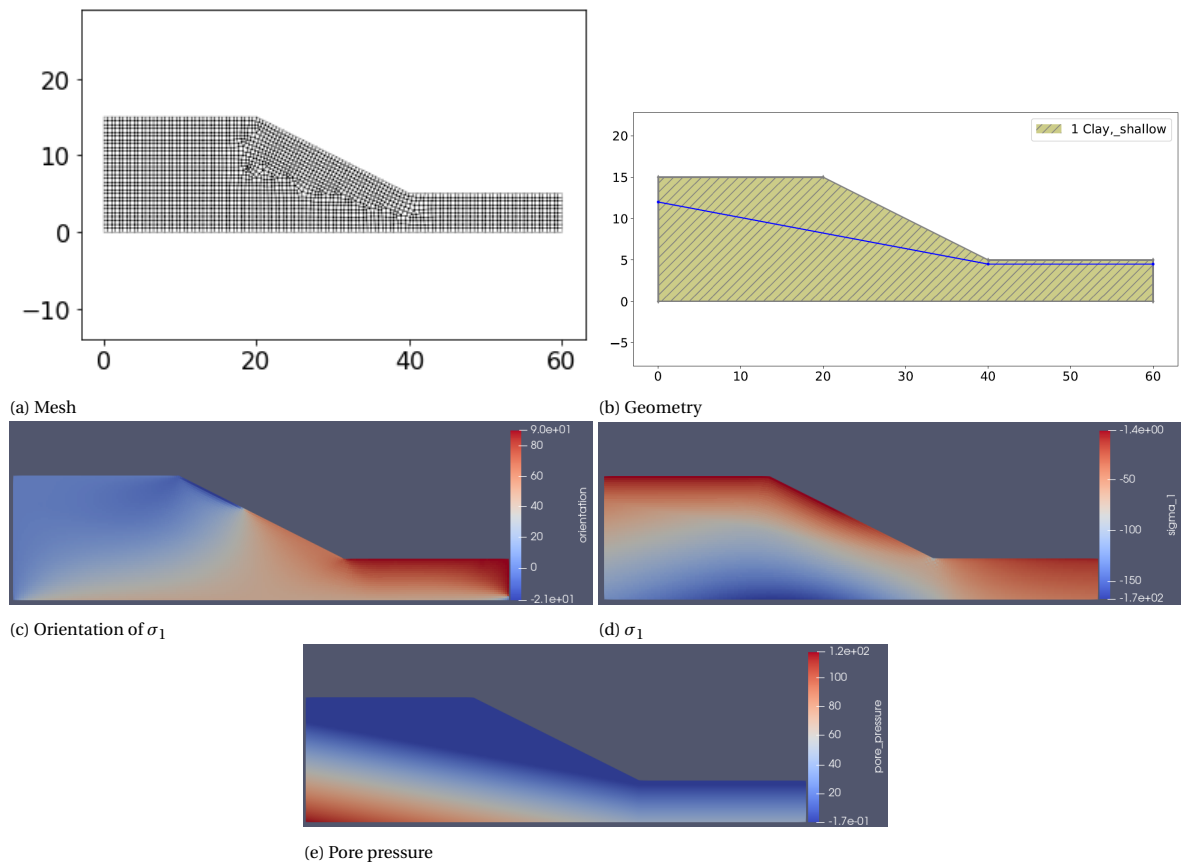
(e) Pore pressure

Figure 4.1: Illustrations of the mesh (a), geometry and layering (b), the orientation and magnitude of the major principal stress (c & d) and pore pressure of the ground model.

γ_m is a model factor and FOS_d is the safety factor obtained from a simulation with design values. The design value is the 5 or 95 percentile values of the distributions of strength parameters and loads divided or multiplied by a material factor, respectively. The terms in the brackets represent a calibrated relation between the factor of safety obtained with the design values of all stochastic parameters. 0.41 and 0.15 are the calibration values of the mean and standard deviation, respectively. There is no further knowledge about the calibration procedure and the determination of these values.

The formulation is intended to be used for all primary dikes in the Netherlands, making it too general and is relatively inaccurate (but conservative) in case it is applied to specific cases. In order to have a better estimation of the failure probability from the factor of safety the First Order Second Moment (FOSM) method will be used. A deterministic analysis is performed with mean values of stochastic variables. The factor of safety result will be used as a mean. The standard deviation of FOS will be approximated using the FOSM method. The stochastic variables are assumed to be distributed lognormally. The FOS results are therefore also distributed lognormally. The mean and standard deviation can be used to determine the cumulative probability for 1.0 in a lognormal distribution. Software like Excel and python have functions to calculate the cumulative probability that approximate this equation.

$$p_f = 0.5 + 0.5 erf\left(\frac{\mu_{ln}}{\sqrt{2}\sigma_{ln}}\right) \tag{4.2}$$

The standard deviation is approximated using a first order Taylor expansion alongside with the second moments (standard deviations) of the soil parameters(Fenton and Griffiths, 2008). Mathematically the relation is:

$$\sigma^2_{f(X_1, X_2, ..., X_n)} = \sum_{i=1}^{n}\left(\frac{\partial f}{\partial X_i}\right)^2 \sigma^2_{X_i} \tag{4.3}$$

X_i represent the soil parameters and f is a limit state equation. The limit state equation for the FEM code would be the FOS result minus 1. The FEM code uses complex algorithms to compute a FOS from the individual displacements of elements. It is extremely difficult if not impossible to formulate a proper limit state equation. Therefore the partial derivatives will be approximated numerically using central difference differentiation.

$$\sigma^2_{FOS} = \sum_{i=1}^{n}\left(\frac{FOS(\mu_{X_i} + \sigma_{X_i}) - FOS(\mu_{X_i} - \sigma_{X_i})}{2\sigma_{X_i}}\right)^2 \sigma^2_{X_i} \tag{4.4}$$

FOS is the result of a deterministic analysis with mean input values except the variable for which the partial derivative is approximated for. The value used for this variable is shown in brackets. It is crucial to do the approximation with values close to the mean(Fenton and Griffiths, 2008). Values one standard deviation from the mean serve as a safe crude approximation.

A second use of the FOSM method is to perform a sensitivity analysis on the contribution of a single parameter's variability to the variability of the FOS. Keeping the previous approach in mind, the following mathematical expression can be approximated to come up with a sensitivity value.

$$Sen_{X_i} = \frac{\left(\frac{\partial f}{\partial X_i}\right)^2 \sigma^2_{X_i}}{\sum_{i=1}^{n}\left(\frac{\partial f}{\partial X_i}\right)^2 \sigma^2_{X_i}} \tag{4.5}$$

4.2. Results: Ultimate state strength

Sensitivity   Before starting the comparison of the results between RFEM and the deterministic analysis, it would be interesting to investigate the influence of the model parameters on the FOS. It should be kept in mind that the sensitivity is problem specific as it strongly depends on f.e. the dike geometry and layering. However it is good enough for a general indication. The sensitivity analysis will include the influence of the Poisson's ratio. Although the physical value is 0.5 in undrained conditions, for the sake of the analysis, this assumption will be disregarded. The variation of ν is assumed to follow a uniform distribution between 0.2 and 0.5. It's mean and standard deviation are chosen accordingly.

Results of the sensitivity analysis is summarised in table 4.3. The FEM code depends strongly on SHANSEP parameter S. This strong influence can be explained by the linear dependency of the SHANSEP strength to

(a) $\nu = 0.263$, magnitude

(b) $\nu = 0.437$, magnitude

(c) $\nu = 0.263$, orientation
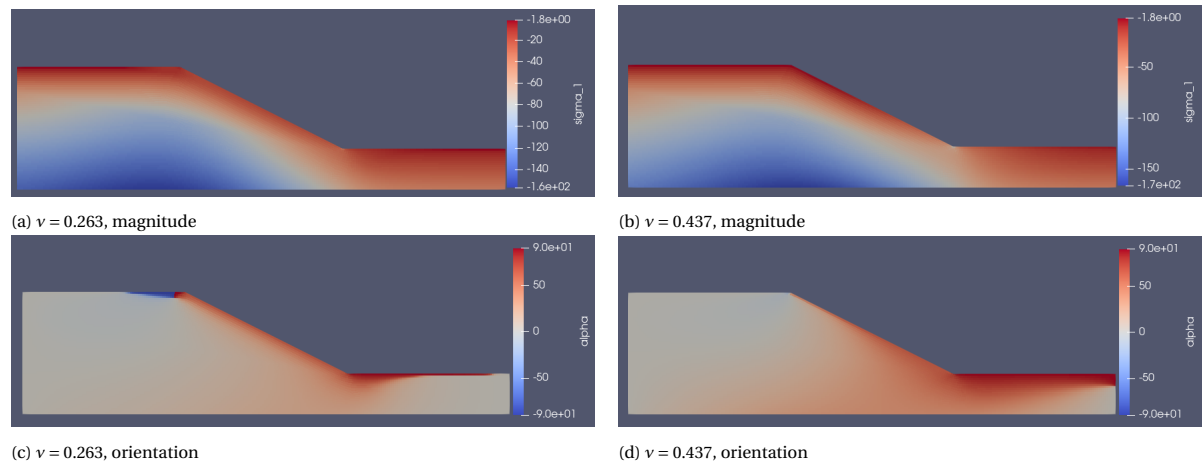
(d) $\nu = 0.437$, orientation

Figure 4.2: A comparison of the orientation and magnitude of the major principal stress for $\nu = 0.263$ (a & c) and $\nu = 0.437$ (b & d). The major principal stress seems to be rotated in a smaller portion distributed a the toe of the dike and along the surface of the slope for smaller values of Poisson's ratio. The rotation is more significant and deeper for higher values of Poisson's ratio.

this parameter. The dependency of m and POP is surprisingly smaller. Their values are only significant to the undrained shear strength at the first few meters of depth. This reduces their impact on the stability of a high slope.

Variation in the expected range of volumetric weight, both dry and wet seem to have little effect on the stability. The self weight of the soil affects the stress field, both the shear stress acting as a load as well as the confining pressures acting as a resistance are influenced by their value. A larger influence would theoretically be expected. The proportions in which they influence loads and resistances depend on the geometry. As the results are close to $FOS = 1.0$, the proportions should lie relatively close and therefore cancel each other out. It is also interesting to see that an increase in dry volumetric weight seems to have negative effect and a positive effect is observed for its wet counterpart.

The Young's modulus and Poisson's ratio are elastic parameters meaning that their expected impact on the stability, which is governed by plasticity, should be very limited. This is true for the Young's modulus. Surprisingly, it is observed that variation in Poisson's ratio is quite significant passing by any other parameter except S. Inspecting stress fields reveal that the stress field is influenced significantly by the Poisson's ratio (see figure 4.2). The way initial stresses are computed could explain this influence. The volumetric weight is integrated over the areas of elements numerically. This value is saved as vertical loads. The horizontal components are computed from elastic constitutive equations (eq. 2.10). The Poisson's ratio being the ratio between strains in two perpendicular directions, a higher value would lead to higher computed horizontal forces. The shear stresses (forces) are calculated from the interaction of all nodal horizontal and vertical loads. According to equation 3.6, higher shear stresses lead to a larger rotation. Higher overall stress leads to higher principal stresses and thus higher SHANSEP strength.

Deterministic analysis/FOSM   In the sensitivity analysis all model parameters were assumed to be stochastic. Although the volumetric weights are spatially variable, in our comparison only the SHANSEP parameters will be assumed to be stochastic in order to highlight their effect. This assumption is acceptable as the sensitivity analysis pointed out that the (ground) model is relatively insensitive to those model parameters.

The estimated probability of failure is around 16% (see figure 4.4b). This value is very high as the maximum failure probability for a single cross section is below 1/10000.

The strength field and slip surface resulting from the mean analysis is shown in figure 4.5. Its factor of safety is 1.178. The slip surface is not circular and has more of an oval shape. It cuts through the crest close to the slope and ends very close to the toe. Contrary to expectations from chapter 3, the failure mechanism is deeper, probably caused by the addition of a phreatic surface. In the moment equilibrium, the weight of the dry soil close to slope is counteracted by a wet soil in the foundation layer. The relative decrease in effective stress due to the buoyant weight of wet soil causes the s_u of the foundation layer to decrease affecting the slip surface. The path of the slip surface is now not merely defined by weaker zones of the strength field.

	S	m	POP	γ_d	γ_w	E	ν
μ	0.25	0.9	25kPa	$17 kN/m^3$	$17\ kN/m^3$	1.0 MPa	0.35
σ	0.025	0.05	3.75 kPa	$0.85\ kN/m^3$	$0.85\ kN/m^2$	0.25 MPa	0.867

(a) Variable input

	S	m	POP	γ_d	γ_w	E	ν
$FOS(\mu_{X_i} + \sigma_{X_i})$	1.1469	1.0562	1.075	1.0344	1.05	1.0422	1.1156
$FOS(\mu_{X_i} - \sigma_{X_i})$	0.9375	1.0281	1.0094	1.0531	1.0344	1.0422	0.9984
$\left(\dfrac{\partial f}{\partial X_i}\right)$	4.188	0.281	0.0087	-0.011	0.0092	0	0.677
$\left(\dfrac{\partial f}{\partial X_i}\right)^2 \sigma^2$	0.0109	0.0002	0.0011	8.74E-05	6.08E-05	0	0.0034
Sensitivity	0.693	0.012	0.068	0.006	0.004	0	0.217

(b) Sensitivity analysis

Figure 4.3: Sensitivty analysis on the ultimate state strength approach. The approximation of the partial derivative is based on central difference differentiation with a step size of one standard deviation from the mean. The mean and standard deviation values are partly improvised within expected ranges. Table 2b of Eurocode 7 is consulted for input values of the volumetric weights and Young's modulus.

	S	m	POP	γ_d	γ_w	E	ν
μ	0.25	0.9	25kPa	$17 kN/m^3$	$17\ kN/m^3$	1.0 MPa	0.49
σ	0.025	0.05	3.75 kPa	-	-	-	-

(a) Input

	θ_x	θ_y	μ	σ	p_{f1}	p_{f2}	nreal
FOSM	-	-	1.178	0.123	0.158	-	7
RFEM 1	2.0m	0.75m	1.147	0.015	1.2E-11	0.0	500
RFEM 2	6.0m	1.0m	1.141	0.026	7.0E-05	0.0	500
RFEM 3	20.0m	2.0m	1.139	0.045	0.015	0.0	500

(b) Failure probability
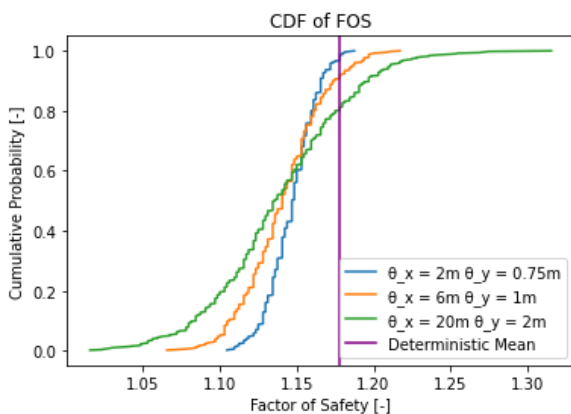
(c) CDF of FOS results
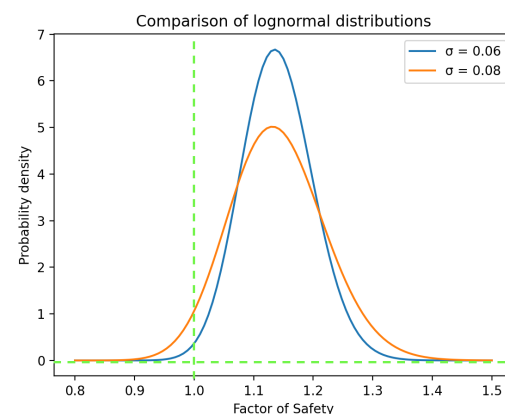
(d) pdf of FOS results

Figure 4.4: Comparison of the probability of failure estimated for the deterministic approach and three RFEM analyses with different values of correlation lengths. The code used in those analyses are developed for the ultimate state strength assumption. The correlation lengths are improvised with some in realistic ranges (RFEM 2 & 3). The probability of failure is the area bound by the two green lines and the probability density. The standard deviation do not correspond to the analyses, but are chosen high on purpose to enhance the visualization.

(a) Undrained Shear strength
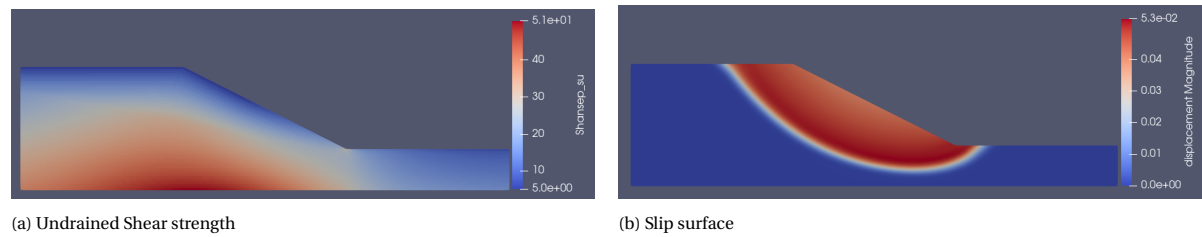
(b) Slip surface

Figure 4.5: The undrained shear strength field and slip surface of the deterministic analysis.

RFEM   Three RFEM analyses were run with three combinations of correlation lengths. each analysis comprises of 500 realizations. An easy way to estimate the probability of failure is to divide the amount of realisations with a factor of safety lower than one by the total number of realisations.

$$p_{f,RFEM} = \frac{NREAL_{FOS<1}}{NREAL} \tag{4.6}$$

The problem of this approach is that the accuracy that 500 realisations give is insufficient to estimate at a required accuracy of about 1/10000 for a single cross section. Therefore a second method similar to the FOSM estimation is utilised. The mean and standard deviation of the factor of safety results are computed. The probability of failure is the cumulative probability at $FOS = 1.0$ of a lognormal distribution with these statistical parameters with equation 4.2. The estimated mean, standard deviation of the distributions and the resulting failure probabilities is summed up in figure 4.4.

The mean of the of RFEM simulations are relatively close to each other. There seems to be a decrease of the mean for higher correlations lengths. The use of a higher scale of fluctuation results in less fluctuations between strong and weak zones along the slip surface. As the slip surface prefers the least path of resistance, less averaging between zones happen resulting in a general drop in strength.

The spread of FOS outcomes expressed as the standard deviation shows the opposite trend compared to the mean; A higher scale of fluctuation gives higher spread in results. Again, more fluctuations in weak and stronger zones result in averaging towards a mean, decreasing the spread in results.

As the mean of every results analysis is very close, the effect of a lower spread is reflected back in the probabilities of failure. As mentioned earlier, the probability of failure is the CDF of a lognormal distribution at $FOS = 1.0$. A way of visualising this is taking the area under a lognormal distribution for $FOS \leq 1.0$. At equal mean, a larger spread will result in more extreme values (larger tail on both sides) thus a larger area under the distribution (see figure 4.4d)

The probability of failure estimated by equation 4.6 for every simulation is 0.0. However, p_{f1} of analyses RFEM 2&3 fall within the required accuracy for a single cross section. The choice not to rely on p_{f2} was valid.

RFEM resulted is a wide range of slip surfaces. However, the following statements about the slip surfaces can be made.

- Slip surfaces tend to cut through weak zones of the random fields. The most influential parameter is S followed by POP. The random field of parameter m seems to be relatively insignificant (figure 4.6).

- The depth of the slip surface is controlled by horizontal weak zones close to the toe. The lowest point of the arc is observed to prefer such a weak zone. The lateral position is found to be controlled by a weak zone around the crest. The lowest point of the arc is wide for analyses with high horizontal correlation lengths (figure 4.7). There is no significant difference in the width between correlation lengths $\theta_x = 6m$ and $\theta_x = 20m$.

Comparison   The mean FOS of the FOSM method is higher compared to any RFEM simulation. There is a bias of slip surfaces to go through weaker parts of random fields, causing the general shear strength along slip surfaces to be lower than the average strength of the field.

Despite having a higher mean FOS, the failure probability is substantially higher in the FOSM analysis. To put it in perspective, the FOSM analysis resulted in a p_f one order of magnitude higher than the most conservative RFEM simulation. This difference is significant.

(a) Slip surface

(b) Undrained shear strength

(c) Parameter S

(d) Parameter m

(e) Pre-overburden pressure
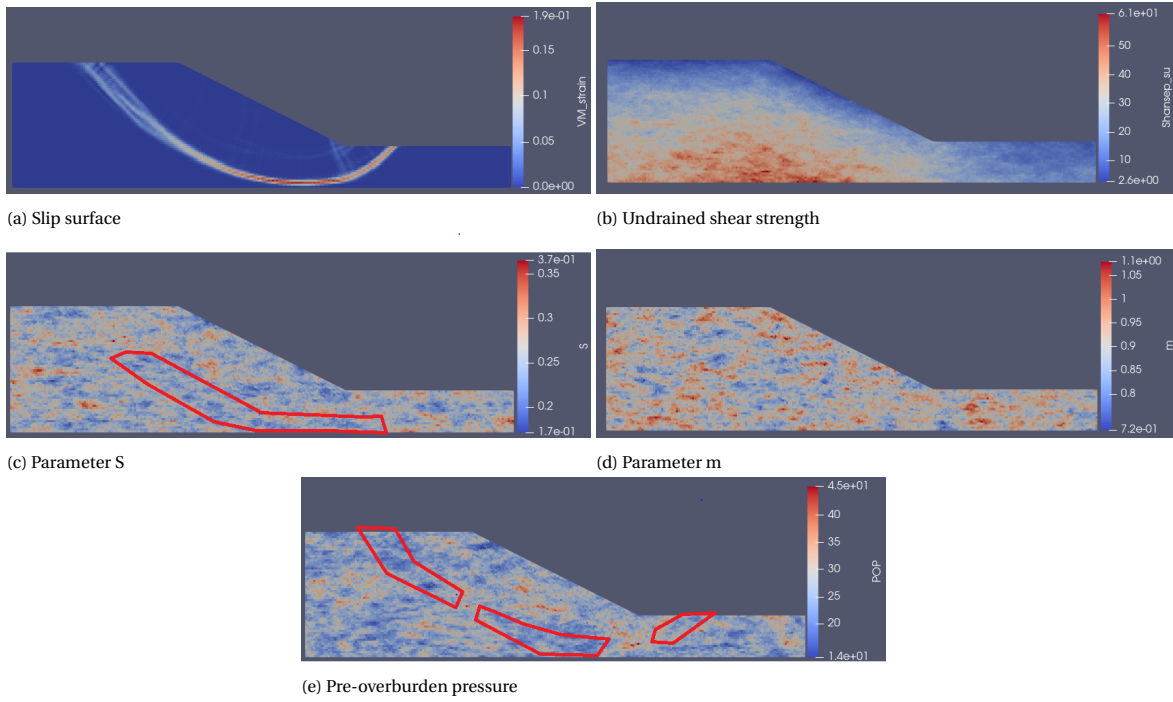
Figure 4.6: Slip surface (a), random fields (c,d & e) and undrained shear strength field (b) of a single evualuation of RFEM 1, $\theta_x = 2m$ $\theta_y = 0.75m$. The slip surface goes through clearly at a weak area in POP in the crest and weak zones of S and POP at its lowest points. Note that the slip surface goes through a relatively strong zone of parameter m. The factor of safety of this evaluation is 1.1344

(a) Slip surface

(b) Undrained shear strength

(c) Parameter S

(d) Parameter m

(e) Pre-overburden pressure
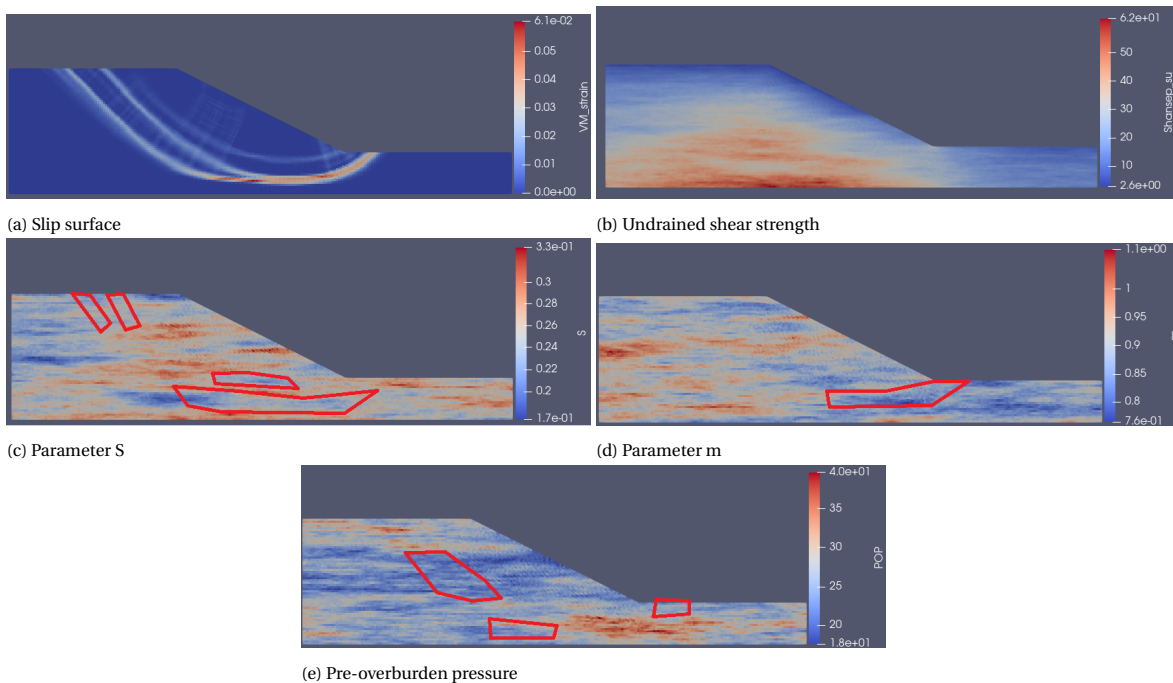
Figure 4.7: Slip surface(a), random fields (c,d&e) and undrained shear strength field (b) of a single evaluation of RFEM 3, $\theta_x = 20m$ $\theta_y = 2.0m$. The lowest part of the slip surface is wider due to a wider weak zones in parameter S and POP.The factor of safety of this evaluation is 1.2047.

Theoretically, the scale of fluctuation of a deteministic analysis is infinite, ($\theta_{det} = \infty$). Considering this fact, FOSM follows the trend found in the RFEM analyses; the probability of failure increases with increasing scale of fluctuation.

(a) Undrained Shear strength

(b) Slip surface
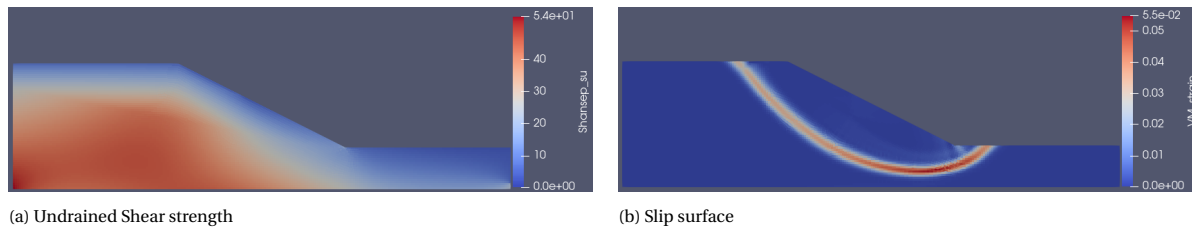
Figure 4.8: Strength field and failure mechanism of a deterministic analysis with mean values using the CADP model. The factor of safety of this evaluation is 1.197.

4.3. Results: CADP

Sensitivity In the CADP apporach, the S value corresponding to peak shear strength in trixial compression is required. As the model parameters in those analyses are not correlated to any real data, a theoretical value 40% larger is taken. The sensitivity of model parameters in the continuous ADP approach are tabulated in 4.1. The mean and standard deviation of parameter S is changed preserving its coefficient of variation.
The continous ADP approach is observed to be less dependent on the Poisson's ratio. The value of parameter S dominates this model.

The effect of the additional parameter, $s_{u,TXE}/s_{u,TXC}$,on the factor of safety is quite small. This is surprising as SHANSEP strength strongly depends on the reduction factor resulting from this variable. A $\frac{s_{u,TXE}}{s_{u,TXC}}$ value of 0.3 would indicate a slowly increase in reduction up to 70% from top to bottom, which is significant. However, taking the standard deviation into account, 60% of the values are expected to deviate 0.05 from the mean, a reduction or increase in strength of around 16% at the maximum (and slowly decreasing along the slip surface) will indeed not make significant difference.

There is an inverse relation between FOS and Poisson's ratio. Findings in figure 4.2 showed us that an increase in Poisson's ratio increased the rotation of the major principal stress. The rotation was amplified. An amplification of the rotation results in higher overall reduction factors and thus lower strength.

Deterministic analysis/FOSM Figure 4.8 shows the strength field and slip surface of the FOSM realisation with mean input values. The slip surface is an oval shaped deep arc cutting through the crest and a few meters from the toe. Small branches are observed perpendicular to the major slip surface passing through the toe. Another branch is parallel to the major slip surface with few meters of vertical separation. The factor of safety of this slip surface is calculated to be 1.197. The FOSM estimation of the standard deviation considering only SHANSEP parameters to be random variables is 0.126 giving, together with the mean, a failure probability of 12.7% in a lognormal distribution.

	S	m	POP	γ_d	γ_w	E	ν	$\frac{s_{u,TXE}}{s_{u,TXC}}$
μ	0.35	0.9	25kPa	$17 kN/m^3$	$17\ kN/m^3$	1.0 MPa	0.35	0.3
σ	0.035	0.05	3.75 kPa	$0.85\ kN/m^3$	$0.85\ kN/m^2$	0.35 MPa	0.867	0.05

(a) Variable input

	S	m	POP	γ_d	γ_w	E	ν	$\frac{s_{u,TXE}}{s_{u,TXC}}$
$FOS(\mu_{X_i} + \sigma_{X_i})$	1.3313	1.2281	1.2484	1.2000	1.2188	1.2109	1.2000	1.2281
$FOS(\mu_{X_i} - \sigma_{X_i})$	1.0906	1.1937	1.1719	1.2219	1.2000	1.2109	1.2219	1.1922
$\left(\frac{\partial f}{\partial X_i}\right)$	3.44	0.344	0.0102	-0.013	0.011	0	-0.126	0.359
$\left(\frac{\partial f}{\partial X_i}\right)^2 \sigma^2$	0.0145	0.0003	0.0015	0.0001	8.84E-05	0	0.0001	0.0003
Sensitivity	0.857	0.018	0.087	0.007	0.005	0	0.007	0.019

(b) Sensitivity calculation

Table 4.1: Sensitivity analysis performed on the continuous ADP approach.(a) presents input variables and (b) shows the results.

	S	m	POP	γ_d	γ_w	E	ν	$\dfrac{s_{u,TXE}}{s_{u,TXC}}$
μ	0.35	0.9	25kPa	$17 kN/m^3$	$17\ kN/m^3$	1.0 MPa	0.49	0.3
σ	0.035	0.05	3.75 kPa	-	-	-	-	-

(a) Input

	θ_x	θ_y	μ	σ	p_{f1}	p_{f2}	nreal
FOSM	-	-	1.197	0.126	0.137	-	7
RFEM 1	2.0m	0.75m	1.166	0.016	3.5E-13	0.0	500
RFEM 2	6.0m	1.0m	1.164	0.027	6.6E-06	0.0	500
RFEM 3	20.0m	2.0m	1.165	0.045	4.6E-03	0.0	500

(b) results
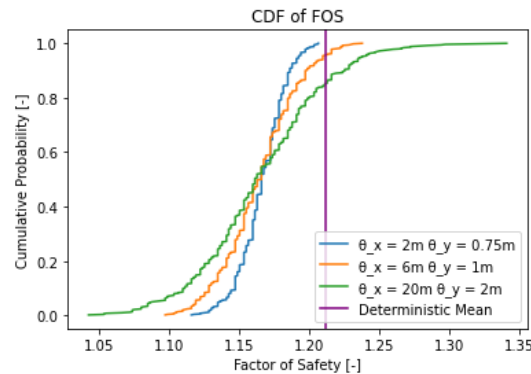
(c) CDF of FOS results

Figure 4.9: The input values (a), and results (b & c) of the continuous ADP approach.

RFEM   Figure 4.9 shows the distribution of factor of safety and the estimated failure probabilities. The mean values of the RFEM analyses are relatively close to each other and there seems to be no clear trend with respect to the scale of fluctuation. The standard deviation and probability of failure increase with increasing scale of fluctuation. Averaging to the mean has it's part on this.

Slip surfaces do not follow the weak zones of the strength field. They rather go through weak zones locally caused by local weak zones in the random fields of parameters S, m and POP. The most influential random fields are parameter S and POP. The depth of the major slip surface tend to go through a wide weak zone in the foundation layer close to the toe. Some minor slip surfaces are observed perpendicular and parallel to the slip surface.

Comparison   Despite taking the value of parameter S 40% higher compared to the ultimate state strength analysis, the resulting mean is comparable. This indicates the great impact of the reduction factor on the factor of safety. It is interesting to see that the sensitivity analysis presents an opposite picture, the sensitivity factor of 0.019 is very low. However, the sensitivity analysis gives an indication what the effect will be of change in parameter value of a certain model. The effect of adding new features to a certain model cannot be tested using a sensitivity analysis based on FOSM. The sensitivities of the other parameters have increased slightly. The increases are insignificant.

μ_{FOS} calculated by FOSM is larger than all RFEM analyses. The estimated standard deviation and failure probability are also larger and follow the trend found in the RFEM analyses. The FOSM analyses could be considered as an RFEM analysis with infinite correlation length $\theta_{det} = \infty$.

4.4. Comparison of models & summary
In this chapter the deterministic/FOSM approach is compared to RFEM. It was found that the ultimate state strength model is mostly sensitive to SHANSEP parameter S and the Poisson's ratio. The CADP model is most sensitive to parameter S and is found to be less and inversely related to the Poisson's ratio.

(a) Slip surface

(b) Undrained shear strength

(c) Parameter S

(d) Parameter m

(e) Pre-overburden pressure
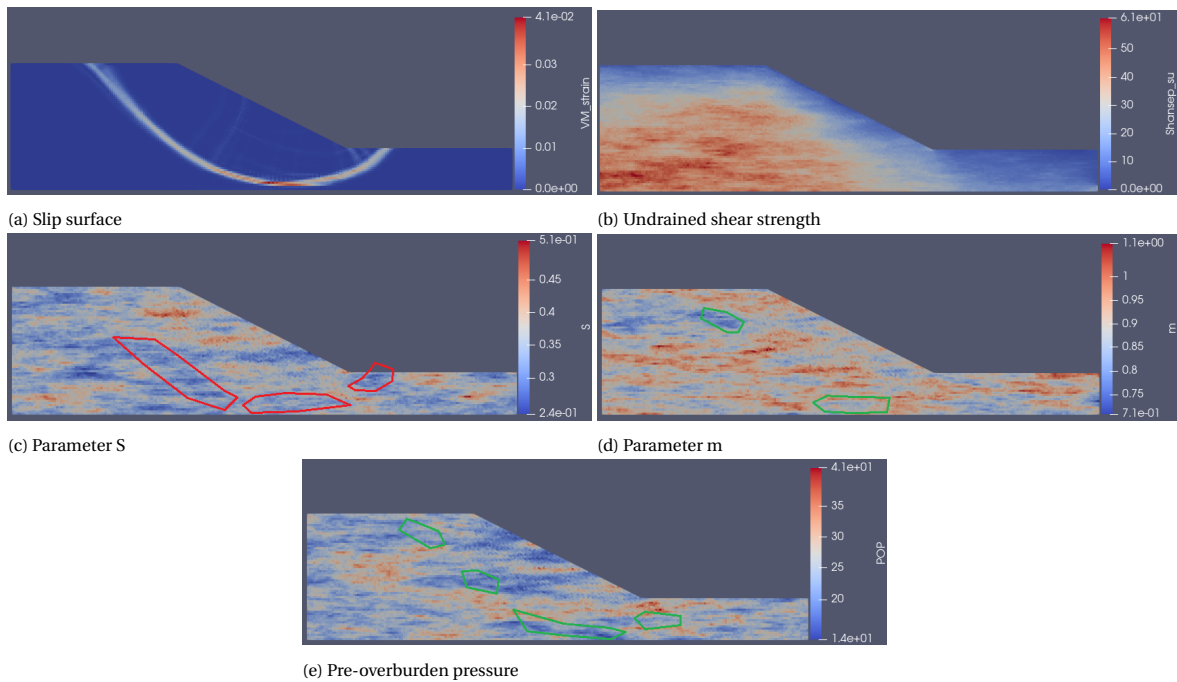
Figure 4.10: Slip surface(a), random fields (c,d & e) and undrained shear strength field (b) of a single evaluation of RFEM 2, $\theta_x = 6m$ $\theta_y = 1m$. The factor of safety of this evaluation is 1.1531.

If the deterministic analysis is considered as a RFEM analysis with $\theta_{det} = \infty$, there there seems to be a slight downward trend in the mean of FOS distributions with increasing scale of fluctuation in the ultimate state strength model. This trend is not observed in the CADP model. The standard deviation increased in both models with increasing correlation length. This is reflected back in the probability of failure.

In both models the mean of FOS is higher in FOSM. The slip surfaces in the RFEM analysis tend to go through local weak zones, decreasing the average strength and FOS result.

It should be noted that the value of S was tuned well as the mean and standard deviation are close to their ultimate state strength model counterpart. This could indicate that the use of the CADP approach is unnecessary. A side by side comparison with real soil data is required to make a definitive comment.

In both models, the estimated probability of failure was at least one order of magnitude larger compared to the most conservative RFEM analysis. Although being conservative in stability analysis is beneficial, one could argue that the use of a conservative estimate of a correlation length will be more beneficial to avoid unnecessary and costly over-engineering of slopes.

5

Case study; Broekermeerdijk

In this chapter. the performance of the ultimate state strength model will be tested using real geotechnical investigation data. The results of RFEM simulations and a deterministic analysis will be compared and discussed.

The data is part of an investigation of Arcadis on the stability of the Broekermeerdijk nearby the city of Amsterdam. The data consists of a single cross section in and (statistical) input parameters for D-stability.

The cross section does not show any complex geometries and consists of three cohesive soil layers out of which the behaviour of the two upper layers are modelled with SHANSEP. The upper of the two is dike material and the other is a very soft peat layer. The third layer is a more permeable sandy clay layer and it's behaviour is modelled with Mohr-Coulomb. Figure 5.1a shows the cross section in D-Stability. This cross section was too large to evaluate with the advanced FEM code efficiently.

An adapted version of the cross section 5.1b is modelled in the advanced code in which parts that are found to be unnecessary are left out in order to reduce the amount of elements that are produced and evaluated. The canal, the dike itself and some distance away from the dike's toe are thought to be important for the analysis. The cross-section is cut-off vertically at the sand layer as sands are stiff compared to cohesive layers which makes it the perfect bottom boundary.

A small distributed load was modelled on top the dike simulating traffic loads. There were difficulties modelling those loads in the FEM code and are therefore left out. The mesh 5.1c consists of regular and irregular quadrilaterals with a maximum size of 0.5m by 0.5m.

Input parameters are summed up in table 5.1d. The original data did not include elastic moduli. Table 2B of Eurocode 7 is consulted to select a proper value of Young's modulus considering the soil type and its volumetric weight. Minding the guidelines in WBI2017, the assumption to model the cohesive soils with the SHANSEP model inherently indicates undrained behaviour. Therefore a Poisson's ratio of 0.49 is assumed. A proper value of 0.3 is found to be suitable for the drained sandy clay layer.

5.1. Deterministic analysis

Figure 5.2a shows the magnitude of the major principal stress. Due to the very low buoyant weight ($0.19 kN/m^3$) of the peat layer, the major principal stress is very low under the canal and other side of the dike. The weight in the middle is relatively high due to the weight of dike material.

The effect of the major principal stress is reflected back to the undrained shear strength field 5.2c, the dike body has a higher shear strength relative to both sides of the dike. The shear strength in the upper clay layer is higher compared to the peat layer as the POP is significantly higher. The POP is significant to the SHANSEP strength of shallow layers.

The failure mechanism 5.2d is an oval shaped arc with two branches on the right handside; a branch that finishes the arc close to the dike's toe and another branch that continues to slip trough the boundary of the peat and sandy clay layer and eventually rise to the surface far away. The factor of safety is 1.98.

5.2. RFEM

Three RFEM simulations with 500 evaluations each and different combinations of correlation lengths are run. The scales of fluctuations are assumed to be the same in every soil layer and are chosen arbitrarily. A
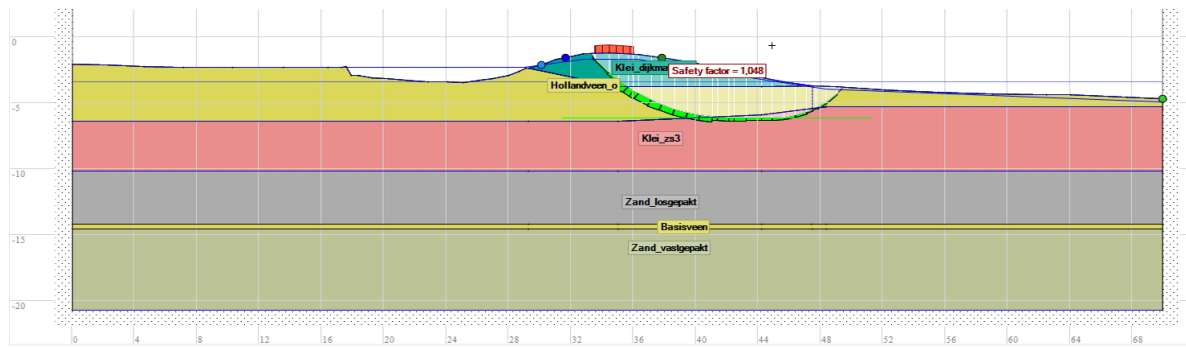
(a) Cross section in D-Stability
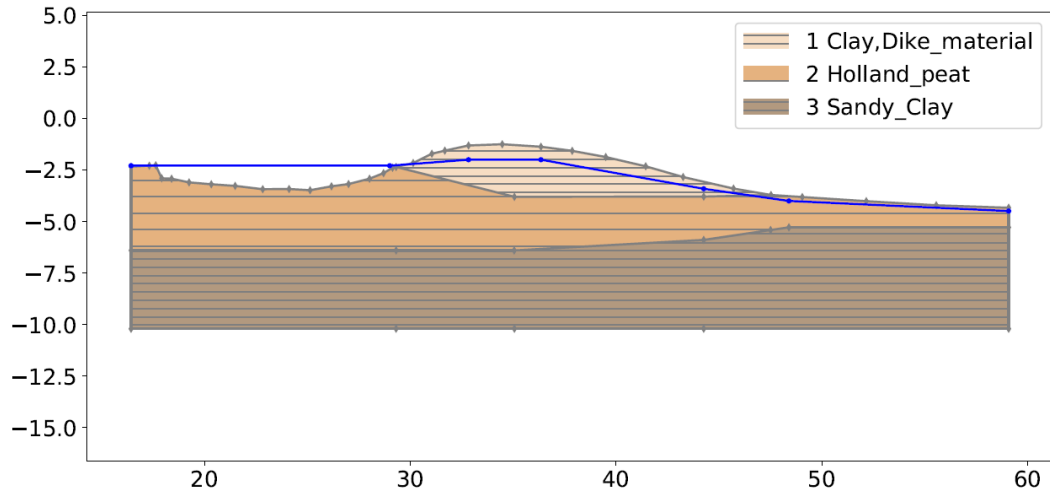
(b) Adapted cross section
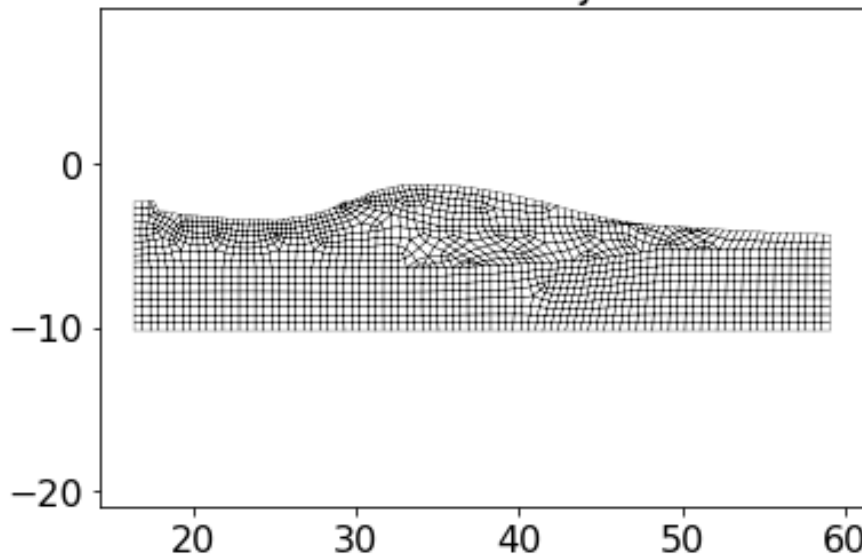
(c) Mesh

	μ_S	σ_S	μ_m	σ_m	μ_{POP}	σ_{POP}	γ_d	γ_w	E	ν
Layer 1	0.31	0.03	0.9	0.03	32.55 kPa	7.5 kPa	$13.9 \frac{kN}{m^3}$	$13.9 \frac{kN}{m^3}$	1 MPa	0.49
Layer 2	0.39	0.024	0.9	0.03	10.228 kPa	2.2 kPa	$10 \frac{kN}{m^3}$	$10 \frac{kN}{m^3}$	0.2 MPa	0.49
	c		μ_ϕ	σ_ϕ			γ_d	γ_w	E	ν
Layer 3	0		33.8 °	1°			$19.74 \frac{kN}{m^3}$	$19.74 \frac{kN}{m^3}$	5 MPa	0.3

(d) Adapted cross section

Figure 5.1: Cross section in D-Stability(a) and an adapted version of cross section (b), the mesh (c) and input values (d) in the evaluation of the stability of the Broekermeerdijk.
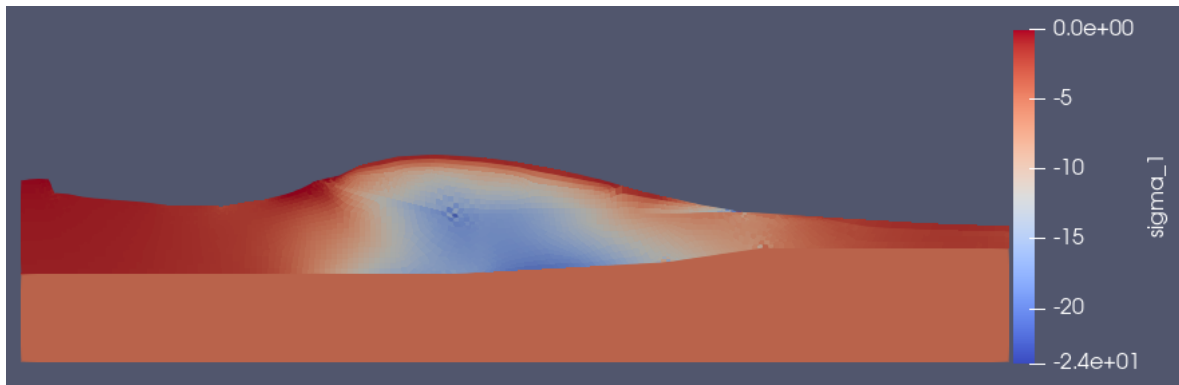
(a) Major principal stress
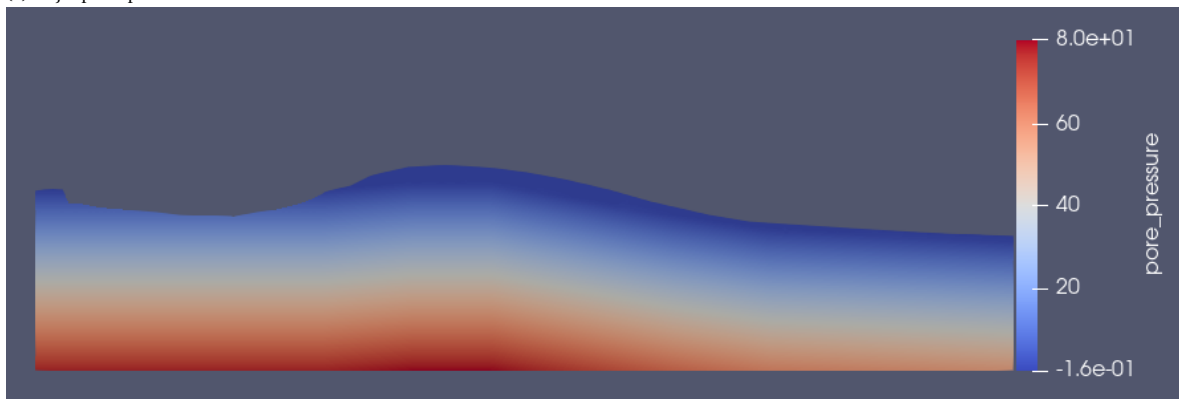
(b) Pore pressure
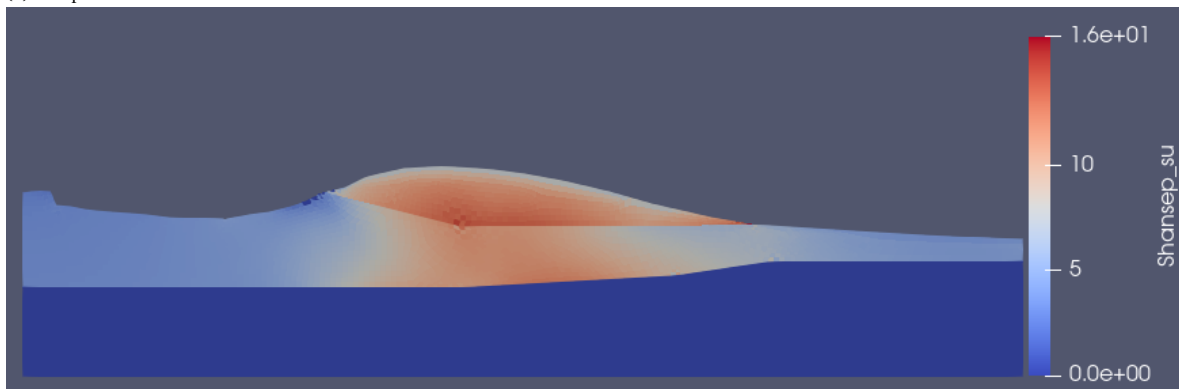
(c) Undrained Shear Strength
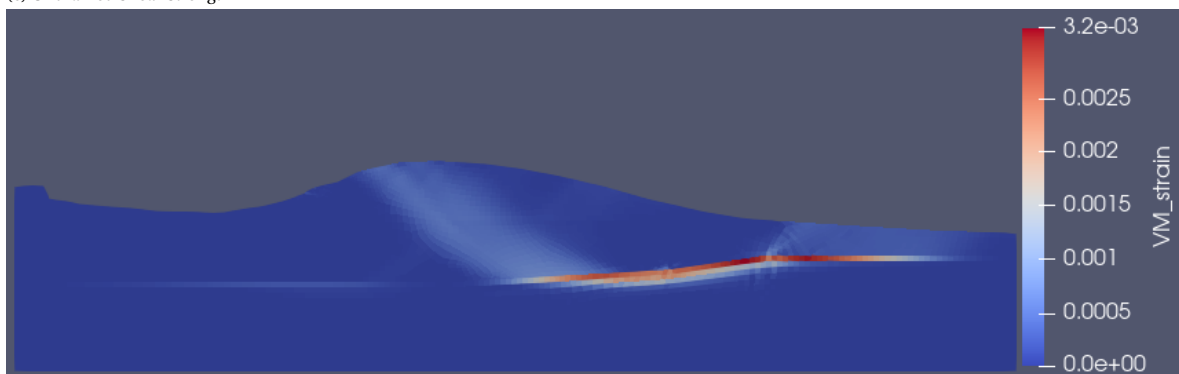
(d) Failure mechanism

Figure 5.2: The major principal stress (a), pore pressure field (b), undrained shear strength (c) and failure mechanism (d) of the deterministic analysis.
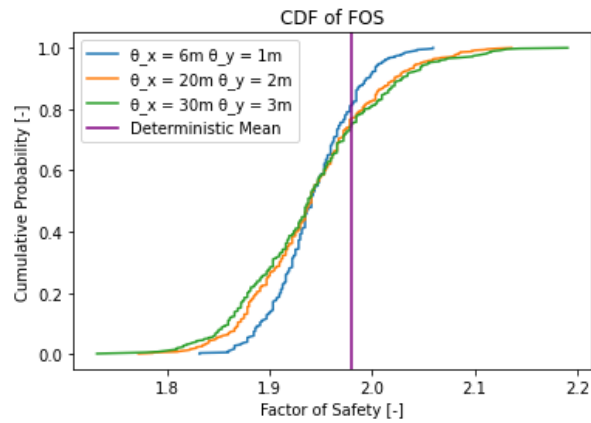
Figure 5.3: Cumulative distribution of RFEM analyses on a cross section of the Broekermeerdijk.

simulation with very low values was not desirable as, considering the mesh size, alliasing could occur.

Figure 5.4a shows the undrained shear strength field of a single evaluation of the RFEM analysis with $\theta_x = 6m$ and $\theta_y = 1m$. Due to the combination of the vertical correlation length and the thickness of the peat layer, the vertical variation is not obvious. However, some variation is noticed also in the random fields of parameter S and POP (figures 5.4c&5.4d).

Although some vertical variation exists, the major slip surface 5.4b is observed to be the same as the deterministic analysis in all evaluations. This geometry is thought to be forced as the arc the slip surface makes intersects with a stiffer layer, making the boundary of the two layers the lowest zone with low resistance. Some small lateral variation (less than a meter) is observed at the top part of the slip surface.

Although the geometry of the slip surfaces did not change, the use of different values of correlation length resulted in different distributions of FOS outcomes. There is a small descending trend in their mean with increasing correlation length. The mean of the deterministic analysis is higher than in any RFEM simulation. The spread in results show that the standard deviation increases with increasing correlation length. This trend is caused by averaging towards the mean at decreasing correlation length as explained in the previous chapter.

5.3. Comparison single layer analysis

The results of the Broekermeerdijk case study show that even in instances where a certain failure mechanism is forced by a combination of dike geometry and stratigraphy, the results are in line with the observations made in the single layer analysis regarding the factor of safety; (1) a deterministic evaluation with mean values gives a higher factor of safety that the mean of FOS outcomes of any RFEM analysis, (2) the spread in FOS outcomes increases with increasing correlation length and (3) this is translated to higher failure probabilities. The findings of this chapter confirms the findings of the previous chapter.

(a) Undrained shear strength

(b) Slip surface

(c) Parameter S

(d) Pre-overburden pressure
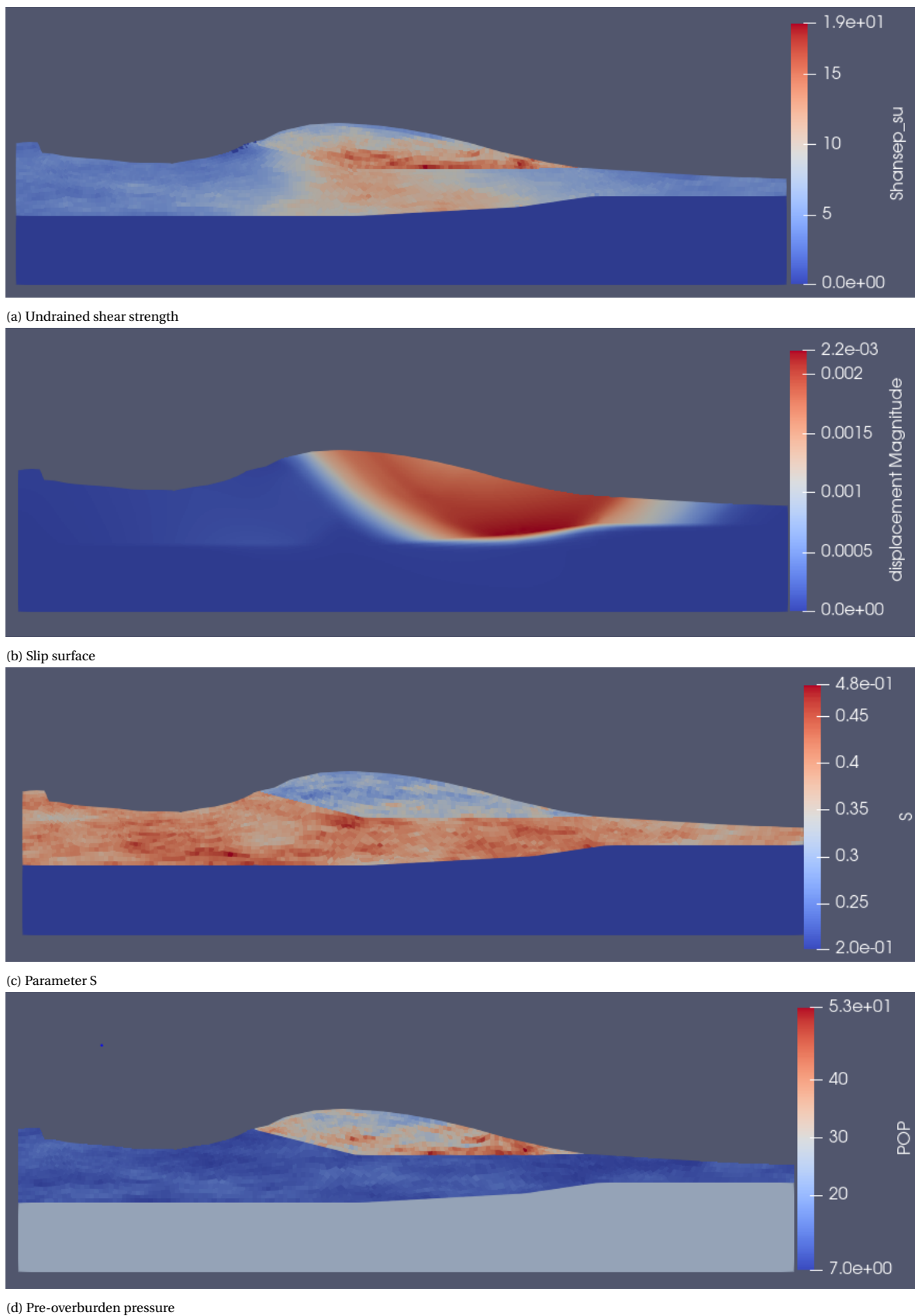
Figure 5.4: The undrained shrea strength (a), failure mechanism (b) and random fields (c,d) of a single realisation out of a RFEM analysis consisting of 25 realisations. Only minor insignificant changes in slip surface are observed in the remaining slip surfaces.

6

Discussion & Conclusion

The main objective of this thesis is to develop a FEM code that combines the effects of stress dependent variation of the SHANSEP constitutive model with the natural variation of strength parameters reached through the Random Finite Element Method to investigate preliminarily what difference the outcome would yield against a deterministic analysis. The outcome could be used to determine if further investigation is necessary on the application of RFEM to the assessment of Dutch Dikes in the future. The thesis will be concluded with a discussion on the most important findings by answering the research questions formulated in the introduction.

In what ways can the variation of random field be combined with variation of shear strength created SHANSEP? Which method is practical?

The SHANSEP formulation relates the undrained shear strength to the vertical effective stress and three model parameters. Model parameters S and m are objective in the sense that their values are stress independent. They are observed to show variation whether through physical causes (natural variations) and measuring uncertainties. A similar variation is observed for POP estimations from both CPT tests and laboratory test. Therefore a good starting point would be to consider the three model parameters as stochastic variables. Following examples in literature, the random variables are assumed to be distributed lognormally. There are no indications of a trend in the mean and standard deviation of any random variable. The only exception are local increases of POP (overconsolidation) due to surface loads from non-natural source, which imposes a horizontal trend. These effects are disregarded. The Cholesky decomposition method is found to be suitable for the generation of random fields.

In chapter 3 it is explained that the major principal stress is believed to be a more objective representation of the stress conditions in contrast to the vertical effective stress used in the original formulation. It is the most compressive stress irrespective of (the orientation of) the stress field.Laboratory test data show that the model parameters determined for the original SHANSEP formulation needs adjustments in case the consolidation happens in rotated stress fields. The adjustments are believed to be related to the ratio between vertical effective stress and major principal stress. The reason that the original formulation works well in k_0-consolidation and triaxial compression could be related to the fact that the vertical effective stress is equal to the major principal stress in those conditions. As stress fields in a dike body are rotated, the use of the major principal stress is will be more objective.

Soils are inherently anisotropic, meaning that their behaviour is direction dependent. Furthermore, the ADP method for dikes distinguishes three shearing modes in which the soils' behaviour is highly correlated to three different laboratory tests. The anisotropy in both the stress paths of the shearing modes and the soil behaviour causes discrepancy of mobilised shear strength at equal shear strain. This needs attention in the light of the strain compatibility assumption. There are two approaches formulated to deal with this.

The first approach is the use of the ultimate state strength. The mobilised shear strength is equal at the ultimate state strength. The Dutch guidelines recommend the use of 25% shear strain in triaxial tests.

The second approach is to use the mobilised shear strength at a certain shear strain. This is achieved using

a workaround in our linear elastic perfectly plastic SHANSEP constitutive model. The workaround requires determining the SHANSEP parameters at a certain shear strain, preferably at peak triaxial comppression and reduce the undrained shear strength for the other shearing modes depending on the orientation of the major principal stress with respect to the vertical plane.This way a continuous reduction in undrained shear strength is achieved.

How can be guaranteed that random fields will not result in physically impossible circumstances ?

There were no instances found were the use of random fields on SHANSEP parameters resulted in physically impossible circumstances as anticipated at the beginning of the project. The main concern was that the generation of random fields for POP would result in instances where a point would have higher pre-consolidation pressures with respect to points deeper down on a horizontal surface. This is impossible as deeper layers are older and thus are subjected to the same surface loads as their neighbours on top of them. However, this representation disregards any secondary source of overconsolidation (chemical, biological and hydrological) which makes the overconsolidation varying randomly, also with depth.

A physically impossible circumstance is having a negative value for the model parameters with the use of a normal distribution. This is easily counteracted by the general assumption of using a lognormal distribution.

What difference in failure mechanism, factor of safety and probability of failure does the use of RFEM yield with respect to a deterministic analysis?

A review of generated RF evaluation in chapter 4 show that, for both approaches, the slip surfaces calculated by RFEM tend to go through local weak spots in the random fields. The random fields of parameter S and POP were found to be more influential.

In both models, the estimated probability of failure by FOSM was at least one order of magnitude higher compared to RFEM. The FOSM analysis is therefore conservative. As the mean of FOS of FOSM is equivalent to a deterministic analysis with mean values, it is expected that a deterministic approach is conservative too. The lower failure probability is explained by a lower spread in FOS outcomes from the RFEM model. A lower correlation length causes the slip surface to alternate more between weak and strong zones leading to averaging towards the mean of the strength.

Chapter 5 shows that although generally slip surfaces computed by RFEM prefer weak zones in random fields, for cross-sections that have a preferential slip surface due to geometry and stratigraphy, the slip surfaces do not vary. However, the factor of safety still does vary and show a similar trend as found in chapter 4. A larger correlation length increases the standard deviation of the outcomes. The results are a confirmation of the findings in chapter 4.

6.1. Recommendations

The major limitation of this project is the inability to model the stress-strain behaviour of cohesive soils accurately. The use of the viscoplastic algorithm forces the use of a linear elastic perfectly plastic constitutive model. Those models are unable to capture anisotropic behaviour of clays. A potential improvement would be the use of the SHANSEP/NGI-ADP constitutive model in conjunction with elastoplasticity. Although this is already implemented into PLAXIS which does not have the ability to create random fields. It could be investigated whether a constitutive model that capture the full behaviour of soil will give different results.

As the results of this thesis are based on numerical models, a confirmation with experimental methods would improve the validity of the results. However, it is has to be kept in mind that it is difficult or almost impossible to set up an experiment in which the scale of fluctuation of soil parameters is controlled. A solution would be to fail an existing dikes or build up dikes, where the statistical data is determined with a geotechnical investigation.

The FOSM method is conservative. The most conservative RFEM simulation has an estimated probability of failure which is one order of magnitude lower. As the approach of the Dutch guidelines are probably are even more conservative due to its general nature, Dutch policy makers could look into RFEM, rather than the methods of slices with partial factors, to estimate failure probabilities. A suggested method is using conservative values of correlation lengths.

Bibliography

Agaiby, S. S., & Mayne, P. W. (2019). CPT Evaluation of Yield Stress Profiles in Soils. *Journal of Geotechnical and Geoenvironmental Engineering, 145*(12), 04019104. https://doi.org/10.1061/(asce)gt.1943-5606.0002164

Anandarajah, A., Kuganentira, N., & Zhao, D. (1996). VARIATION OF FABRIC ANISOTROPY OF KAOLINITE IN TRIAXIAL LOADING. *Journal of Geotechnical Engineering, 122*(8), 633–640.

Bishop, A. W. (1955). The use of the slip circle in the stability analysis of slopes. *Geotechnique, 5*(1), 7–17. https://doi.org/10.1680/geot.1955.5.1.7

Cormeau, I. (1975). Numerical stability in quasi-static elasto/visco-plasticity. *International Journal for Numerical Methods in Engineering, 9*(1), 109–127. https://doi.org/10.1002/nme.1620090110

Duncan, J. M., & Seed, H. B. (1966). Anisotropy and Stress reorientation in Clay. *Journal of the Soil Mechanics and Foundations Division, 92*(SM5), 21–50.

Fenton, G. A., & Griffiths, D. V. (2008). *Risk Assessment in Geotechnical Engineering.* John Wiley & Sons.

Green, D. K., Douglas, K., & Mostyn, G. (2015). The simulation and discretisation of random fields for probabilistic finite element analysis of soils using meshes of arbitrary triangular elements. *Computers and Geotechnics, 68*, 91–108. https://doi.org/10.1016/j.compgeo.2015.04.004

Jardine, R. J., & Menkiti, C. O. (1999). THE UNDRAINED ANISOTROPY OF K0 CONSOLIDATED SEDIMENTS. *Twelfth European Conference on Soil Mechanics and Geotechnical Engineering*, 1101–1108.

Koning, M. D., Goeman, D. G., Bakker, H. L., Haasnoot, J. K., & Bisschop, C. (2019). Determination of SHANSEP parameters by laboratory tests and CPTu for probabilistic model-based safety analyses Détermination de paramètres SHANSEP par essais en laboratoire et CPTu pour analyses à base de modèle probabilistes de sécurité, 1–9. https://doi.org/10.32075/17ECSMGE-2019-0073

Ladd, C. C. (1991). Stability Evaluation During Staged Construction. *Journal of Geotechnical Engineering, 117*(4), 540–615.

Ladd, C. C., & Foott, R. (1974). New Design Procedure For Stability of Soft Clays. *Journal of the geotechnical engineering division, 100*(7), 763–786.

Leroueil, S., & Vaughan, P. R. (1990). The general and congruent effects of structure natural soils and weak rocks. *Géotechnique, 40*(3), 467–488.

Lewin, P. I. (1973). The influence of stress history on plastic potential. *Proceedings of the symposium on the role of plasticity in soil mechanics*, 96–107.

Low, H. E., Maynard, M. L., Randolph, M. F., & Degroot, D. J. (2011). Geotechnical characterisation and engineering properties of Burswood clay. *Geotechnique, 61*(7), 575–591. https://doi.org/10.1680/geot.9.p.035

Mesri, G. (1975). Discussion. *Journal of the geotechnical engineering division, 101*(GT4), 409–412.

Ministerie van Infrastructuur en Milieu. (2016a). Fenomenologische beschrijving, 208.

Ministerie van Infrastructuur en Milieu. (2016b). *Voorschriften toetsen op veiligheid niet-primaire waterkeringen in rijksbeheer* (tech. rep.).

Ministerie van Infrastructuur en Milieu. (2017). Regeling veiligheid primaire waterkeringen 2017 Bijlage III Sterkte en veiligheid. (april 2016), 169.

Ministerie van Infrastructuur en Waterstaat. (2017). Schematiseringshandleiding Macrostabiliteit. (december 2016), 173.

Nishimura, S., Minh, N. A., & Jardine, R. J. (2007). Shear strength anisotropy of natural London Clay. *Géotechnique, 57*(1), 49–62. https://doi.org/10.1680/ssc.41080.0009

Panagoulias, S., & Brinkgreve, R. B. J. (2017). *SHANSEP NGI-ADP - Model description and verification examples* (tech. rep.). POV Macrostabiliteit. https://www.povmacrostabiliteit.nl/wp-content/uploads/2015/03/SHANSEP%7B%5C_%7DNGIADP.pdf

Pineda, J. A., Suwal, L. P., Kelly, R. B., Bates, L., & Sloan, S. W. (2016). Characterisation of Ballina clay. *Geotechnique, 66*(7), 556–577. https://doi.org/10.1680/jgeot.15.P.181

Schofield, A., & Wroth, P. (1968). *Critical State Soil Mechanics.*

Smith, I. M., Griffiths, D. V., & Margetts, L. (2014). *Programming the Finite Element Method* (5th). John Wiley & Sons.

Tanaka, H., Shiwakoti, D. R., & Tanaka, M. (2003). Applicability of SHANSEP method to six different natural clays, using triaxial and direct shear tests. *Japanese Geotechnical Society, 43*(3), 43–55.

Van, M. A. (2001). New Approach for Uplift Induced Slope Failure. *International conference on Soil Mechanics and Geotechnical Engineering*, 2285–2288.

Van de Meij, R. (2012). Afschuiving langs een vrij glijvlak. *Geotechniek*.

van den Eijnden, A. P., & Hicks, M. A. (2017). Efficient subset simulation for evaluating the modes of improbable slope failure. *Computers and Geotechnics, 88*, 267–280. https://doi.org/10.1016/j.compgeo.2017.03.010

van Duinen, A. (2014). *Ongedraineerde schuifsterkte bij toetsspoor macrostabiliteit in WTI 2017 - informatie voor besluitvormingsproces* (tech. rep.). Deltares.

Vanmarcke, E. (2010). *Random Fields: Analysis and synthesis*. World Scientific Publishing Co. Pte. Ltd.

Vrijling, J. K., Schweckendiek, T., & Kanning, W. (2011). Safety Standards of Flood Defenses. *3rd International Syposium on Geotechnical Safety and Risk (ISGSR 2011)*, (July 2014).

Zhang, G., & Wang, M. (2019). Development of Eight-Node Curved-Side Quadrilateral Membrane Element Using Chain Direct Integration Scheme (SCDI) in Area Coordinates (MHCQ8-DI). *Arabian Journal for Science and Engineering, 44*(5), 4703–4724. https://doi.org/10.1007/s13369-018-3521-7

A

Shape functions of 8 node quadrilaterals

$$N1 = \frac{1}{4}(1-\xi)(1-\eta)(-\xi-\eta-1) \tag{A.1}$$

$$N2 = \frac{1}{2}(1-\xi)(1-\eta^2) \tag{A.2}$$

$$N3 = \frac{1}{4}(1-\xi)(1+\eta)(-\xi+\eta-1) \tag{A.3}$$

$$N4 = \frac{1}{2}(1-\xi^2)(1+\eta) \tag{A.4}$$

$$N5 = \frac{1}{4}(1+\xi)(1+\eta)(\xi+\eta-1) \tag{A.5}$$

$$N6 = \frac{1}{2}(1+\xi)(1-\eta^2) \tag{A.6}$$

$$N7 = \frac{1}{4}(1+\xi)(1-\eta)(\xi-\eta-1) \tag{A.7}$$

$$N8 = \frac{1}{2}(1-\xi^2)(1-\eta) \tag{A.8}$$

The shape functions of 8 node quadrilaterals. Shape functions are used in the conversion between local and global coordinates.

Random field generator

The random field generator starts with the definition of two classes containing model and soil parameters. This is followed by two functions which are translated and adapted from the FEM program. Thirdly, the coordinates of the integration points are calculated. Finally, the random fields are generated and saved into text files.

```python
"""
Created on Fri May 21 16:21:05 2021

Random field generator FEM

@author: Esat Unal
"""
import numpy as np
import os
import scipy.spatial as sp
import time

start = time.time()
iversion = 0 # 0 for principal stress, 1 for no correction factor applied
os.chdir(r"C:\Users\e-una\Desktop\vergelijksesc\sesc010") # Define path of FEM program

class geom:
    w1 = 20.
    s1 = 20.
    w2 = 20.
    h1 = 10.
    h2 = 5.
    nx1= 20
    nx2= 10
    ny1= 20
    ny2= 10

    nfield = 1

    geometry_data = np.array([w1,s1,w2,h1,h2,nx1,nx2,ny1,ny2,nfield]).reshape([-1,1])

    np_types = 1
    nye = ny1 + ny2
    nels = nx1*nye + ny2*nx2
    nn = (3*nye+2)*nx1 + 2*nye + 1 + (3*ny2+2)*nx2
```

```python
        nip  = 4
        ntip = nels * nip
        ndim = 2

        thetax = 15.
        thetay = 1.5

class SP:
    pars_mean = 0.2
    pars_cov  = 0.1
    pars_std_ln = np.sqrt(np.log(1+pars_cov**2))
    pars_mean_ln = np.log(pars_mean) - 0.5 * pars_std_ln**2

    parm_mean = 0.8
    parm_cov  = 0.1
    parm_std_ln = np.sqrt(np.log(1+parm_cov**2))
    parm_mean_ln = np.log(parm_mean) - 0.5 * parm_std_ln**2

    pop_mean = 25
    pop_cov  = 0.1
    pop_std_ln = np.sqrt(np.log(1+pop_cov**2))
    pop_mean_ln = np.log(pop_mean) - 0.5 * pop_std_ln**2

def emb2Dgeom(iel,geom):

    w1 = geom.w1
    s1 = geom.s1
    w2 = geom.w2
    h1 = geom.h1
    h2 = geom.h2
    nx1 = geom.nx1
    nx2 = geom.nx2
    ny1 = geom.ny1
    ny2 = geom.ny2
    one = 1
    pt5 = 0.5

    nxe=nx1+nx2
    nye=ny1+ny2
    nt=nx1*ny1
    nc=(3*nye+2)*nx1+2*ny1
    facx=s1/ny1
    facy=h1/ny1
    facb=(w1+s1)/nx1
    facs=0.
    if ny2!=0:
        facs=h2/ny2
    frh=0.0
    if nx2!=0:
        frh=w2/nx2
    if iel<=nt:
        iq=np.int((iel-1)/nx1+1)
        ip=np.int(iel-(iq-1)*nx1)
    else:
        iq=np.int((iel-nt-1)/nxe+ny1+1)
        ip=np.int(iel-nt-(iq-ny1-1)*nxe)
```

```python
    num   = np.zeros([8])
    coord = np.zeros([8,2])
    if ip<=nx1:
        num[0]=(ip-1)*(3*nye+2)+2*iq+1
        num[1]=num[0]-1
        num[2]=num[0]-2
        num[3]=(ip-1)*(3*nye+2)+2*nye+iq+1
        num[4]=ip*(3*nye+2)+2*iq-1
        num[5]=num[4]+1
        num[6]=num[4]+2
        num[7]=num[3]+1
        if iq<=ny1:
            coord[0,0]=(ip-one)*(wl+iq*facx)/nx1
            coord[2,0]=(ip-one)*(wl+(iq-1)*facx)/nx1
            coord[4,0]=ip*(wl+(iq-1)*facx)/nx1
            coord[6,0]=ip*(wl+iq*facx)/nx1
            coord[0,1]=-iq*facy
            coord[2,1]=-(iq-1)*facy
            coord[4,1]=-(iq-1)*facy
            coord[6,1]=-iq*facy
        else:
            coord[0,0]=(ip-one)*facb
            coord[2,0]=(ip-one)*facb
            coord[4,0]=ip*facb
            coord[6,0]=ip*facb
            coord[0,1]=-h1-(iq-ny1)*facs
            coord[2,1]=-h1-(iq-ny1-1)*facs
            coord[4,1]=-h1-(iq-ny1-1)*facs
            coord[6,1]=-h1-(iq-ny1)*facs
    else:
        num[0]=nc+(ip-nx1-1)*(3*ny2+2)+2*(iq-ny1)+1
        num[1]=num[0]-1
        num[2]=num[0]-2
        num[3]=nc+(ip-nx1-1)*(3*ny2+2)+2*ny2+iq-ny1+1
        num[4]=nc+(ip-nx1)*(3*ny2+2)+2*(iq-ny1)-1
        num[5]=num[4]+1
        num[6]=num[4]+2
        num[7]=num[3]+1
        coord[0,0]=wl+s1+(ip-nx1-1)*frh
        coord[2,0]=coord[0,0]
        coord[4,0]=wl+s1+(ip-nx1)*frh
        coord[6,0]=coord[4,0]
        coord[0,1]=-h1-(iq-ny1)*facs
        coord[2,1]=-h1-(iq-ny1-1)*facs
        coord[4,1]=-h1-(iq-ny1-1)*facs
        coord[6,1]=-h1-(iq-ny1)*facs

    coord[1:6:2,:]=pt5*(coord[0:5:2,:]+coord[2:7:2,:])
    coord[7,:]=pt5*(coord[6,:]+coord[0,:])
    return coord, num

def shapefun(iip,coord):
    sq3 = np.sqrt(1./3)
    xi  = np.array([-sq3,sq3,-sq3, sq3])
    etan = np.array([sq3,sq3,-sq3,-sq3])
```

```python
        ksi = xi[iip]
        eta = etan[iip]

        etam=0.25*(1.-eta)
        etap=0.25*(1.+eta)
        xim=0.25*(1.-ksi)
        xip=0.25*(1.+ksi)

        fun = np.zeros([8])
        fun[0] = 4.*etam*xim*(-ksi-eta-1.)
        fun[1] = 32.*etam*xim*etap
        fun[2] = 4.*etap*xim*(-ksi+eta-1.)
        fun[3] = 32.*xim*xip*etap
        fun[4] = 4.*etap*xip*(ksi+eta-1.)
        fun[5] = 32.*etap*xip*etam
        fun[6] = 4.*xip*etam*(ksi-eta-1.)
        fun[7] = 32.*xim*xip*etam

        '''
        fun[0] = 0.25 * (1-ksi) * (1-eta) * (-ksi -eta -1)
        fun[1] = 0.5 * (1-ksi) * (1-eta**2)
        fun[2] = 0.25 * (1-ksi) * (1+eta) * (-ksi +eta -1)
        fun[3] = 0.5 * (1-ksi**2) * (1+eta)
        fun[4] = 0.25 * (1+ksi) * (1+eta) * ( ksi +eta -1)
        fun[5] = 0.5 * (1+ksi) * (1-eta**2)
        fun[6] = 0.25 * (1+ksi) * (1-eta) * ( ksi -eta -1)
        fun[7] = 0.5 * (1-ksi**2) * (1-eta)
        '''

        coord_ip = np.zeros([2])
        for i in range(0,8):
            coord_ip = coord_ip + fun[i]*coord[i,:]

        return coord_ip

# Find coordinates of integration points
g_num = np.zeros([8,geom.nels])
g_coord = np.zeros([geom.ndim,geom.nn])
g_coord_ip = np.zeros([geom.ndim,geom.ntip])
for iel in range(0,geom.nels):
    coord , num = emb2Dgeom(iel+1,geom)
    num = num.astype(int)
    g_num[:,iel] = num
    g_coord[:,num-1] = np.transpose(coord)
    for iip in range(0,geom.nip):
        coord_ip = shapefun(iip,coord)
        g_coord_ip[:,iel*geom.nip+iip] = np.transpose(coord_ip)

# Cholesky decomposition + Distance matrix
coord_x = np.reshape(g_coord_ip[0,:],[-1,1])
coord_y = np.reshape(g_coord_ip[1,:],[-1,1])
Dx = sp.distance_matrix(coord_x,coord_x)
Dy = sp.distance_matrix(coord_y,coord_y)
corr = np.exp(-2 * np.sqrt((Dx/geom.thetax)**2+(Dy/geom.thetay)**2))
sqrt = np.linalg.cholesky( (np.exp(corr)-1) / (np.exp(1)-1))
```

```python
# Create random fields
pop_rdnl = sqrt @ np.random.normal(0.,1.,size = [geom.ntip,geom.nfield])
pop = np.exp(pop_rdnl * SP.pop_std_ln + SP.pop_mean_ln)

pars_rdnl = sqrt @ np.random.normal(0.,1.,size = [geom.ntip,geom.nfield])
pars = np.exp(pars_rdnl * SP.pars_std_ln + SP.pars_mean_ln)

parm_rdnl = sqrt @ np.random.normal(0.,1.,size = [geom.ntip,geom.nfield])
parm = np.exp(parm_rdnl * SP.parm_std_ln + SP.parm_mean_ln)


# Save text files
np.savetxt('pop.txt',np.transpose(pop))
np.savetxt('pars.txt',np.transpose(pars))
np.savetxt('parm.txt',np.transpose(parm))
np.savetxt('geometry.txt',geom.geometry_data)

if iversion == 0:
    os.system(r'FEMpstress.exe')
elif iversion == 1:
    os.system(r'nored.exe')
else:
    print("SHANSEP version not understood")


end = time.time()
print("This script took %0.4f seconds to run." %(end-start))
```

C

Orientation of principal stresses
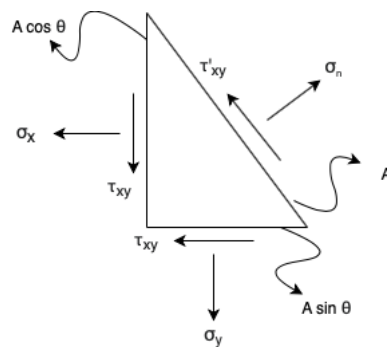
Figure C.1: Schematisation of the force equilibrium that needs to be solved in order to transform cartesian stresses to any orientation.

Consider the (force) stress equilibrium in figure C.1. σ_x and σ_y are the cartesian stresses in horizontal and vertical direction, τ_{xy} is the shear stress and σ_n and τ'_{xy} are the normal stress and shear stress for any orientation θ, the angle between the shear stress and vertical plane. This angle is the same as the angle between the normal stress and the vertical plane. A is the length of the line on which σ_n acts. For a general representation in which θ is variable, the lengths of lines on which the horizontal and vertical normal stresses act are $A\cos\theta$ and $A\sin\theta$, respectively.

From force equilibrium the, projected shear stress (τ'_{xy}) can be expressed mathematically as:

$$\tau'_{xy} = 0.5(\sigma_y - \sigma_x)\sin\theta\cos\theta) + \tau_{xy}(\cos^2\theta - \sin^2\theta) \tag{C.1}$$

$\tau'_{xy} = 0$ in the principal stress convention. Using trigonometric identities $2\sin\theta\cos\theta = \sin 2\theta$ and $\cos^2\theta - \sin^2\theta = \cos 2\theta$,the formulation becomes:

$$0.5(\sigma_y - \sigma_x)\sin 2\theta + \tau_{xy}\cos 2\theta = 0 \tag{C.2}$$

Some rearrangement gives:

$$\frac{\sin 2\theta}{\cos 2\theta} = \frac{-2\tau_{xy}}{\sigma_y - \sigma_x} \tag{C.3}$$

Which is equal to:

$$\tan 2\theta = \frac{2\tau_{xy}}{\sigma_x - \sigma_y} \tag{C.4}$$

Equation C.4 gives an orientation between -45°and +45°of any principal stress (σ_1 and σ_3). A correction of 90 degrees needs to be applied in case the orientation of the minor principal stress is calculated. The formulation will give the orientation of the minor principal stress if the orientation exceeds 45 degrees. The result will be a
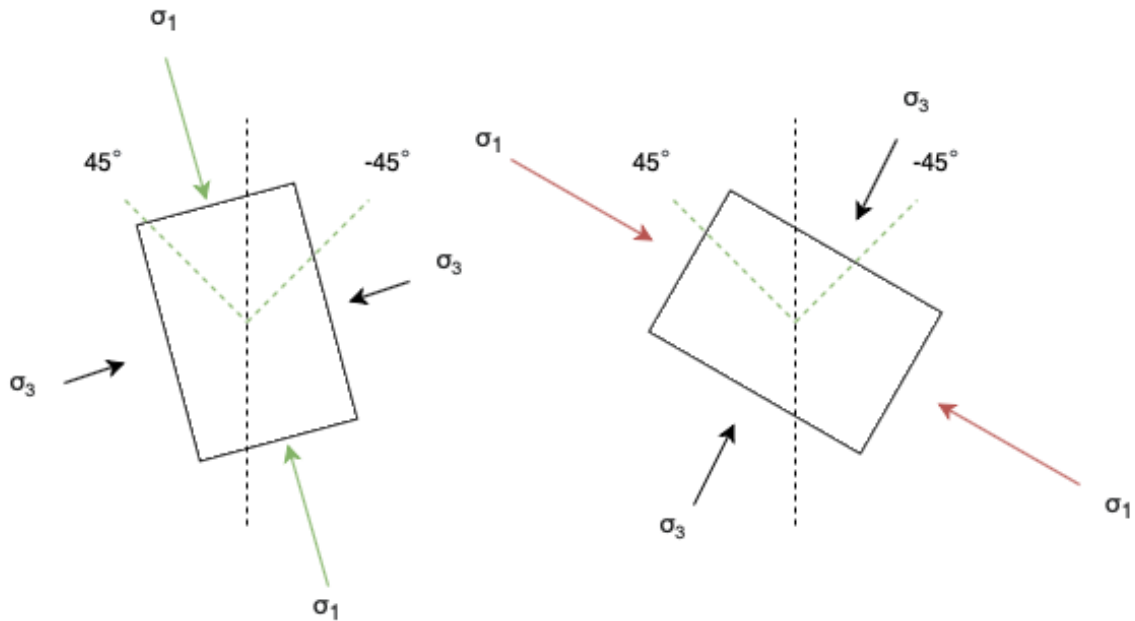
Figure C.2: Orientations equation C.4 gives without correction.

negative orientation. Adding 90 degrees to any negative value will not do the trick as negative σ_1 orientation would also be falsely corrected. However, it is expected that the horizontal stress is larger than the vertical stress in case the orientation of of σ_1 is larger than 45°. This will be used as a second requirement of the correction.

The same is expected to happen for orientations smaller than -45°. In this case the requirements is a positive orientation with a larger horizontal stress with respect to the vertical stress.

$$IF[(\alpha > 0 \ AND \ \sigma_3 > \sigma_1 \quad OR \quad (\alpha < 0 \ AND \ \sigma_3 > \sigma_1)] \quad THEN \quad \alpha = \alpha + 90 \tag{C.5}$$

D

Python script random field generator

```python
"""
Created on Fri May 21 16:21:05 2021

Random field generator FEM

@author: Esat Unal
"""
import numpy as np
import os
import scipy.spatial as sp
import time

start = time.time()
iversion = 0 # 0 for principal stress, 1 for no correction factor applied
os.chdir(r"C:\Users\e-una\Desktop\vergelijksesc\sesc010") # Define path of FEM program

class geom:
    w1 = 20.
    s1 = 20.
    w2 = 20.
    h1 = 10.
    h2 = 5.
    nx1= 20
    nx2= 10
    ny1= 20
    ny2= 10

    nfield = 1

    geometry_data = np.array([w1,s1,w2,h1,h2,nx1,nx2,ny1,ny2,nfield]).reshape([-1,1])

    np_types = 1
    nye = ny1 + ny2
    nels = nx1*nye + ny2*nx2
    nn = (3*nye+2)*nx1 + 2*nye + 1 + (3*ny2+2)*nx2
    nip = 4
    ntip = nels * nip
    ndim = 2
```

```
    thetax  =  15.
    thetay  =  1.5


class  SP:
    pars_mean  =  0.2
    pars_cov   =  0.1
    pars_std_ln  =  np.sqrt(np.log(1+pars_cov**2))
    pars_mean_ln  =  np.log(pars_mean)  -  0.5  *  pars_std_ln**2

    parm_mean  =  0.8
    parm_cov   =  0.1
    parm_std_ln  =  np.sqrt(np.log(1+parm_cov**2))
    parm_mean_ln  =  np.log(parm_mean)  -  0.5  *  parm_std_ln**2

    pop_mean  =  25
    pop_cov   =  0.1
    pop_std_ln  =  np.sqrt(np.log(1+pop_cov**2))
    pop_mean_ln  =  np.log(pop_mean)  -  0.5  *  pop_std_ln**2


def  emb2Dgeom(iel ,geom ):

    w1  =  geom.w1
    s1  =  geom.s1
    w2  =  geom.w2
    h1  =  geom.h1
    h2  =  geom.h2
    nx1  =  geom.nx1
    nx2  =  geom.nx2
    ny1  =  geom.ny1
    ny2  =  geom.ny2
    one  =  1
    pt5  =  0.5


    nxe=nx1+nx2
    nye=ny1+ny2
    nt=nx1*ny1
    nc=(3*nye+2)*nx1+2*ny1
    facx=s1/ny1
    facy=h1/ny1
    facb=(w1+s1)/nx1
    facs=0.
    if  ny2!=0:
        facs=h2/ny2
    frh=0.0
    if  nx2!=0:
        frh=w2/nx2
    if  iel<=nt:
        iq=np.int((iel-1)/nx1+1)
        ip=np.int(iel-(iq-1)*nx1)
    else:
        iq=np.int((iel-nt-1)/nxe+ny1+1)
        ip=np.int(iel-nt-(iq-ny1-1)*nxe)
    num   =  np.zeros([8])
    coord  =  np.zeros([8,2])
    if  ip<=nx1:
        num[0]=(ip-1)*(3*nye+2)+2*iq+1
```

```
            num[1]=num[0]-1
            num[2]=num[0]-2
            num[3]=(ip-1)*(3*nye+2)+2*nye+iq+1
            num[4]=ip*(3*nye+2)+2*iq-1
            num[5]=num[4]+1
            num[6]=num[4]+2
            num[7]=num[3]+1
            if iq<=ny1:
                coord[0,0]=(ip-one)*(wl+iq*facx)/nx1
                coord[2,0]=(ip-one)*(wl+(iq-1)*facx)/nx1
                coord[4,0]=ip*(wl+(iq-1)*facx)/nx1
                coord[6,0]=ip*(wl+iq*facx)/nx1
                coord[0,1]=-iq*facy
                coord[2,1]=-(iq-1)*facy
                coord[4,1]=-(iq-1)*facy
                coord[6,1]=-iq*facy
            else:
                coord[0,0]=(ip-one)*facb
                coord[2,0]=(ip-one)*facb
                coord[4,0]=ip*facb
                coord[6,0]=ip*facb
                coord[0,1]=-h1-(iq-ny1)*facs
                coord[2,1]=-h1-(iq-ny1-1)*facs
                coord[4,1]=-h1-(iq-ny1-1)*facs
                coord[6,1]=-h1-(iq-ny1)*facs
        else:
            num[0]=nc+(ip-nx1-1)*(3*ny2+2)+2*(iq-ny1)+1
            num[1]=num[0]-1
            num[2]=num[0]-2
            num[3]=nc+(ip-nx1-1)*(3*ny2+2)+2*ny2+iq-ny1+1
            num[4]=nc+(ip-nx1)*(3*ny2+2)+2*(iq-ny1)-1
            num[5]=num[4]+1
            num[6]=num[4]+2
            num[7]=num[3]+1
            coord[0,0]=wl+s1+(ip-nx1-1)*frh
            coord[2,0]=coord[0,0]
            coord[4,0]=wl+s1+(ip-nx1)*frh
            coord[6,0]=coord[4,0]
            coord[0,1]=-h1-(iq-ny1)*facs
            coord[2,1]=-h1-(iq-ny1-1)*facs
            coord[4,1]=-h1-(iq-ny1-1)*facs
            coord[6,1]=-h1-(iq-ny1)*facs

    coord[1:6:2,:]=pt5*(coord[0:5:2,:]+coord[2:7:2,:])
    coord[7,:]=pt5*(coord[6,:]+coord[0,:])
    return coord , num

def shapefun(iip,coord):
    sq3 = np.sqrt(1./3)
    xi  = np.array([-sq3,sq3,-sq3, sq3])
    etan = np.array([sq3,sq3,-sq3,-sq3])

    ksi = xi[iip]
    eta = etan[iip]

    etam=0.25*(1.-eta)
```

```python
    etap=0.25*(1.+eta)
    xim=0.25*(1.-ksi)
    xip=0.25*(1.+ksi)

    fun = np.zeros([8])
    fun[0] = 4.*etam*xim*(-ksi-eta-1.)
    fun[1] = 32.*etam*xim*etap
    fun[2] = 4.*etap*xim*(-ksi+eta-1.)
    fun[3] = 32.*xim*xip*etap
    fun[4] = 4.*etap*xip*(ksi+eta-1.)
    fun[5] = 32.*etap*xip*etam
    fun[6] = 4.*xip*etam*(ksi-eta-1.)
    fun[7] = 32.*xim*xip*etam

    '''
    fun[0] = 0.25 * (1-ksi) * (1-eta) * (-ksi -eta -1)
    fun[1] = 0.5 * (1-ksi) * (1-eta**2)
    fun[2] = 0.25 * (1-ksi) * (1+eta) * (-ksi +eta -1)
    fun[3] = 0.5 * (1-ksi**2) * (1+eta)
    fun[4] = 0.25 * (1+ksi) * (1+eta) * ( ksi +eta -1)
    fun[5] = 0.5 * (1+ksi) * (1-eta**2)
    fun[6] = 0.25 * (1+ksi) * (1-eta) * ( ksi -eta -1)
    fun[7] = 0.5 * (1-ksi**2) * (1-eta)
    '''

    coord_ip = np.zeros([2])
    for i in range(0,8):
        coord_ip = coord_ip + fun[i]*coord[i,:]

    return coord_ip

# Find coordinates of integration points
g_num = np.zeros([8,geom.nels])
g_coord = np.zeros([geom.ndim,geom.nn])
g_coord_ip = np.zeros([geom.ndim,geom.ntip])
for iel in range(0,geom.nels):
    coord , num = emb2Dgeom(iel+1,geom)
    num = num.astype(int)
    g_num[:,iel] = num
    g_coord[:,num-1] = np.transpose(coord)
    for iip in range(0,geom.nip):
        coord_ip = shapefun(iip,coord)
        g_coord_ip[:,iel*geom.nip+iip] = np.transpose(coord_ip)

# Cholesky decomposition + Distance matrix
coord_x = np.reshape(g_coord_ip[0,:],[-1,1])
coord_y = np.reshape(g_coord_ip[1,:],[-1,1])
Dx = sp.distance_matrix(coord_x,coord_x)
Dy = sp.distance_matrix(coord_y,coord_y)
corr = np.exp(-2 * np.sqrt((Dx/geom.thetax)**2+(Dy/geom.thetay)**2))
sqrt = np.linalg.cholesky( (np.exp(corr)-1) / (np.exp(1)-1))

# Create random fields
pop_rdnl = sqrt @ np.random.normal(0.,1.,size = [geom.ntip,geom.nfield])
pop = np.exp(pop_rdnl * SP.pop_std_ln + SP.pop_mean_ln)
```

```
pars_rdnl = sqrt @ np.random.normal(0.,1.,size = [geom.ntip,geom.nfield])
pars = np.exp(pars_rdnl * SP.pars_std_ln + SP.pars_mean_ln)


parm_rdnl = sqrt @ np.random.normal(0.,1.,size = [geom.ntip,geom.nfield])
parm = np.exp(parm_rdnl * SP.parm_std_ln + SP.parm_mean_ln)



# Save text files
np.savetxt('pop.txt',np.transpose(pop))
np.savetxt('pars.txt',np.transpose(pars))
np.savetxt('parm.txt',np.transpose(parm))
np.savetxt('geometry.txt',geom.geometry_data)

if iversion == 0:
    os.system(r'FEMpstress.exe')
elif iversion == 1:
    os.system(r'nored.exe')
else:
    print("SHANSEP version not understood")


end = time.time()
print("This script took %0.4f seconds to run." %(end-start))
```

E

Modifications simple FEM code

```
! ---------------------- Calculate strength & initial plasic points ------------------------
gravlo1 = gravlo
CALL spabac(kv,gravlo1,kdiag)
gravlo1(0) = 0.
DO iel = 1,nels
        num = g_num(:,iel)
    coord = TRANSPOSE(g_coord(:,num))
    g = g_g(:,iel)
    eld = gravlo1(g)

        DO i = 1,nip
                CALL bee8(bee,coord,points(i,1),points(i,2),det)
                eps = MATMUL(bee,eld)
                sigma = MATMUL(dee,eps)

                CALL principal(pstress,sigma,orr,iel)
                stre((iel-1)*nip+i,:) = pstress(1)
                orrvec((iel-1)*nip+i,:) = orr
                pstress = - pstress
                !write(502,*) sigma(1),sigma(2),sigma(3),sigma(4),pstress

        ocr = (pstress(1) + pop((iel-1)*nip+i,:) )/pstress(1)
        shansepsu = pstress(1) * pars((iel-1)*nip+i,:) * ocr**parm((iel-1)*nip+i,:)

        corrfactor = 1 - ((1-0.1)/90) * (ABS(orr))
        cfactorvec((iel-1)*nip+i,:) = 1 - corrfactor
        WRITE(502,*) corrfactor , orr
                rfc((iel-1)*nip+i,:) = MAX(shansepsu*corrfactor,1.0)
                ! check yield
                CALL invar(sigma,sigm,dsbar,lode_theta)
                DO ireal = 1,nreal
            CALL mocouf(zero, rfc((iel-1)*nip+i,ireal),sigm,dsbar,lode_theta,f)
            plastic((iel-1)*nip+i,ireal) = f
        END DO
        END DO
END DO
```

```fortran
SUBROUTINE principal(pstress,stress,orr,iel)
 !
 ! This subroutine calculates and returns the principal stresses of a plane strain
 ! stress tensor.
 !
 IMPLICIT NONE
 INTEGER, INTENT(IN)::iel
 REAL*8,INTENT(IN)::stress(4)
 REAL*8,INTENT(OUT)::pstress(3),orr
 REAL*8::p,q,sx,sy,sz,txy,l(3),temp,pi

 pi = 2*ACOS(0.0)

 sx  = stress(1)
 sy  = stress(2)
 txy = stress(3)
 sz  = stress(4)

 p = sx + sy
 q = sx * sy - txy**2

 l(1) = sz
 l(2) = (p + SQRT(p**2 - 4*q))/2
 l(3) = (p - SQRT(p**2 - 4*q))/2

 IF (l(1) < l(2)) then
    IF (l(2) > l(3)) then
        IF (l(1) < l(3)) THEN
            temp = l(2)
            l(2) = l(3)
            l(3) = temp
        ELSE
            temp = l(1)
            l(1) = l(3)
            l(3) = l(2)
            l(2) = temp
        END IF
    ELSE
    END IF
 ELSE
    IF (l(2) < l(3)) THEN
        IF (l(1) < l(3)) THEN
            temp = l(1)
            l(1) = l(2)
            l(2) = temp
        ELSE
            temp = l(1)
            l(1) = l(2)
            l(2) = l(3)
            l(3) = temp
        END IF
    ELSE
        temp = l(1)
        l(1) = l(3)
        l(3) = temp
    END IF
```

```
  END IF

  pstress(1) = l(1) ! principle stresses are sorted in ascending order in l, in pstress we want them in
  pstress(2) = l(2)
  pstress(3) = l(3)

  orr       = 0.5 * ATAN((2*txy)/(sx-sy)) * (180/pi)
  IF (orr < 0 .AND. iel > 210) THEN
      orr = 90 + orr
  END IF
  RETURN
END SUBROUTINE principal
```

A part of the whole code of the FEM program. The calculation of stresses and the subroutine are all modifications to the program.

F

Modifications to advanced code

```
!-----|----------------------------------------------------------|
      SUBROUTINE SHANSEP(s_shan,m_shan,sigma1,sigma2,sigmap,su,ocr,sesc,orr,pop_shan,sigmap2)
!-----|----------------------------------------------------------|
      !
      use RFEM_MOD, only : nst
      use MAIN
      implicit none
      !
      double precision :: sigma1(nst),sigma2(nst),sigmap(nst),s_shan,m_shan,      &
                          pi,sigm1,dsbar1,lode_theta1,sigm2,dsbar2,lode_theta2,   &
                          sigmp,dsbarp,lode_thetap,sigmap1,sigmap2,sigmapp,su,     &
                          ocr,orr,corrfactor,sesc,pop_shan,ratio,p1,q1,p2,q2
      !
      CALL invar(sigma1,sigm1,dsbar1,lode_theta1)
      CALL invar(sigma2,sigm2,dsbar2,lode_theta2)
      !
      pi = acos( -1.d0 )
      p1 = sigma1(1) + sigma1(2)
      q1 = sigma1(1) * sigma1(2) - sigma1(3)**2
      sigmap1 = (p1 - SQRT(p1**2 - 4*q1))/2
      !
      p2 = sigma2(1) + sigma2(2)
      q2 = sigma2(1) * sigma2(2) - sigma2(3)**2
      sigmap2 = (p2 - SQRT(p2**2 - 4*q2))/2
      !
      orr = 0.5 * ATAN((2*sigma2(3))/(sigma2(1)-sigma2(2))) * (180/pi)
      IF (orr < 0. .AND. sigma2(1) < sigma2(2)) THEN
          orr = 90. + orr
      ELSEIF (orr > 0. .AND. sigma2(1) < sigma2(2)) THEN
          orr = orr - 90.
      END IF
          corrfactor = 1 - (((1-sesc)/90) * (ABS(orr)))
      !
      !
          ocr = max(1.d0, abs((sigmap1-pop_shan)/sigmap2))
          su  = max(0.d0, corrfactor*s_shan*-sigmap2*(ocr**m_shan))
      !
!-----|----------------------------------------------------------|
      END SUBROUTINE SHANSEP
```

```
!-----|----------------------------------------------------------|
```

In the SHANSEP subroutine unnecessary parts were removed and everything after the definition of orr is added.

In subroutine OPEN AND READ the data file is expanded to include a definition of POP and s_u^{TXE}/s_u^{TXC} (sesc).

```
read(10,*) !\\ --- SOILS ---
! LINE 6
DO il = 1,nbl
    read(10,*) l_layer(il,1)                  !; write(id_log,'(A,1I12.1)') 'LAYER NBS
: ',l_layer(i,1)          ! LINE 10
    read(10,*) stype(il)                      ! 1: Drained- c' phi', 2: Undrained- Shansep S m
    ! - - - - - - - - - - - - -
    [ mean_const, mean_linear, std, cov, omega ],lognormal
    read(10,*) param(1:5,1,il,1),dist(1,il)   ! c' or Shansep S
    read(10,*) param(1:5,2,il,1),dist(2,il)   ! tan(phi') or Shansep m
    read(10,*) param(1:5,3,il,1),dist(3,il)   ! gamma_dry
    read(10,*) param(1:5,4,il,1),dist(4,il)   ! gamma_wet
    read(10,*) param(1:5,5,il,1),dist(5,il)   ! psi
    read(10,*) param(1:5,6,il,1),dist(6,il)   ! E
    read(10,*) param(1:5,7,il,1),dist(7,il)   ! vee
    read(10,*) param(1:5,8,il,1),dist(8,il)   ! POP
    read(10,*) param(1:5,9,il,1),dist(9,il)   ! sesc
    ! - - - - - - - - - - - - -
    read(10,*) theta(il,1:2)                   ;! scale of fluctuations              ;
    !
    WRITE(ID_LOG,'(36A)') ('--',j=1,36)
    WRITE(ID_LOG,'(A,1I3.1,A,1I4.1)') '     UNIT ',i,' | LAYER ID =',l_layer(il,1)
    WRITE(ID_LOG,'(36A)') (' -',j=1,36)

    WRITE(ID_LOG,'(A,5D12.3)') 'c or S        | ',param(1:5,1,il,1)
    WRITE(ID_LOG,'(A,5F12.3)') 'tan(phi) or m| ',param(1:5,2,il,1)
    WRITE(ID_LOG,'(A,5D12.3)') 'gamma_dry     | ',param(1:5,3,il,1)
    WRITE(ID_LOG,'(A,5D12.3)') 'gamma_wet     | ',param(1:5,4,il,1)
    WRITE(ID_LOG,'(A,5F12.3)') 'psi           | ',param(1:5,5,il,1)
    WRITE(ID_LOG,'(A,5D12.3)') 'E (Young)     | ',param(1:5,6,il,1)
    WRITE(ID_LOG,'(A,5F12.3)') 'v (Poisson)   | ',param(1:5,7,il,1)
    WRITE(ID_LOG,'(A,1F12.3)') 'THETA_1       | ',theta(il,1)
    WRITE(ID_LOG,'(A,1F12.3)') 'THETA_2       | ',theta(il,2)
END DO
```